DOCTOR OF PHILOSOPHY

Metabolic Factors Determining Outcome in Chemotherapy Studies with Pazopanib

Sharp, Stephanie Lora

Award date:
2014

DOCTOR OF PHILOSOPHY

Metabolic Factors Determining Outcome in Chemotherapy

Studies with Pazopanib

Stephanie Lora Sharp

2014

University of Dundee

UNIVERSITY OF DUNDEE

Metabolic Factors Determining Outcome in Chemotherapy: Studies with Pazopanib

by

Stephanie Lora Sharp

A thesis presented to the University of Dundee for the degree of Doctor of Philosophy

January 2014

Contents

Appendix 1

Candidate's Declaration

I hereby declare that the results described in this thesis are entirely my own work, except where otherwise stated. The writing and composition of this thesis was carried out by myself. Furthermore, I affirm that the contents of this thesis are original, and have not been submitted for the attainment of any other degree. I further state that all sources have been appropriately cited. This work was carried out in the Medical Research Institute, University of Dundee, under the supervision of Professor Roland Wolf and Dr Colin Henderson.

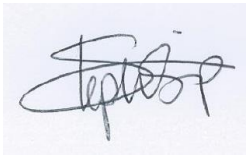

Stephanie Lora Sharp

Supervisor's Declaration

I confirm that Stephanie Sharp has completed at least 9 terms in the Division of Cancer Research at the Medical Research Institute, fulfilling the conditions of Ordinance 39, University of Dundee, and is thereby eligible to submit this thesis for the Degree of Doctor of Philosophy.

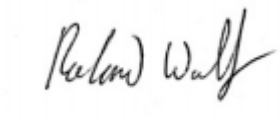

Professor Roland Wolf

Summary

Understanding of human pathology has been greatly advanced by the use of 'model organisms', such as yeast and Drosophila. While these models have led to great advances in the treatment of human disease, they are limited by variations in physiology, metabolism, and genetic background.

The development of humanised mice, in which the gene or genes of interest have been excised from the genome and replaced with the functional human counterpart, may have the potential to bridge the gap between preclinical mouse models and human disease.

The work carried out in this thesis utilises a number of transgenic-animal models where the metabolic pathways involved in the metabolism of drugs have either been deleted or humanised in order to delineate the impact that such systems have on drug metabolism, distribution, and efficacy. These pathways include the cytochrome P450-dependent monooxygenase system and the constitutive androstane and pregnane X nuclear receptors.

The aims of this work were to assess whether these humanised mouse models better represented human drug metabolism and pharmacokinetics compared to wild-type animals. Using a novel anti-cancer agent pazopanib as a test substrate, the work detailed in this thesis assesses differences in the pharmacokinetic profile of pazopanib in various humanised and knock out animal models, as well as differences in toxicological responses. Furthermore, this project looks at variations in the efficacy of pazopanib in syngeneic tumours in humanised and wild-type mice.

The techniques used in this work include liver microsome preparations and drug stability assays *in vitro*, pharmacokinetic profiling of drugs, and syngeneic tumour growth studies *in vivo.* Drug stability studies *in vitro* identified a species difference in pazopanib metabolism between wild-type mouse and human liver microsomes. Furthermore, this difference was attenuated in humanised CYP3A4/3A7 mouse liver microsomes when compared with human liver microsomes, suggesting that humanised mice represent a better model for human pazopanib metabolism *in vitro.* This species difference in metabolism was reflected in *in vivo* pharmacokinetic studies with humanised CYP3A4/3A7/hCAR/hPXR mice exhibiting significantly decreased maximum plasma concentration, clearance and half-life of pazopanib compared to wild-type mice. Finally, this work addresses the efficacy of pazopanib in a mouse derived B16 melanoma tumour growth study *in vivo.* Pazopanib retarded the growth of melanoma tumours in both wild-type and humanised CYP3A4/3A7/hCAR/hPXR mice. Overall survival was reduced in animals which has been induced using Aroclor-1254, which suggests that induction of the cytochrome P450 system does induce the turnover of pazopanib thereby reducing bioavailability and efficacy *in vivo.*

List of Figures

Chapter 1. Introduction

List of Tables

Acknowledgements

I would like to extend my most sincere thanks to my supervisors, Professor Roland Wolf, and Dr Colin Henderson, for affording me the opportunity to pursue this research within the Molecular Pharmacology Group. Their support, advice and understanding, has proven to be the cornerstone of this endeavour. It has been a privilege to work here. Many thanks extend to all of the members of the Molecular Pharmacology Group, past and present. Very special thanks go to Lesley "Skippy" McLaughlin, who provided excellent advice and insight regarding mass spectrometry and *in vitro* assay development. Thank you to Catherine Meakin and Julia Carr for the management and supply of animals used in these studies. Thank you to Cheryl Wood and Kathryn Campbell, who played a significant role in teaching and aiding me with tissue sectioning and cell culture respectively. Furthermore, I acknowledge my family and friends who have been supportive of this work. I extend my deepest thanks, firstly to my mother, and friend, Ms Gillean McNeill, without whom this work would not have been possible. Thanks to my father, Mr Brian Sharp, for his encouragement, faith and support, and my grandmother Mrs Evelyn Sharp, for lengthy talks on the phone. Thank you also to my uncle, Mr Donald Campbell, who stands by me through yet another mission. Thank you to my beloved brother, Mick, who keeps me sane, and advised me that I can "transform into a beaker"… Heartfelt thanks to my friend and advisor, Dr Paul Skett, for his good humour and advice. I also wish to mention Dr Joy McCarthy of UCT, Mr Robert "Bobbin" Hallam, and Miss Caroline Purslow. Thank you all. Finally, I would like to acknowledge my grandparents, David and Elinor Wilkie, to whom I dedicate this work.

Chapter 1

Introduction

1.1 Current Chemotherapeutic Strategies

Modern chemotherapeutic strategies have evolved from advances in our understanding of the molecular mechanisms involved in the progression of cancer. Advancements in molecular profiling, radiologic and imaging technology have allowed insights into the growth patterns, metabolism and heterogeneity of many tumours, while the use of genetic techniques have provided tools with which predictions can be made regarding the likelihood of disease recurrence and drug sensitivity in individual patients (Walko and McLeod 2008).

The traditional approach to treating cancers was with broad spectrum cytotoxic compounds such as ifosfamide and cyclophosphamide. While these drugs are effective at halting tumour cell growth, and killing cancerous cells, their major flaw is their lack of selectivity for cancerous tissue. This results in a narrow therapeutic index, with significant damage to healthy cells, and an often severe side effect profile (Brock 1996). The ultimate goal in anticancer drug development is to improve the efficacy and selectivity of cancer treatment by exploiting the differences between cancer cells and normal cells (Balis 2002).

1.2 Limitations of Current Strategies

In 2003, an article published by DiMasi and Grabowski gave an in depth account of the costs incurred in developing new drugs. The figure quoted was approximately $900 million over a 12 to 15 year investment period. Factors contributing to these escalating costs included failures by pharmaceutical companies to terminate research on drugs which fail approval tests in good time, lengthy development processes and underutilization of emerging development technologies (DiMasi, Hansen et al. 2003). Existing, ‘traditional’ chemotherapeutics have been widely

criticised for limited efficacy, development of resistance, and vast inter-patient outcomes. It is therefore of paramount importance to assess whether or not these drugs could be better utilised by understanding optimum dosing strategies in particular cancers and patients. This not only would reduce the cost of licensing new drugs, many of which are abandoned due to funding shortages and stringent FDA guidelines for clinical trials, but would potentially improve patient prognosis.

1.3 Drug Metabolism

Under most circumstances, drugs and xenobiotics which enter the body are metabolized in order for that drug to be excreted either in the bile or urine. Generally, drugs are broken down into metabolites of increasing polarity in order for this to be achieved. Polar groups may be created by oxidation, reduction or hydrolysis reactions, or, alkyl groups may be removed to reveal polar groups within the compound itself. These metabolites may then be conjugated to glutathione, methyl, sulphate, acetyl, glucose or amino acid groups in further reactions. These metabolites may exist in different ratios and with differing volumes of distribution. They may also be excreted at different rates (Gillette 1971). Understanding these reactions and pathways is of crucial importance as the metabolism of a drug may have significant effects on its pharmacokinetic and pharmacodynamic activity, with possible consequences for efficacy. Drug metabolism is divided into ‘phase 1’ and ‘phase 2’ metabolism.

1.3.1 Phase 1 Drug Metabolism

Phase 1 metabolism is a functionalization process in which functional, polar groups are revealed or inserted into a compound. This serves to increase the water solubility of the compound and facilitate its excretion by renal and biliary routes, as well as creating substrate groups for Phase 2 metabolism. Phase 1 metabolism involves several enzymatic systems including cytochrome P450 enzymes (P450s), and flavin-containing monooxygenases (FMO) (Gonzalez 2005).

1.3.2 Cytochrome P450 Enzymes

The cytochromes P450 are a superfamily of haem-containing enzymes which are constitutively expressed in the liver, small intestine, lung and kidney, as well as being expressed at lower levels in a variety of other tissues. They are inducible, and are implicated in both xenobiotic metabolism and in the synthesis of endogenous substrates including bile acids, lipids and steroids. They catalyse mixed-function oxidase (MFO) reactions, in which they drive the insertion of a molecular oxygen atom into a vast range of substrates, often creating active metabolites that may go on to act as substrate of Phase 2 metabolism. They exhibit an absorbance peak at 450 nM when they are reduced and bound to carbon monoxide, hence their title ‘P450’ (Omura and Sato 1962). The cytochromes P450 are membrane-bound enzymes which are primarily located in the endoplasmic reticulum (ER), where they catalyse reactions which are necessary for cholesterol and sterol biosynthesis. Certain CYPs are also compartmentalised in other subcellular regions, including the plasma membrane, inner mitochondrial membranes and lysosomes (Neve and Ingelman-Sundberg 2008). Cytochrome P450 mediated oxidation reactions can be described by the following illustration:

$$NADPH + O_2 + RH \xrightarrow{\text{Cytochrome P450}} NADP+ + H_2O + ROH$$

Where RH is the substrate of the reaction, and ROH, the oxidised product.

1.3.2.1 Cytochrome P450 Structure and Function

The cytochromes P450 constitute a large, complex superfamily of proteins, which share a highly variable sequence homology. In eukaryotic cells, P450s are membrane bound, in either the mitochondria or the endoplasmic reticulum (ER). Both mitochondrial and ER-bound enzymes require electron donation in order to function. Mitochondrial P450s, also known as "class 1" P450s receive NADPH-derived (mitochondrial) electrons from a two-protein redox chain, (FAD reductase → iron-sulphur protein→ P450), whereas microsomal, or, "class 2" P450s receive NADPH-derived electrons directly from a flavin mononucleotide (FMN) /flavin adenine nucleotide (FAD)-containing reductase (Hasemann, Kurumbail et al. 1995).

1.3.2.2 NADPH-Cytochrome P450 Reductase

Cytochrome P450 reductase (POR), is an integral membrane protein which is able to donate electrons to cytochrome P450, as well as other electron acceptors including microsomal haem-oxygenase and cytochrome b_5. POR is an unusual enzyme in the sense that it contains both a FMN and a FAD prosthetic group. POR contains four structural domains from the N- to C- termini; the FMN-binding domain, the connecting domain, the FAD- and the NADPH-binding domains. The two electron-accepting domains of POR makes it an ideal "transducer" of reducing entities, as NADPH is a two-electron donor, while cytochrome P450 is a two-electron acceptor, however, these two electrons are accepted sequentially (Wang, Roberts et al. 1997).

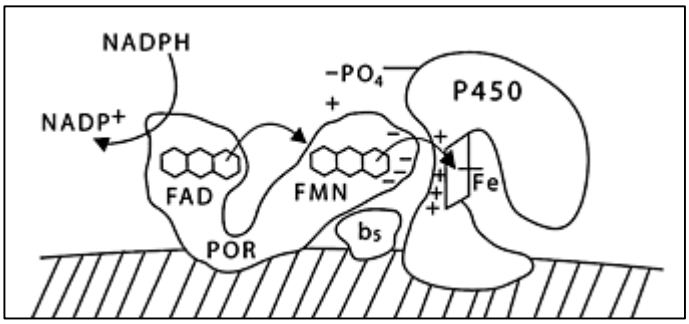

Figure 1.1 Diagram of NADPH- Cytochrome P450 Reductase

(Scott and Miller 2008).

1.3.2.3 Cytochrome P450 Catalytic Cycle

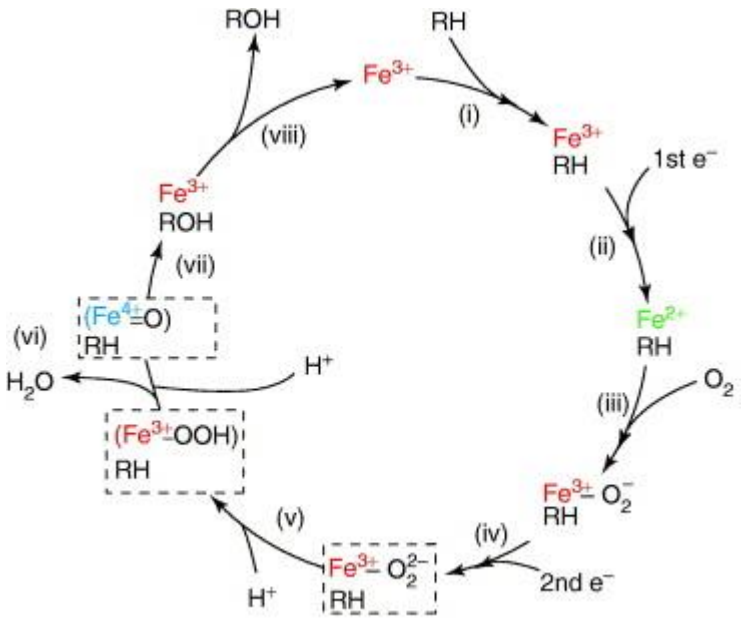

(i) The resting ferric (Fe^{3+}) form of P450 binds to substrate (RH)

(ii) The substrate-enzyme complex is reduced by a single electron (e^-) to the ferrous (Fe^{2+}) state

(iii) Molecular oxygen (O_2) binds to the reduced complex.

(iv) A second electron is received from the redox partner NADPH/NADH.

(v) H_2O is released through a reaction between the molecular oxygen and protons from the surrounding medium, leaving an activated oxygen atom.

(vi) The activated oxygen atom interacts with the substrate molecule.

(vii) The substrate becomes hydroxylated and is released from the cycle.

(viii) The cycle may then continue upon further substrate binding.

(McLean, Clift et al. 2006)

1.3.2.4 Metabolism, Resistance and the Cytochrome P450 System

The metabolism of a particular drug may have a direct impact on its duration of efficacy. This is an important consideration in which the P450s are implicated.

Xenobiotics may act to induce or supress the expression and activity of certain P450 isoforms. If there is an inhibition of P450s by a given drug, metabolism of any compound which is a substrate to the inhibited P450 will be slowed and higher levels will remain in the body for a greater length of time. This may lead to the requirement to lower the drug dose to avoid toxicity. The opposite is true of drugs causing an induction of P450s. The induction of a CYP enzyme isoform responsible for the metabolism of a drug may reduce its expected therapeutic capacity due to diminished plasma concentrations. A higher dose of the parent drug may therefore be required for effective therapy, with further dosage reviewing as and when the inducer effects are withdrawn (Saxena, Tripathi et al. 2008). It is also important to consider the potential effect of co-administered drugs, given to alleviate co-morbidities and side-effects of chemotherapy, such as analgesics and anti-emetics. Self-medications and herbal preparations, while often seen by patients as innocuous, may fall into the same category. Many of these drugs are metabolised by way of the P450 system and therefore have the potential to change the pharmacokinetics of an anti-cancer drug. This may render the drug ineffective, or cause it to be present at toxic or lethal doses (Marechal, Yu et al. 2006).

CYP3A4 is one of the most highly inducible P450s and consequently the concomitant administration of CYP3A4 inducers such as dexamethasone limits the oral availability of drugs which are substrates for this enzyme, thus lowering the dose *in vivo* and potentially leading to a loss of efficacy.

Several well described examples of clinical drug-drug interactions leading to loss of efficacy involve the anti-fungal agent rifampicin. One such study by Backman *et al.* showed that the AUC of the CYP3A4 substrate midazolam was decreased to 2-4 % of control by a 5-day pre-treatment with rifampicin 600 mg daily in healthy human subjects. This was attributed to the potent CYP3A4 induction in the liver and intestine caused by rifampicin (Backman, Kivisto et al. 1998)

1.4 Phase 2 Drug Metabolism

While metabolite products of phase 1 metabolism may be directly excreted from the body, many undergo further biotransformation by phase 2 enzymes. Phase 2 drug metabolising enzymes are responsible for the conjugation of phase 1 xenobiotic products with endogenous molecules. These conjugations generally result in further polarisation of molecules which increases the ease with which they may be excreted. These conjugations occur primarily through methylation, esterification, acetylation, glucuronidation, sulfation, and glutathione and amino acid conjugation. Phase 2 enzymes include quinone reductases (QR), methyltransferases, epoxide hydrolases (EPH), N-acetyltransferases (NAT), glutathione S-transferases (GST), UDP-glucuronosyltransferases (UGT), and sulfotransferases (SULT) (Hinson and Forkert 1995). Similarly to phase 1 drug metabolising enzymes, phase 2 enzymes are almost ubiquitously expressed, however they are significantly enriched in the liver, intestines, kidney and lung (Chen, Tang et al. 2012).

1.5 Phase 3 Drug Metabolism

Phase 3 drug metabolism is the most recently described phase of drug metabolism and refers to the active transport of drugs across cell membranes by drug transporters (Omiecinski, Vanden Heuvel et al. 2011). Research into phase 3 drug metabolism and transport dates back to 1976 when Juliano and Ling discovered a membrane bound glycoprotein on the surface of Chinese hamster ovary cells which modulated drug permeability. They named this complex "permeability glycoprotein" (P-glycoprotein), which was the first member of what now are collectively referred to as the ATP-binding cassette (ABC) family of drug transporters (Juliano and Ling 1976). In addition to the ABC transporters, other important xenobiotic transporters include the organic anion transporters and organic cation transporters and the organic anion-transporting polypeptides of the of the solute carrier families, *SLC22A* and *SLCO*s (Hagenbuch 2010). Drug transport can contribute to the development of drug resistant phenotypes through the transport of drugs out of cells and away from their site of action.

1.6 The Role of Nuclear Receptors: CAR and PXR

Regulation of the detoxification response by the body to xenobiotics is regulated at a transcriptional level by nuclear receptors (NR) in humans and animals. The nuclear receptor family of ligand-activated transcription factors includes the steroid, retinoid, and thyroid hormone receptors as well as many orphan receptors, whose physiological ligands remain unknown.

The expression of cytochrome P450 enzymes is regulated on a transcriptional level by the nuclear receptors- pregnane X receptor (PXR), the vitamin D3 receptor (VDR) the constitutive androstane receptor (CAR), and the aryl hydrocarbon (AH) receptor.

PXR was first described in 1998 (Kliewer, Moore et al. 1998) and shown to respond to a variety of compounds such as xenobiotics, natural and synthetic steroid hormones, and dietary phytoestrogens (Blumberg, Sabbagh et al. 1998). Its binding domain is largely hydrophobic, with a binding volume of 1150 $Å^3$. It is flexible and able to accommodate a vast array of substrates (Watkins, Wisely et al. 2001).

Since its discovery, PXR has been found to be activated by a range of structurally related compounds such as rifampicin, phenobarbital, hyperforin, paclitaxel and tamoxifen (Harmsen, Meijerman et al. 2009). When unbound, PXR is located in the cytoplasm. When bound to and activated by a ligand, the PXR-ligand complex translocates to the nucleus where it forms a heterodimer with retinoid-X-receptor (RXR). PXR then interacts with DNA response elements located on its target genes, and in doing so, PXR is able to up-regulate its target genes though transcriptional induction (Ihunnah, Jiang et al. 2011). The most well-known of these target genes is CYP3A4, however CYP2C9, CYP2B6, CYP2C19, CYP3A5, and UGT1A1, among others, are also implicated (Krausova, Stejskalova et al. 2011). This raises the concern of auto-induction, where a given anti-cancer agent may in fact induce its own metabolism. This has been seen in the use of the alkylating pro-drug cyclophosphamide, which is metabolised to 4-hydroxycyclophosphamide and aldophosphamide by several enzymes including, CYP3A4, CYP2A6, CYP2B6, CYP2C8, CYP2C9 and CYP2C19 (Scripture, Sparreboom et al. 2005). Cyclophosphamide has

been shown to induce mRNA levels of CYP2C8, CYP2C9 and CYP3A4 and in doing so, accelerates the rate of its own clearance resulting in a need for increasing doses of cyclophosphamide to maintain its therapeutic effect (Hassan, Svensson et al. 1999).

CAR shares approximately 40 % homology in the ligand binding domain with PXR, and is most abundantly expressed in the liver (Moore, Parks et al. 2000). Similarly to PXR, CAR acts as a xenosensor for drugs and exogenous compounds, however, it is also involved in the regulation of bile acid and cholesterol homeostasis (Rezen, Tamasi et al. 2009). CAR, like PXR, is sequestered in the cytoplasm when unbound. Upon binding to a ligand, CAR translocates to the nucleus where it forms a heterodimer with RXR and binds to phenobarbital-responsive elements of CYP2B genes, leading to an up-regulation in their expression (Xie, Barwick et al. 2000).

a)

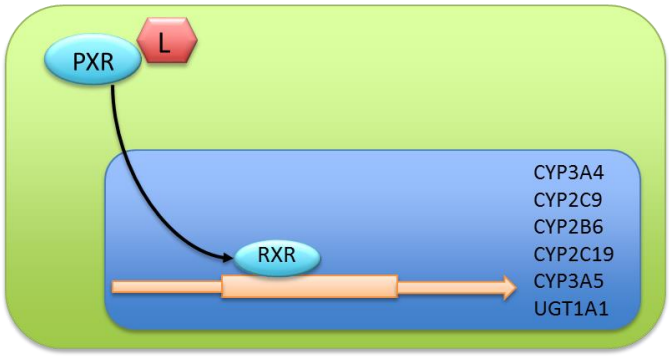

b)

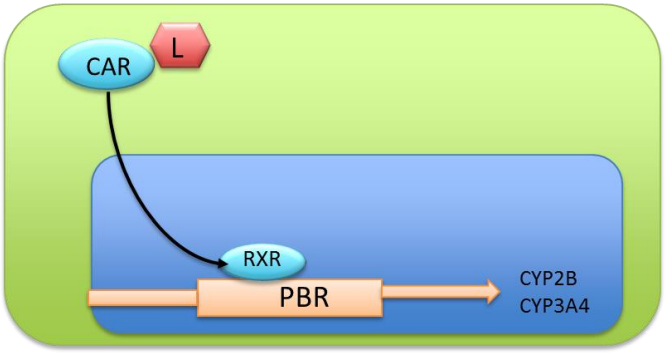

Figure 1.2. Schematic of PXR and CAR Translocation and Transcription

When unbound, a) PXR and b) CAR are sequestered in the cytoplasm. Upon ligand binding, the receptor-ligand complex translocates to the nucleus where they form a heterodimer with RXR, leading to the transcription and expression of target genes.

1.6.1 PXR and Drug Resistance

PXR is also implicated in the development of multi-drug resistance (MDR). In a study by Harmsen *et al*. human colon adenocarcinoma-derived LS180 cells treated with a range of anticancer drugs including vincristine, vinblastine and cyclophosphamide showed increased P-glycoprotein (Pgp) induction when co-transfected with a PXR expression plasmid. Pgp is a member of the ATP Binding-Cassette (ABC) transporter family of proteins, which facilitate the transport of drugs out of cells. Pgp induction is regarded as one of the major mechanisms of the development of resistance to anti-cancer drugs (Szakacs, Paterson et al. 2006). When PXR was knocked down and cells treated with the anticancer drugs, no Pgp induction was seen. These data strongly suggest a role for PXR in Pgp-related drug resistance (Harmsen, Meijerman et al. 2009).

Interest in pharmacogenetics, the heritable variations in metabolic pathways amongst a population, is growing rapidly as knowledge of the area develops. There is an increasing focus on patient targeted therapy, with a view to improving the outcome of treatments that may be effective in one patient and have little to no effect on another. Ultimately, selecting patients for certain treatments based upon the presence or absence of a molecular predictor, or a patient's own genetic background would improve the efficacy of treatment, and reduce costs of treatments significantly (Carden, Sarker et al. 2010). There have been several recent studies in which PXR activation has been associated with resistance to chemotherapy. One such study by Raynal et al. described a positive relationship between PXR expression and activity levels in human colon cancer cells, and resistance to irinotecan therapy. They noted that PXR expression was highly varied

between tumour samples, and suggest that genotyping individual tumours for PXR could improve patient survival by identifying suitable candidates for specific therapies. Furthermore they suggest that PXR down-regulation may be a novel approach to circumvent PXR-mediated chemotherapy resistance (Raynal, Pascussi et al. 2010).

1.7 Drug Transporters

Many drugs are sufficiently lipophilic to diffuse across cell membranes; however, many are anions or cations and their transport across cell membranes depends on the function of a variety of drug transporters. In recent years, drug transporters have become more widely recognised as significant determining factors with regards to drug metabolism and pharmacokinetics. (DeGorter, Xia et al. 2012). Most drug transporters belong to one of two major superfamilies of transporters; ATP-binding cassette (ABC) and solute-linked carrier (SLC). Drug transporters are, in many ways, comparable to P450s in the sense that they are differentially expressed in various tissues, are subject to polymorphisms, and are implicated in pharmacokinetics and drug-drug interactions (Zhang, Strong et al. 2006).

1.8 Difficulties Associated with Current Chemotherapeutic Regimens

It is not uncommon for initially successful chemotherapy to suddenly lose its efficacy during a course of treatment, as the tumour develops resistance to the drug. There are many mechanisms by which tumour cells may develop resistance, as many cells from a given patient have different genetic make-up. This is dependent on both the tissue of origin of the cancerous cells as well as the expression patterns of oncogenes, activity of tumour suppressors and random

genetic variations attributed to the 'mutating phenotype' of many cancers. Subsequently, all cancers may express a variety of drug-resistant genes and transporters. As a result, even the most selective and effective anti-cancer drug may allow accelerated growth of other, resistant cell types and a shift in the phenotype and genetic make-up of the cancer (Gottesman 2002). This is illustrative of a need for a new approach to cancer therapy in place of, or alongside drugs which target neoplastic cells. There is emerging awareness of the interactions between the tumour, host, and 'microenvironment' of the cancer, as well as mounting interest in potential therapies which focus on the non-cancerous stromal cells of the tumour microenvironment, with which the tumour interacts in order to aid its survival (West and van de Rijn 2007). In a study by Orimo *et al.* Carcinoma-associated fibroblasts (CAFs) were isolated from six human invasive mammary carcinomas which were obtained from mastectomies. Separate fibroblasts were also extracted from normal, non-cancerous tissue obtained from reductive mammoplasty as a comparative control. These fibroblasts were combined with MCF-7 Ras human breast cancer cells and administered subcutaneously to nude mice as a human xenograft. Their results show that CAFs are significantly more competent at enhancing tumour growth compared with normal fibroblasts (Orimo, Gupta et al. 2005). Tumour heterogeneity is a driving factor for the development of many cancers. A tumour may arise from one or more tumour initiating cells (TICs), all of which may express a different set of mutated oncogenes, affording them the ability to evolve drug-resistance pathways and grow even when challenged with several treatment strategies. As a result of heterogeneity, tumours may develop morphologically distinct zones containing populations of both mutated and normal cells. This may be affected by the development of the tumour micro-vasculature, as

these cell populations often have different nutritional requirements (Calderwood 2013).

1.9 History of Pharmacogenetics

The oestrogen receptor was first identified in the 1960's on the basis of its ability to bind radiolabeled oestrogen. Within the following decade the oestrogen receptor had become a predictive biomarker of the hormone-responsiveness of breast tumours (Osborne 1998).

Approximately 70 % of all breast cancers express oestrogen or progesterone receptors and are classified as 'Oestrogen Positive'. Tamoxifen is a selective antagonist for the oestrogen receptor and has been used for almost thirty years as a breast cancer chemotherapeutic, making it one of the very first molecularly targeted drugs to be approved by the FDA in the 1970s (Higgins and Stearns 2010).

The success of tamoxifen paved the way for many more molecularly targeted drugs that have revolutionised the way in which chemotherapy regimens are designed. In 1989, Hudziak and colleagues described a monoclonal antibody which they had generated to target the ERBB2 protein encoded for by the HER-2/neu proto-oncogene. This was based on a previous finding by Slamon and colleagues that this gene is overexpressed by up to 30% in certain breast and ovarian cancers (Slamon, Godolphin et al. 1989). Hudziak showed that *in vitro, '*4D5', as the monoclonal antibody was coined, was able to target ERBB2 expressing cells selectively to cause a decrease in proliferation as well as a down regulation of ERBB2 itself (Hudziak, Lewis et al. 1989). Presently, a modified version of 4D5, trastuzumab is now a front line therapy in HER-2 positive breast cancer. Trastuzumab may be given as a

monotherapy, to act via antibody dependent cytotoxicity to inhibit ERBB2 signalling, or in combination with broader cytotoxic drugs (Gelmon 2008).

These advances are promising; however, there are still many questions surrounding the use of genetic testing. These issues range from the financial implications of genotyping patients during a course of treatment, the time that such a process would require as well as the rather more ethical dilemma of the impact that a negative genetic result may have on a patient's morale who is subsequently denied a particular treatment (Hapgood 2003). Despite these concerns, it is clear that more work in this area is needed to identify successful drugs, such as tamoxifen and trastuzumab, for a broader spectrum of cancers. Given the sheer number of genes involved in cancer development, there is no shortage of potential targets; however there has been limited progress in the development of clinical, 'personalised' drugs since trastuzumab. The situation changed in 2007 when AstraZeneca revived interest in pharmacogenetics by launching clinical trials of olaparib, for breast and ovarian cancer (Tutt, Robson et al. 2010).

Despite the promise that these drugs show, and the distinct pathways and mutations they target, the question still remains, what percentage of patients will respond? As mentioned earlier, variations in an individual's capacity to metabolise a drug may, in some cases, render it completely ineffective in some patients, regardless of their particular variations. Therefore it is important to look beyond the drug and to assess the metabolic capacity of the patient. Ideally, single nucleotide polymorphism (SNP)-based phase 1 optimisation ought to be carried out; however, due to fiscal and ethical constraints, this is not a routine procedure (Yap, Sandhu et al. 2010).

1.10 Considerations in Personalised Therapy

There is profound inter-patient variability in the outcome of cancer treatment. This must be related either to the physiology and genetics of the tumour itself or to the genetics and phenotypic characteristics of the patient. In the latter case, an important determinant of therapeutic outcome is the absorption, metabolism and disposition of the anti-tumour agents themselves. In some patients rapid elimination of the drugs used can lead to lack of efficacy, in others prolonged exposure to the anti-tumour agent can result in life-threatening drug side effects. The metabolism of a particular drug is heavily dependent on the drug metabolising enzymes (DME) present in a particular patient. DMEs are subject to significant variation and may be profoundly affected by chronic co-medications administered alongside a chemotherapeutic agent. For example, dexamethasone is as corticosteroid, commonly prescribed to a majority of cancer patients for the alleviation of pain, nausea and chronic fatigue that can be caused by anti-cancer agents (Yennurajalingam, Frisbee-Hume et al. 2013). Dexamethasone is a PXR ligand, and therefore an inducer of CYP3A4 in man (Pascussi, Drocourt et al. 2001). Anti-cancer drugs which are also metabolised by CYP3A4 may be metabolised more rapidly in patients also receiving dexamethasone compared to patients not receiving dexamethasone.

In humans, the DMEs with the highest impact on drug disposition are the cytochrome P450 enzymes. These enzymes are responsible for phase 1 metabolism of xenobiotics and toxins and often functionalise a drug to allow further metabolism by phase 2 enzymes. Certain pro-drugs, such as cyclophosphamide are also converted to their active form by the action of P450 enzymes (Pass, Carrie et al.

2005). Of these enzymes, certain isoforms have been found to be highly polymorphic, generating distinct phenotypes in humans. Of these, CYP2C9, CYP2C19 and CYP2D6 (Gough, Miles et al. 1990) are highly polymorphic and together they account for approximately 40% of hepatic phase 1 metabolism. CYP2D6 is perhaps the most widely studied isoform as its polymorphisms result in distinct and clinically relevant phenotypes known as poor, intermediate, efficient or ultra-rapid metabolisers of CYP2D6 drugs which include common medications such as various tricyclic antidepressants and beta blockers. This polymorphism has direct effects on approximately 50 % of all pharmacotherapeutics in current use, with normal doses causing adverse reactions, or no response at all (Rodriguez-Antona and Ingelman-Sundberg 2006).

It is clear that in order to develop more efficacious cancer therapies, novel drugs must be identified which possess some degree of selectivity for tumour cells, but also that have a favourable pharmacokinetic profile. Drugs must be selected based on specific pathways dysregulated in any particular tumour. Several novel drugs have recently been described such as those discussed previously, that have been passed into clinical trials on the basis of their favourable qualities, namely - low toxicity, selectivity and efficacy. The general aim of this research is to establish the metabolism of these compounds in order to define their suitability for a particular patient. Furthermore, established anti-cancer drugs must be revisited with regards to polypharmacy and co-medication. It is highly possible that greater efficacy could be achieved with these drugs through a better understanding of the interactions of co-administered medications on their metabolism.

There is increasing awareness of the effects of polypharmacy on patient outcomes. This is a poorly-defined term that incorporates drug-drug interactions, improper medication administration, and excessive or conflicting drug administration (Bushardt, Massey et al. 2008). Polypharmacy has been linked to higher incidences of drug-related problems and poorer outcomes. This is a major implication in the outcome of chemotherapy, as many drugs impact on, or depend on the same metabolic enzymes, including the CYP450 system, for their efficacy and clearance (Marechal, Yu et al. 2006).

1.11 Drug Toxicity and Idiosyncratic Reactions

Idiosyncratic drug reactions are adverse reactions to a drug which are specific to an individual. Idiosyncratic reactions are toxic reactions that a patient may experience, which does not routinely occur in the general population of patients receiving a therapeutic dose of the drug in question. In this respect, idiosyncrasy is not related to 'drug overdose', where the dose of drug received is greater than the intended therapeutic dose, which may result in adverse reactions. An adverse reaction may be referred to as an idiosyncratic reaction, providing that the adverse response is not a consequence of the observed action or function of the drug. For example, arrhythmia caused by prolonged exposure to verapamil would not be considered an idiosyncrasy, as verapamil is a calcium channel blocker when used in a therapeutic setting, and arrhythmia may result purely from the blockade of the cardiac calcium channel. In other words, adverse reactions which are predictable are not considered to be idiosyncratic. The term idiosyncratic is often used in the same context as 'type B reactions', hypersensitivity, and allergy (Uetrecht 2007). As idiosyncratic reactions cannot be explicated based upon the pharmacology of the drug, they are largely

unexplained. While there has been a great deal of research into drug toxicity in terms of dosing strategies, and metabolism of parent compounds to toxic metabolites, the basic mechanisms of idiosyncratic reactions remain largely unknown (Knowles, Uetrecht et al. 2000). One well described example of a rare idiosyncrasy with drug treatment is hepatotoxicity in patients treated with the non-steroidal anti-inflammatory drug (NSAID), diclofenac. Diclofenac is a widely prescribed drug worldwide for the treatment of rheumatic conditions and pain management. Like other NSAIDs, diclofenac acts via inhibition of cyclo-oxygenase (COX) 1 and -2, and in doing so inhibits the synthesis of leukotrienes, prostacyclin and prostaglandins. No dose-response relationship between diclofenac dose or duration and hepatotoxicity exists, neither is it possible to reproduce diclofenac-induced hepatotoxicity in animal models, which confounds attempts to define the mechanism by which it occurs in patients. This has led to a number of patient-specific biomarkers of susceptibility to diclofenac-induced injury to be investigated, including polymorphisms in CYP450s, class 1 and class 2 major histocompatibility molecules, and mitochondrial dysfunction however, these have not been shown to be involved in clinical studies (Boelsterli 2003).

1.12 Drug-Induced Liver Injury

The liver is central to the metabolism of virtually all foreign compounds which enter the body, making the liver a common site of drug-induced toxicity seen in patients. Drug-induced liver injury may be 'dose-dependent', such as acute liver toxicity in acetaminophen overdose (Craig, Bates et al. 2011), or chronic and progressive such as cirrhosis and fibrosis resulting from prolonged ethanol consumption (Bardou-Jacquet, Legros et al. 2013), In some cases, hepatotoxicity may be transient,

beginning shortly after commencement of drug therapy, and subsiding with continued treatment. Such transient hepatotoxicity occurs in approximately 10 – 20 % of patients receiving isoniazid, with little consequence (Nolan, Goldberg et al. 1999). The nature of hepatic injury can be categorized into a number of disease states, including cytotoxic injury, cholestatic injury, phospholipidosis, fatty liver, cirrhosis, fibrosis, hepatic tumours, hepatitis, and necrosis. Despite the broad spectrum of hepatic injury that can result from drug therapies and drug abuses alike, hepatic injury is often 'silent', with no overt symptoms of underlying disease until more severe injury has occurred. Common 'late stage' symptoms are often vague and include, malaise, fatigue, abdominal swelling or discomfort, dark coloured urine, nausea, confusion, and in some cases, jaundice. While the liver has a great capacity for regeneration, if damage extends beyond a certain stage, total liver failure can occur. At this stage, liver transplantation is the only treatment available.

1.12.1 Diagnosis and Evaluation of Hepatic Injury

The subtle, and non-specific symptoms of liver damage in the early stages, coupled with the impracticalities of performing core liver biopsies to ascertain histopathological changes of the earlier stages of hepatotoxicity makes the mechanisms of hepatic disease progression difficult to delineate in humans. While liver biopsies remain useful in cases of diagnostic uncertainty, coexisting disorders can confound diagnosis, and following transplantation of the liver, there are risks of complications including bleeding, damage to biliary ducts, and pneumothorax. Furthermore, diseased tissue is not always evenly distributed throughout the liver, and consequently, biopsies may not detect underlying disease (Carey and Carey

2010). Currently, liver function is routinely evaluated using blood tests to analyse plasma levels of liver enzymes. These include tests for aminotransferases alanine transaminase (ALT) and aspartate transaminase (AST), elevations of which are often indicative of hepatocellular injury. AST is present in cytosol and mitochondria in the liver, cardiac and skeletal muscle, kidney, brain, pancreas, lung, and several blood cell types. ALT is a cytosolic enzyme found in its highest concentrations in the liver and resultantly is more specific to the liver. Hepatocellular injury causes the release of these transaminases into the circulation where they may be detected in blood tests (Limdi and Hyde 2003).

1.13 Pre-Clinical Models of Human Disease

Therapeutic testing in humans is severely constrained by practical and ethical considerations. Similarly so, the use of large mammals and non-human primates in medical research incurs high costs and complex ethical concerns. Furthermore, while these models have led to great advances in the treatment of human disease, they are limited by variations in physiology, metabolism, and genetic background, and lack of genetically inbred strains (Macchiarini, Manz et al. 2005).

The laboratory mouse is the most widely used and genetically amenable rodent species in pre-clinical research, offering several advantages over other species. Mice are among the smallest laboratory rodents available and may be housed in large numbers at a low cage density at comparatively low maintenance and husbandry costs when compared to rats, or larger species. Mice have a short gestation period of approximately 3 weeks, with females generally producing 5 to 10 pups in a litter.

Furthermore, most mouse strains exhibit immediate postpartum oestrus (Muruganandan and Sinal 2008).

1.13.1 Limitations of Mice as Pre-Clinical Models

While functional counterparts for almost all human genes have been identified in the mouse, numerous species differences in the expression, activity and inducibility of the cytochrome P450 enzymes have been described between mice and humans. The mouse genome contains 102 putatively functional genes, and 88 pseudogenes, whereas the human genome contains 57 putatively functional genes and 58 pseudogenes within 7 main CYP gene clusters. In total, there are 36 orthologous pairs of CYP genes in mice and humans, and while these particular genes would be suitable to study in mice, with relation to human biology, the vast expansion of the Cyp gene clusters in mice means that many genes are not comparable between species. For example, the Cyp2d cluster in mice contains 9 full length putatively functional genes, whereas the human has only one; CYP2D6. CYP2D6 is of clinical importance as it encodes for an enzyme responsible for the metabolism of a broad range of over 40 clinically used drugs including a number of antidepressants, neuroleptics, beta-blockers and anti-arrhythmics (Ingelman-Sundberg 2005). Patients lacking functional CYP2D6 are at risk of toxic drug reactions due to an inability to clear CYP2D6 substrates from the body, while conversely, patients overexpressing CYP2D6 may fail to maintain therapeutic levels of a drug due to overly rapid metabolism. It is likely that the vastly expanded Cyp2d cluster in the mouse is responsible for more extensive functions than in the human, rendering the mouse as an unsuitable model for studies involving CYP2D6 substrates (Nelson, Zeldin et al. 2004).

In order to address the disconnect between mouse and human data, powerful humanised mouse models have been generated. Humanisation of mice involves the replacement of a murine gene or genes with its functional human ortholog *in vivo*. In this way, humanised mice more closely mimic human drug metabolism, improve the predictability of drug responses and speed up the drug discovery process

1.13.2 Humanised Mice

Humanised mice are set to become the gold standard in pre-clinical modelling. They have been shown to better reflect human responses to xenobiotics in several different fields of study including research into HIV transmission (Denton, Estes et al. 2008), Parkinson's disease (Yamakado, Moriwaki et al. 2012) and Alzheimer's disease (Hickman, Allison et al. 2008). They are stable models in the sense that many generations of mice can be bred and still retain and express the human transgene.

Genetically modified mice including *nude* and severe combined immunodeficient (SCID) mice have been used for many years to study human tumour growth, and to test emerging therapies. The *nude* mouse carries a mutation in the HNF-3/forkhead homolog 11 gene. These mice are athymic, and hairless, hence the name *'nude'.* Due to the lack of a functional thymus in these animals, they are unable to produce mature T-cells, rendering them immunocompromised (Balciunaite, Keller et al. 2002). They have proven to be highly useful in immunology research, and are a popular model for leukaemia (Potter, Shen et al. 1984), HIV and AIDS (Ensoli, Markham et al. 1994), leprosy (Lancaster, McDougall et al. 1984) and tumour growth studies (Swami, Krishnan et al. 2011), as they are unable to reject human tissue xenografts. Similarly to *nude* mice, SCID mice are immunodeficient, lacking both functional B- and T-lymphocytes, as well as natural killer (NK) cells. SCID mice

are homozygous for recessive mutations of the protein kinase, DNA activated, catalytic polypeptide (*Prkdc*) gene, which encodes for a protein kinase involved in the repair of double stranded DNA breaks (Maruyama, Suemizu et al. 2002). Their attenuated capacity for double stranded DNA break repair makes them particularly sensitive to non-genotoxic carcinogens, and a useful model for investigating radiation induced DNA damage (Takahashi, Asakawa et al. 2002). SCID mice are more severely compromised than nude mice, and there have been several studies demonstrating improved invasion of metastatic human tumour xenografts in SCID mice than in nudes. This is likely due to T-cell-independent immune responses to metastasis in the nude mouse (Xie, Brunner et al. 1992).

Unlike the *nude* and SCID models, humanised mice retain a fully functional immune system. This is useful when considering tumour models, as the immune response may affect tumour progression and development. Moreover, chemotherapeutic agents which impair the immune system may be better evaluated in early stages of development.

CYP3A4 is the most highly expressed of the human CYP3A enzymes in the liver. It is highly promiscuous and is implicated to some degree in the metabolism of the majority of clinically-used drugs (Ekroos and Sjogren 2006). However, mice do not possess a CYP3A4 ortholog; of the eight cyp3a genes identified in the mouse, the most highly expressed is Cyp3a11, which does not exhibit the same substrate specificity as CYP3A4. This led to the generation of several humanised mouse models which are able to metabolise drugs using the functional human CYP3A4 enzyme.

A study by van Herwaarden *et al.* in 2005 described the generation of the FVB.129P2-Cyp3a13^{tm1Ahs} Del(5Cyp3a57-Cyp3a59)1Ahs Tg(APOE-CYP3A4)A1Ahs mouse line. This is a humanised 3A4 mouse line in which all 8 murine Cyp3a genes had been removed or disrupted and replaced with a transgene containing human CYP3A4 under the control of a liver specific promoter-human apolipoprotein E (APOE) (Taconic, tADMET™ model number 9048). These animals constitutively express high levels of human CYP3A4 in the liver alone, and may be used alongside the 8-gene knock out line (Taconic, tADMET™ model number 9011) to investigate the relative contribution of CYP3A4 in the liver to the overall metabolism of a drug. In their study, these mice were administered midazolam and cyclosporine A, both of which are CYP3A4 substrates. Their findings showed a greater rate of clearance of both drugs in the humanized mice compared to wild-type mice. Such findings provide strong evidence that humanised mice provide a more accurate model for testing drugs compared to wild-type mice. In particular, drugs such as cyclosporine A, which have a narrow therapeutic index may be better understood by using these transgenic models, which could improve patient care in the clinic (van Herwaarden, Smit et al. 2005). These models are becoming increasingly complex, with some lines possessing multiple transgenes to investigate interactions of various enzymes with drug transporters and nuclear receptors.

In recent years, powerful models with which to study pharmacogenetic variations have been developed that are proving to be invaluable tools in determining how susceptible a particular drug may be to cytochrome P450 polymorphisms, in particular, CYP2D6 and CYP3A4. One such model is the Hepatic Reductase Null (HRN) mouse (Pass, Carrie et al. 2005). The rationale for this model was based on

the understanding that the P450s are nearly ubiquitously expressed and a global knock out is embryonically lethal. There is also significant functional redundancy among the P450s, which belong to a large family of enzymes. P450s exhibit overlapping substrate specificities and often the loss of one enzyme only, will be compensated by the action of another isoform. However, all P450 enzymes receive an electron from the electron donor cytochrome P450 oxidoreductase (*Por*), and so, by conditionally deleting this protein in the liver it is possible to inactivate the hepatic P450 enzymes only (Henderson, Otto et al. 2003). By administering xenobiotics to these mice and measuring the levels of the parent compound and metabolites in the plasma over a period of time, it is possible to determine whether or not a drug is a P450 substrate, and consequently, whether it will be affected by potential polymorphisms in these enzymes (Henderson, Otto et al. 2003). It would then be possible to administer the drug to humanized mouse models of cancer and/models with modified P450 isoform expression to see if efficacy is lost, or enhanced, in different genetic scenarios (van Schaik 2008).

1.14 Transgenic Technology

Transgenic animals are animals which have been genetically altered in such a way so that they express the functional gene or genes of an animal of another species. This differs from knockout technology, whereby the gene of interest is removed from the genome of the model organism and not substituted with another gene. By using such genetic technology, it is possible to study the effect an absent or non-functional gene may have on the pharmacology of drugs, or to compare the response of wild type and transgenic animals to certain drug regimens. The generation of transgenic mice may be achieved by several methods, most common

are the embryonic stem cell method, and the pronucleus injection method. The pronucleus injection method involves the harvest of freshly fertilized eggs prior to the fusing of the male and female pro-nuclei. The male pronucleus is injected with the gene of interest and the embryo is implanted into a pseudo-pregnant female at the early blastocyst stage (Ittner and Gotz 2007). Alternatively, the embryonic stem cell method involves the harvest of embryonic stem cells from the inner cell mass (ICM) of mouse blastocysts. These cells are pluripotent, and retain the ability to differentiate into any cell line if cultured under the correct conditions. Any alterations made to these cells may be transmitted though breeding the embryonic stem cell method involves isolating embryonic stem cells and transfecting them with the gene or genes of interest before being injected back into the ICM of the blastocysts (Gossler, Doetschman et al. 1986).

1.14.1 Cre/LoxP System

Cre recombinase/*loxP* system is a site-specific recombination technology which may be used to create deletions, insertions, translocations and inversions of DNA and genes in cells. Cre recombinase is a 38kD protein derived from the P1 bacteriophage and is a member of the integrase family of recombinases. It functions by catalysing the recombination between two *loxP* recognition sites, also derived from the P1 bacteriophage. This system allows alterations to be made in the genome which are inducible, or cell-type specific, which affords many benefits when looking at tissue specific gene function *in vivo* (Nagy 2000). The transgenic animals used in this work were developed by Taconic Artemis, Germany, in collaboration with Professor Roland Wolf and CXR Biosciences Limited, Dundee, using Cre/LoxP transgenic technology.

1.15 Limitations of Humanised Mice

As with all models, humanised mice are not without their limitations. While it is useful to be able to model cancers in the species from which they are naturally derived, the fact remains that we are still unable to mimic the complexity of the human disease progression. Secondly, mouse tumour progression does not offer an exact reflection of human tumours. They often respond differently to chemotherapy compared to human tumours. It is possible to cure many mouse cancers, however this is not reflected in the clinic (Richmond and Su 2008).

Variation in the genetic background of laboratory mice is of particular importance when developing a humanised model. The genetic background may be defined as "the genotype of all other related genes that may interact with the gene of interest" (Yoshiki and Moriwaki 2006). Laboratory mouse strains used today originated from the breeding of domestic varieties of 'fancy mice', a once popular pursuit that originated in Asia in the 1700s. 'Fancy mice' breeding spread to Europe and North America, peaking in its popularity in the late 19th to the early 20th Century with the rediscovery of Mendel's laws of inheritance which allowed selective breeding for desired qualities such as coat colour and behaviour (Wade and Daly 2005). Because of the 'fancy mouse' origins of the laboratory mouse, most strains are a variable genetic blend of four major subspecies; *M. musculus domesticus*, *Mus musculus musculus*, *Mus musculus castaneus*, and *Mus musculus molossinus* which hail from Eastern Europe, Western Europe, South East Asia and Japan respectively (Hedrich and Bullock 2004).

There have been many studies and reports on the effects of genetic background on gene expression and regulation. Such impacts may be extreme in nature, as described by Carlson *et al.* in 1997, who showed that over expression of the

Alzheimer's amyloid precursor protein (APP) in outbred mice produced amyloid plaques associated with Alzheimer's disease in the brain, however over-expression of APP in inbred FVB/N or C57BL/6J mice is lethal (Carlson, Borchelt et al. 1997). Some phenotypes arising from genetic background may be more subtle, with differences arising between sub-strains. To avoid confusion over unexpected results when using mouse models, it is of paramount importance to select a mouse line on a well-defined genetic background, and utilise the correct controls for that strain, preferably, a co-isogenic line (Yoshiki and Moriwaki 2006).

It is worthy of note that while great advances have been made in the field of mouse transgenesis, the rat is the species of choice for a variety of research areas. The physiology of the rat more closely mimics that of humans compared to the mouse, and so they are often used in research into diabetes, cardiovascular disease and age-related disease (Iannaccone and Jacob 2009). Their behaviour is more complex and social than the mouse and their ability to learn tasks and skills makes them a popular model for learning and behavioural studies. Recent advances in rat ES cell technology have led to the generation of new knockout and transgenic rats (Huang, Tong et al. 2011), (Li, Tong et al. 2008). While rats may provide good models for behavioural and learning studies, they are costly to maintain and require more space than mice for high-powered studies. The cost of developing a transgenic rat greatly outweighs the cost of developing a transgenic mouse.

1.16 Application of Humanised Mice to Complex Human Disease

The increasing availability of humanised mice presents a unique opportunity to investigate complex human disease, and compare outcomes with those found in wild-type mice in the hope that better model systems can be identified. Cancer is a

complicated and dynamic disease, especially in later stages of disease progression. Cancer is generally more easily treated when identified early, however this is not always possible, as some cancers do not present with obvious symptoms until an advanced disease state is reached (Smith, Cokkinides et al. 2009).

Metastatic renal cell carcinoma has typically proven very difficult to treat, with patients typically presenting during later stages of disease. This can result in a very poor prognosis and high mortality within 5 years. Renal cell carcinoma is largely resistant to radiation, hormone therapy and chemotherapy which is a great limitation to the armamentarium of traditional treatments (Figlin, Sternberg et al. 2012). Historically, cytokine therapy with Interferon- α and interleukin-2 was considered the most useful treatment option available, with a response seen in 10-20 % of patients (Motzer, Bacik et al. 2004).

Recent studies into the development of the underlying mechanisms of the disease have identified vascular endothelial growth factor (VEGF), a tumour secreted cytokine central to tumour driven angiogenesis, as a key therapeutic target. VEGF is a member of the platelet derived growth factor (PDGF) superfamily of growth factors, along with VEGF-C, D and E, and placenta growth factor (PlGF) (Rini and Small 2005).

The VEGF proteins are dimeric glycoproteins which are over-expressed in the majority of human metastatic tumours as well as many pre-metastatic lesions. They bind to 3 transmembrane tyrosine kinase receptors (VEGFR 1-3) which are enriched in the vascular endothelium in response to hypoxic conditions (Dvorak 2002). Upon binding to the receptor, VEGF causes autophosphorylation of the tyrosine kinase, followed by activation and subsequent phosphorylation of a complex array of second messengers and signalling molecules including those of the Raf, MEK, Erk

pathway, p38MAPK and the Akt pathway, to promote endothelial cell migration, proliferation, survival and vascular permeability (Koch, Tugues et al. 2011) . The VEGF signalling cascade is depicted in **Figure 1.3.**

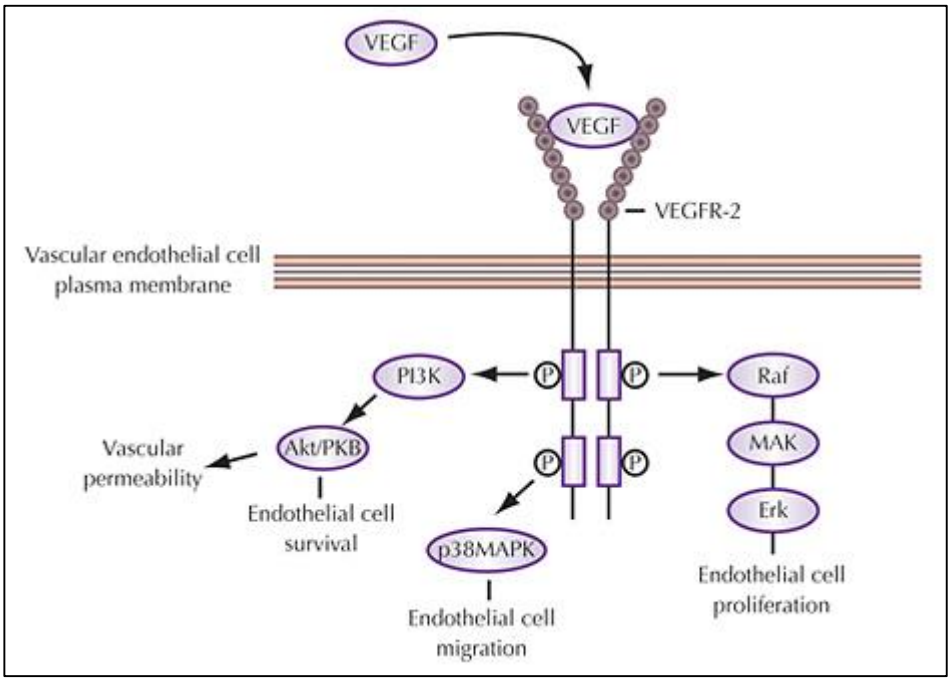

Figure 1.3. Vascular Endothelial Signalling Cascade.

1.16.1 Pazopanib

Pazopanib (Votrient; GlaxoSmithKline, London, UK) is a novel tyrosine kinase inhibitor (TKI), which targets vascular endothelial growth factor receptors (VEGFR) 1, 2, and 3, platelet derived growth factor receptor (PDGFR) -α and -β and stem cell factor receptor (c-kit) tyrosine kinases. The structure of pazopanib is displayed in **Figure 1.4.** Pazopanib exerts its therapeutic effect by inhibiting angiogenesis and reducing blood supply to tumours. Pazopanib is currently licensed for treatment of advanced renal cell carcinoma (RCC), and is undergoing trials for a number of other cancers including glioblastoma (Iwamoto, Lamborn et al. 2010), breast cancer

(Taylor, Chia et al. 2010), thyroid cancer (Bible, Suman et al. 2010) and soft tissue sarcoma (Sleijfer, Ray-Coquard et al. 2009). A clinical trial carried out by Steinberg *et al.* reported a mean progression free survival of patients receiving pazopanib of 9.2 months, compared with the control group which had an average progression free survival time of 4.2 months (Sternberg, Davis et al. 2010).

A study in 2007 showed Pazopanib to be orally bioavailable, with a broad anti-tumour activity *in vivo*, with tumour growth inhibition being seen at doses as low as 10 mg/kg. A plasma concentration of 40 µmol/L was required to inhibit VEGFR phosphorylation and tumour growth *in vivo*. These figures correlate well with clinical trial outcomes, in which the majority of patients achieve efficacious plasma concentrations of 40 µmol/L (approximately 20 µg/ml) at a dose of 800 mg per day (Kumar, Knick et al. 2007).

Pazopanib is known to be a substrate for CYP3A4 and a weak inhibitor of CYP3A4, CYP2C8, and CYP2D6. Consequently, drugs with a low therapeutic index that are substrates of these P450s should not be given in conjunction with Pazopanib. Strong inducers or inhibitors of CYP3A4 should also be avoided. Pazopanib, in addition to interaction with various CYP enzymes, is a substrate for p-glycoprotein, and an inhibitor of uridine-diphosphoglucuronate glucuronosyltransferase 1A1 (UGT1A1). Results from in vitro studies demonstrated that metabolism of pazopanib is mediated primarily by CYP3A4, with minor contributions from CYP1A2 and CYP2C8. There are three principle pazopanib metabolites; GSK1268992, GSK1268997, and GSK1071306 however little is known about their pharmacology. One of the metabolites is known to inhibit the proliferation of VEGF-stimulated human umbilical vein endothelial cells with a similar potency to that of pazopanib, while

the others are 10- to 20-fold less active. Pazopanib itself is considered to be the primary active compound (European Medicines Agency).

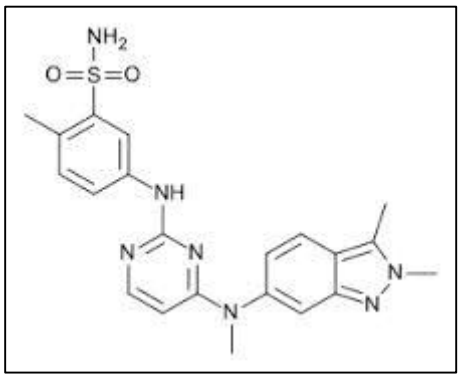

Figure 1.4 Structure of Pazopanib

1.16.2 Pazopanib Dosing and Toxicity

The recommended dose of Pazopanib is 800 mg per day by mouth; however in patients who must use a strong inhibitor of CYP3A4, this may be dropped to 400 mg per day. Similarly, in patients with moderate liver impairment, a dose of 200 mg per day is recommended. Pazopanib carries a black box warning of severe and potentially fatal hepatotoxicity and must not be administered to patients with liver failure or other hepatic impairment (GSK, 2010).

According to a study in 2010 by Hawkins *et al.* Pazopanib hepatotoxicity is fatal in approximately 1 % of patients (Sternberg, Davis et al. 2010). GlaxoSmithKline have reported fatal hepatic failure in 2 of 977 patients enrolled in clinical trials for renal cell carcinoma, and 1 patient in 240 enrolled in a clinical trial with soft tissue sarcoma (GSK).

The mechanisms by which such severe toxicity occurs have not been defined. It is not clear if hepatotoxicity in pazopanib patients is idiosyncratic in nature or whether

it is attributable to variations in metabolism in individuals. Data from clinical trials shows marked variation in plasma concentrations in patients receiving Pazopanib (Hurwitz, Dowlati et al. 2009). In a controlled clinical study with pazopanib for the treatment of RCC, alanine transaminase (ALT) > 3x upper limit of normal (ULN) was reported in 18 % and 3 % of the pazopanib and placebo groups, respectively. ALT > 10x ULN was reported in 4 % of patients who received pazopanib. Concurrent elevation in ALT > 3x ULN and bilirubin > 2x ULN in the absence of significant alkaline phosphatase> 3x ULN occurred in 5/290 (2 %) of patients on pazopanib, and 2/145 (1 %) on placebo (FDA).

Several animal studies have been carried out with repeated doses of pazopanib up to 1000 mg/kg/day in rodents. Liver enzyme elevations were observed in mice at doses of 300 - 1000 mg/kg/day and liver function parameters (aspartate aminotransferase, AST, and alanine aminotransferase, ALT, and/or bile acids) also occurred in individual rats given 300 mg/kg/day for 4 weeks, and alkaline phosphatase (ALP) and ALT were elevated after 26 weeks at 3 mg/kg/day. However, none of the changes in rats were associated with microscopic findings in the liver. No evidence of hepatic toxicity was observed in Cynomolgus monkeys receiving up to 500 mg/kg of pazopanib for up to 52 weeks but 2 monkeys given 500 mg/kg had moderately increased total bilirubin. The mechanism of liver failure and the risk factors pertaining to its development have not been identified and guidelines from GSK regarding pazopanib dosing and treatment suggest monitoring patients liver function and incremental dose-reductions of 200 mg per day, in a step-wise fashion if elevations are noted. There is little information available regarding the effect of reduced dosing on the efficacy of the drug (European Medicines Agency).

1.17 Project Aims

It is clear from the literature that there are a number of shortcomings in the current system by which new drugs are screened and selected for development. Such limitations include rising development costs, and discrepancies between efficacies of drugs in animal models which are not reflected in man. Furthermore, currently used pre-clinical models of human disease are limited by inter-species variation in metabolic pathways, as well as variation in genetic background. These factors are in some cases responsible for dramatic and unexpected effects of new therapies in the clinic. In order to address these limiting factors, it is necessary to investigate ways in which the impact of these variations can be minimised or avoided. Humanised mice represent an exciting new technology with which to accomplish this.

This project will focus on the characterisation and uses of several humanised and knock out mouse models with regards to the novel chemotherapeutic agent, pazopanib. I will investigate whether or not differences in metabolism exist between human and murine microsomal metabolism, and whether the human metabolism of pazopanib can be mimicked using humanised mouse models. Potential differences in pharmacokinetic profiles of pazopanib will also be investigated using wild-type and humanised mouse models, and whether or not this can alter efficacy and toxicity of pazopanib.

Chapter 2

Materials and Methods

2.1 Statistical Analysis and Graphical Software

Data was analysed by means of t-tests, or analysis of variance using Instat, (ANOVA) (GraphPad Instat version 3.01). Pharmacokinetic parameters were calculated using WinNonLin software, version 3.1. A non-compartmental model was used to calculate area under the curve (AUC), terminal half-life, maximum plasma concentration (C_{max}). Enzyme kinetic parameters and Hill coefficients were determined using GraFit (Erithacus Software version 5.0.4) software. *P* values are expressed by asterisks, where * = $P<0.05$, **=$P<0.01$, and ***=$P<0.001$.

2.2 Animals

All animal work undertaken in this thesis was carried out in accordance with the British Home Office Animal (Scientific Procedures) Act 1986. All procedures were approved following ethical review at Dundee University and Cancer Research UK, and conducted under the project licence held by Dr Colin J. Henderson (PIL 60/3956). Mice were housed in open top cages under standard animal house conditions, including a 12 hour light/dark cycle and *ad libitum* access to water and standard RM1 animal diet (SDS, Essex, UK). Breeding mice received RM3 diet (SDS, Essex, UK). Transgenic mice were developed by Professor Roland Wolf in collaboration with Taconic and CXR Biosciences.

2.2.1 C57BL/6NTac-Del(5Cyp3a57-Cyp3a59)1Arte Mouse Line

This mouse is a knock-out for the murine Cyp3a gene cluster. The line was created through the excision of 7 of the 8 mouse Cyp3a genes, including Cyp3a57, -3a16, -3a41, -3a44, -3a11, -3a25 and -3a59, which are located in close proximity to one another within a region of approximately 0.8 Mb, on mouse chromosome 5. The 8th Cyp3a gene, Cyp3a13, is located on the same chromosome approximately 7 Mb removed from the major Cyp3a cluster, and remains in this model, with negligible effect. For the purposes of this thesis, this line will be referred to as “Cyp3ac knock-out”.

2.2.2 C57BL/6-Del(5Cyp3a57-Cyp3a59)1Arte$^{tm1(CYP3A4\text{-}CYP3A7)Arte}$ Mouse Line

The C57BL/6-Del(5Cyp3a57-Cyp3a591Arte$^{tm1(CYP3A4\text{-}CYP3A7)Arte}$ (Taconic, model number 8842-M) mouse line is a novel mouse line containing human CYP3A4 and CYP3A7. Mice were generated from Cyp3a cluster deleted embryonic stem (ES) cells by the insertion of a bacterial artificial chromosome (BAC) containing human CYP3A4 and CYP3A7 via Cre-mediated recombination. Selected ES cells were injected into BALBc-blastocysts, which were inserted into pseudo-pregnant female mice. Resultant progeny were crossed onto a wild type C57BL/6 background. These mice were bred with a Flp-deleter mouse strain which harbours Cre-recombinase in the germline, and efficiently removes the selection markers from the transgene. Further breeding of heterozygous offspring produced homozygous Cyp3a(-/-) and huCYP3A4/CYP3A7(+/+) mice (Hasegawa, Kapelyukh et al. 2011). Throughout this thesis, this line will be referred to as “hCYP3A4/3A7”.

2.2.3 C57BL/6-Nr1i2$^{tm1(NR1I2)Arte}$Nr1i3$^{tm1(NR1I3)Arte}$ Mouse Line

C57BL/6-*Nr1i3*$^{tm1(NR1I3)Arte}$ and C57BL/6-*Nr1i2*$^{tm1(NR1I2)Arte}$ mouse lines containing the functional human nuclear receptors CAR and PXR respectively, were generated by a knock-in strategy which deleted the murine gene of interest and simultaneously inserted the human ortholog. The expression of the human receptors is controlled by the corresponding murine promoter.

In the humanised PXR model, a construct containing exons 2-4, intron 4, exon 5, intron 5, and a fusion of exons 6-9 was knocked onto the translational start ATG sequence of the mouse Pxr gene. In the humanised CAR mouse, the coding region of the mouse Car gene was replaced with the genomic coding region of human CAR, including exons 2–9. As was the case with the humanised 3A4/3A7 mouse line, these animals were crossed onto a FLP recombinase line to give rise to animals expressing human nuclear receptors. These mice were then cross bred to generate the C57BL/6-*Nr1i2*$^{tm1(NR1I2)Arte}$*Nr1i3*$^{tm1(NR1I3)Arte}$ mouse line, which possesses both human CAR and PXR (Taconic, model number 8223-M) (Scheer, Ross et al. 2008). For the purposes of this thesis, this line will be referred to as “hCAR/hPXR”.

2.2.4 C57BL/6-Nr1i3$^{tm1(NR1I3)Arte}$Is(5CYP3A4-CYP3A7;Del5Cyp3a57-Cyp3a59)2ArteNr1i2$^{tm1(NR1I2)Arte}$ Mouse Line

C57BL/6Nr1i3$^{tm1(NR1I3)Arte}$Is(5CYP3A4CYP3A7;Del5Cyp3a57Cyo3a59)2ArteNr1i2$^{tm1(NR1I2)Arte}$ mice possess the human CYP3A4/3A7 cluster, as well as human CAR and PXR. These mice were generated by crossbreeding of h3A4/3A7 mice with hCAR/hPXR mice to create a multiple humanised mouse which may be used in investigations

into autoinduction of drug metabolism (Taconic, model number 11585-M). For the purposes of this thesis, this line will be referred to as “h3A4/3A7/hCAR/hPXR”. A developmental schematic for the generation of this line is displayed in **Figure 2.1.**

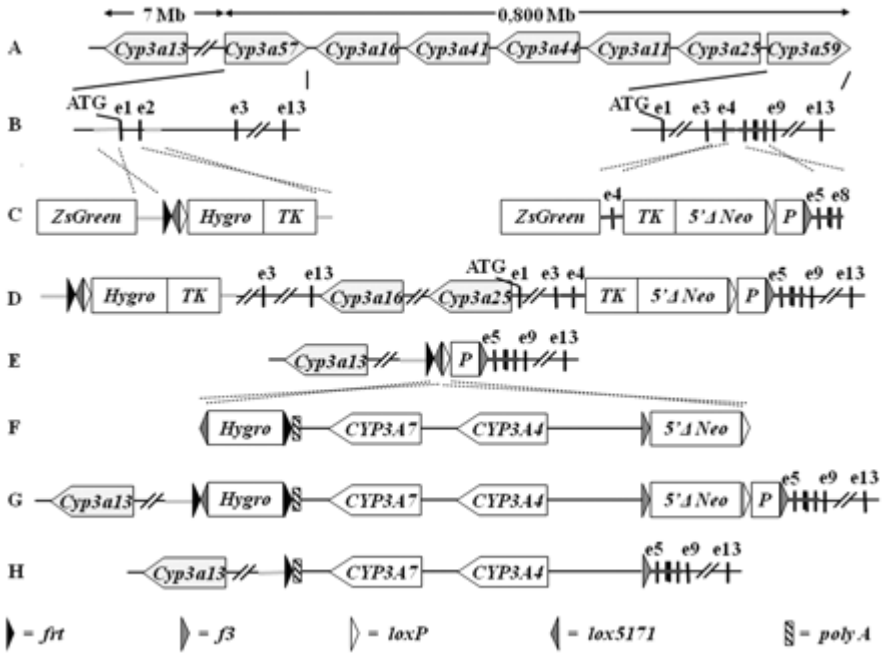

(Hasegawa, Kapelyukh et al. 2011).

Figure 2.1. Strategy for Generating Humanised 3A4/3A7/hCAR/hPXR mice.
A) Schematic representation of the chromosomal organization of functional genes within the mouse *Cyp3a* cluster B) exon/intron structure of Cyp3a57 and Cyp3a59. C) vectors used for targeting of Cyp3a57 and Cyp3a59 by homologous recombination D) genomic organization of the Cyp3a cluster in double-targeted ES cells after homologous recombination. E) Deletion of the mouse Cyp3a cluster after Cre-mediated recombination at the loxP sites F) modified human BAC containing CYP3A4 and CYP3A7 used for Cre-mediated insertion into the Cyp3a knockout locus. G) Targeted mouse Cyp3a locus after Cre-mediated recombination. H) Humanized Cyp3a locus after deletion of the expression cassettes.

2.2.5 Enzyme Induction in Humanised Mouse Lines

The initial study describing the generation of the hCYP3A4/3A7 mouse line, by Hasegawa *et al.* found that the basal expression of the human enzymes in the livers of these models is relatively low, but highly inducible. The levels found in the

intestines are constitutively high, and although they are inducible, the magnitude of induction is not as great as that seen in the liver. The induction of the hCYP3A4/3A7 mouse was achieved by intraperitoneal injection of 10 mg/kg pregnenolone-α-carbonitrile (PCN) on two consecutive days. PCN is a potent activator of murine PXR, and successfully induces the transgene to a level comparable to that found in human tissue. Similarly, the h3A4/3A7/hCAR/hPXR model is inducible using an activator of human PXR, in this case, rifampicin. Rifampicin was given at a dose of 10 mg/kg for three days by intraperitoneal injection to produce an induction equivocal to the induction by PCN in the humanised 3A4/3A7 model (Hasegawa, Kapelyukh et al. 2011).

2.2.6 Hepatic Reductase Null Mouse Line

The hepatic reductase null (HRN™) mouse model is homozygous for a tissue-specific disruption of *Por*, which encodes for P450 oxidoreductase, in the liver. This results in a complete ablation of hepatic microsomal P450 activity. The absence of first pass metabolism in this model makes it an invaluable tool in assessing the role of the P450 system in efficacy, metabolism and toxicology (Henderson 2003).

2.3 Cell Culture

All cell culture experiments were carried out using aseptic techniques. Cells were grown in an incubator at 37°C under 5 % CO_2. Syngeneic mouse tumour cell lines were purchased from Health Protection Agency Culture Collections (HPACC, Salisbury, UK). Cells were cultured in Dulbeccos Modified Eagle Medium, High Glucose (DMEM), GlutaMAX™, Pyruvate (Gibco 31966-021), supplemented with 10

% Fetal Bovine Serum (FBS) (Gibco 10500064) and 1% penicillin-streptomycin (Gibco). At 80-90 % confluency, cells were washed twice with sterile phosphate-buffered saline (PBS) before the addition of 2 ml of trypsin (Gibco) to the flask, which was then incubated at 37°C for 5 min. Medium (8 ml), containing FBS was then added to the flask in order to neutralise the trypsin, and cells were detached from the flask by gentle pipetting. The cell suspension was then transferred into a 15 ml Falcon tube and centrifuged (3 min) at 100 g. The supernatant was aspirated from the falcon and the cell pellet was resuspended in fresh medium (5 ml). Cells were then grown in flasks containing fresh medium (10 ml) at a dilution of 1:10 for 2-3 days until 80-90 % confluency was achieved

2.3.1 Cell Lines

Syngeneic tumour cells were purchased from the Health Protection Agency Culture Collections.

CMT-93 cells are a murine rectal carcinoma cell line (catalogue number: 89111413)

B16-F1 cells are a murine derived melanoma cell line (catalogue number: 92101203)

2.4 Microsomes and *in vitro* Stability

Microsomes are vesicular fractions derived from the endoplasmic reticulum during tissue homogenisation, and they contain the cell's P450 enzymes.

2.4.1 Microsome Preparation from Frozen Tissue

Microsomes were prepared from 0.2-0.4 g of snap frozen tissue samples as previously described by Meehan et al. (Meehan, Forrester et al. 1988). Briefly, tissue samples were thawed in 2 ml Eppendorf tubes. 3x volume of microsome buffer (KCL phosphate, pH7.4 at 4°C) was added to the tissue samples. Small intestines were

harvested using a “squeeze and freeze” technique whereby faecal matter was pushed from the intestine prior to snap freezing in liquid nitrogen. During small intestine tissue processing, 100 mM phenylmethanesulfonylfluoride (PMSF) and protease inhibitor tablets (Roche) were added to the microsome buffer at a concentration of 1 tablet per 10 ml of buffer. Tissue was scissor-minced and homogenised in short bursts using a PT2500E Polytron homogeniser (Kinematica) and kept on ice. Samples were centrifuged at 11,200x g for 20 minutes at 4°C, and the supernatant was transferred into a new Eppendorf tube, taking care to avoid the fatty upper layer. The supernatant was spun a second time at 11,200x g at 4°C to ensure residual debris and fat were removed. The supernatant was placed into precooled ultracentrifuge tubes and balanced to within 0.5 mg. Samples were centrifuged at 226800x g at 4°C for 80 min. The cytosolic fraction was removed to a new tube, and the dried pellet was resuspended in 50-150 µl of microsome storage buffer (0.25 M-sucrose buffered with 10 mM KCL phosphate, pH 7.4). All samples were stored at -80°C. Protein quantification of microsomal fractions was performed by the Bradford technique using the Bio-Rad protein assay reagent (Bradford 1976). A typical standard curve using Bovine Serum Albumin (BSA) as a standard, obtained for Bradford protein quantification can be seen in **Figure 2.1**.

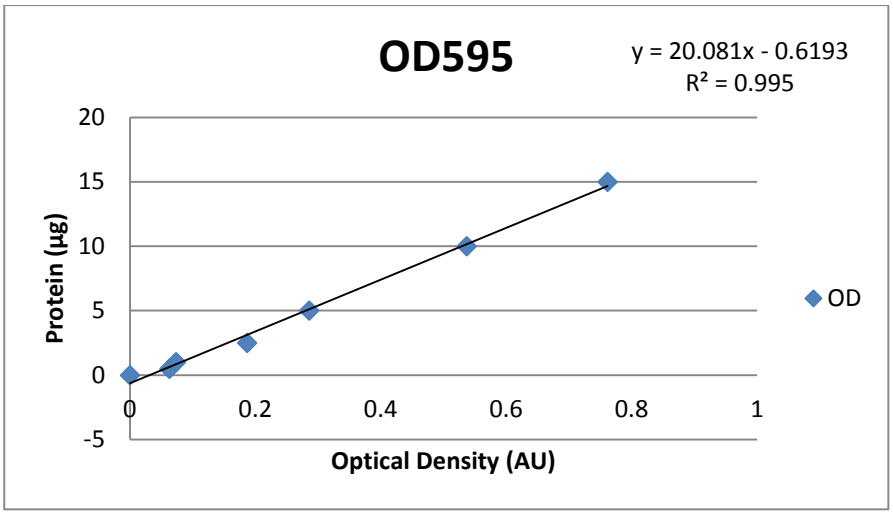

Figure 2.1. Trace depicting a typical linear standard curve of BSA as a 0.1 mg/ml stock against optical density when performing protein quantification.

2.5 Extraction Method Optimisation

In order to optimise the protocol for pazopanib extraction from bloods and protein samples, it was necessary to perform drug extractions from spiked blood samples using various solvents. In order to do so, tubes were set up containing 10 µl of blood containing 0.25 µg/ml of pazopanib. To these tubes, 500 µl of ether, diethyl ether, hexane, dichloromethane or diethyl ether/ dichloromethane (70 %/30 %) mixture was added. Tubes were vortexed for 30 sec, shaken for 20 min and spun down for 5 min at 23755 g. The clear, organic layer was removed into fresh Eppendorf tubes and dried in a speed vac at 30°C. Samples were re-susupended in methanol (80 µl) and water (40 µl). Samples were analysed by liquid chromatography mass spectrometry (LC/MS-MS) (**Section 2.9**).

2.6 Microsomal Incubations of Pazopanib for Liquid Chromatography-Tandem Mass Spectrometry

Incubations and disappearance studies were carried out in triplicate using 0.1 µM pazopanib, 1 mM NADPH, and 100 µg of protein, or, 100 pM of human recombinant P450, made up to a final volume of 700 µl with buffer (50 mM HEPES 30 mM $MgCl_2$ pH 7.4). Boiled protein was used as a control and samples were shaken at 35°C for the duration of the experiment. Substrate disappearance studies were performed by removing 100 µl of the master incubation mixture at 0, 2, 5, 10, 30 and 60 minutes, and transferring the sample into 500 µl of HPLC grade diethyl ether and internal standard solution (60 µl; 6 ng of testosterone). Samples were shaken at 35°C for 20 min and tubes were centrifuged at 23755 xg. The resultant upper layer was removed, spin dried, and resuspended in methanol (80 µl) and water (40 µl) for analysis by liquid chromatography tandem mass spectrometry (LC/MS-MS) (**Section 2.9**).

2.7 Midazolam and Pazopanib Incubations in a Panel of Human Liver Microsomes

To validate the accuracy of predictions made using the panel of microsomes, incubations were carried out using midazolam; a known substrate for CYP3A4. Incubations were performed by preparing 1 master tube for each of the 14 liver samples containing 315 µl of Hepes/$MgCl_2$ buffer containing 50 µM midazolam and 70 µg of protein. Tubes were mixed, and 90 µl of each was added to three reaction tubes, which were warmed to 37°C prior to the addition of 10 µl of 10 mM NADPH to each. Reaction tubes were incubated at 37°C for 10 minutes before the reaction was terminated by the addition of 100 µl of acetonitrile containing 1.4 µM

phenacetin as an internal standard. These were extracted using DEE as described above, and analysed by LC/MS-MS. The rate of production of 1-OH and 4-OH midazolam was calculated using a standard curve for both metabolites and plotted in correlation with the activity of each P450. Details of the individual human liver microsome samples are included in the Appendix.

Pazopanib incubations were carried out in the same way as described for midazolam, using 14 µM pazopanib, and 350 nM testosterone as an internal standard. The peak area of hydroxylated metabolite, as detected by LC-MS/MS was plotted in correlation with the activity of each P450.

2.8 Identification of Pazopanib Metabolite

Incubations were performed to identify potential pazopanib metabolites *in vitro.* Human recombinant CYP3A4 (100 pmol) was incubated with 100 µM of pazopanib, 10 mM NADPH or, the equivalent volume of water for control samples, and made up to 700 µl with HEPES/MgCl buffer. Tubes were incubated at 37°C under agitation for 1 h, and extracted in the same way as described for microsomal incubations. Test and control samples were analysed by scanning LC/MS-MS to identify peak changes between control and test samples. A peak present in test samples only showed a peak representing a mass of 454.14 (**Figure 2.2**), which in comparison to pazopanib at 438.15, is consistent with the expected mass of a hydroxylated metabolite.

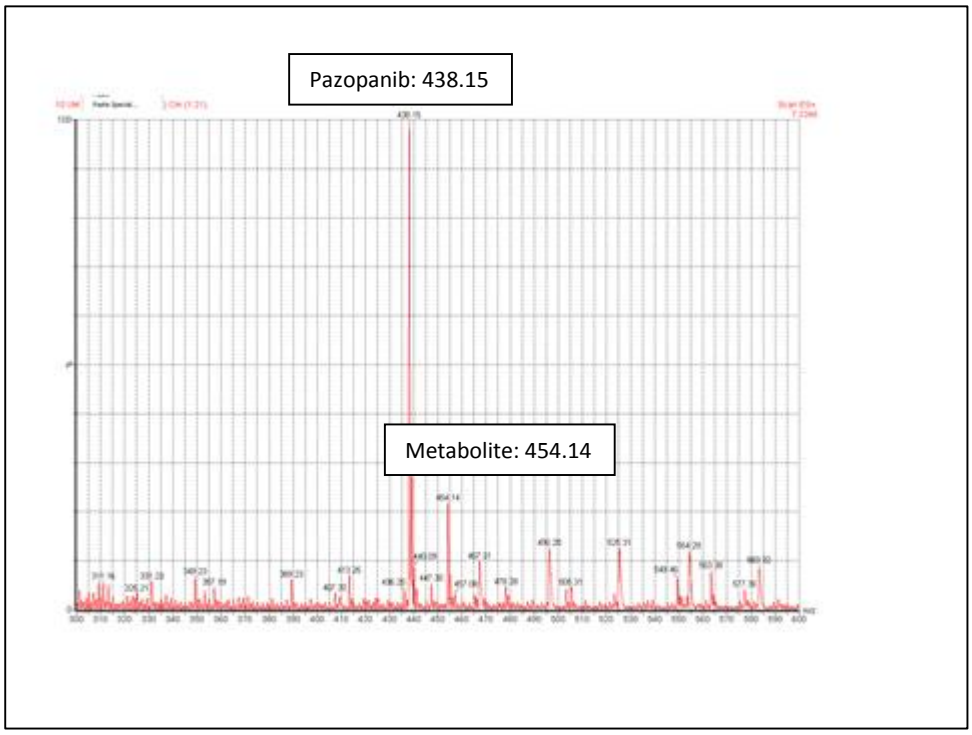

Figure 2.2 Mass spectrometer trace showing pazopanib peaks (438.15) and hydroxyl-pazopanib peak (454.14).

2.9 Mass Spectrometry Conditions for Pazopanib and Midazolam Detection

Parent compound and microsomal product formation from pazopanib and midazolam were analysed by LC/MS-MS (Waters 2795 HPLC and Quattro Micro mass spectrometry system). The voltage and collision energy were optimised for each drug and product. A dwell time of 0.5s was used between multiple reaction monitoring (MRM) transitions.

4-Hydroxy midazolam, 1'-hydroxy midazolam and the internal standard (IS) phenacetin were resolved in 5 min on a Luna C18 (2) (5 µ, 100 Å, 50 x 2.00 mm) column (Phenomenex, Torrance, CA). The injection volume was 10 µl. The following elution program was used at a temperature of 30°C and a flow rate of 0.5 ml/min: Eluent A- 0.1 % formic acid; Eluent B- Acetonitrile; (i) a linear gradient

from 3 % to 50 % was run in 3 min, (ii) mobile phase was held at 50 % B for 30 sec, (iii) linear gradient was run to 60 % B in 30 sec, (iv) solvent composition was returned to 3 % B for equilibration.

Pazopanib, OH-pazopanib and internal standard testosterone, were resolved on a Kinetex C18 (2.6 µ, 100 Å, 50 x 2.1 mm) column (Phenomenex, Torrance, CA). The injection volume was 10 µl. The following elution program was used at a temperature of 30°C and a flow rate of 0.4 ml/min: Eluent A- 0.1 % formic acid; Eluent B- Methanol, 0.1 % formic acid; (i) a linear gradient from 63 % to 75 % B was run for 1.05 min, (ii) mobile phase was held at 75 % for 56 seconds, (iii) linear gradient was reduced to 63 % B for 40 sec, (iv) linear gradient was run from 63 % to 75 % B for 5 sec. Mass spectrometer settings are summarised in **Table 2.1**.

Drug	Ion Mode	MRM Transitions	Cone Voltage (V)	Collision Energy (kV)
Pazopanib	+ve	438.1 > 357.19	50	29
OH-Pazopanib	+ve	454.14 > 436.08	48	29
4-Hydroxy midazolam	+ve	342.4 > 234.3	30	23
1-Hydroxy midazolam	+ve	234.4 > 324.3	30	22
Testosterone (IS)	+ve	289 > 97.07	31	25
Phenacetin (IS)	+ve	180.3 > 110.3	30	30

Table 2.1. Table summarising settings for parent drugs, metabolites and internal standards analysed by LC/MS-MS.

2.10 Enzyme Induction for Pharmacokinetic Studies and Tissue Harvesting

As described in **section 2.2.5**, transgenic mice were induced with appropriate agents prior to the commencement of pharmacokinetic and toxicological experiments.

Following dosing, mice were starved for 2h, and 10 µl of blood was collected from each mouse via a venepuncture made in the tail vein. Samples were transferred to Eppendorf tubes containing heparin (10 µl, 15 IU/ml). Samples were taken at 10, 30, 40, 60, 120, 240, 360, 480, 1440 and 1800 min post-dosing. Following the final time point, mice were killed by a rising concentration of CO_2, livers and small intestines were harvested; tissues were snap-frozen in liquid nitrogen and stored at -80°C for subsequent preparation of sub-cellular fractions, and/or fixed

overnight in Gurr formalin fixative (VWR Prolabo) followed by transfer to 80 % ethanol before processing to wax and sectioning for staining (**Section 2.13**). Blood was collected by cardiac puncture into heparinised tubes, spun for serum and stored at -80°C for subsequent clinical chemistry analysis (**Section 2.11**).

2.11 Biochemical Analysis of Serum

Serum was obtained from terminal blood samples by centrifugation at 23,755 xg for 10 min. The serum was removed to a clean Eppendorf tube and stored at -80°C. Serum samples were sent on dry ice to the Clinical Pathology Service Laboratory at the Mary Lyon Centre (Harwell, Oxfordshire) for biochemical analysis. Serum was tested for creatinine, glucose, total bilirubin, lactate dehydrogenase (LDH) and alanine transaminase (ALT).

2.12 Drug Extraction from Heparinised Blood Samples

Internal standard solution (60 µl; 6 ng of testosterone) was added to each tube. Pazopanib precipitation was carried out by adding diethyl ether (500 µl). Samples were shaken at 30°C for 20 min and spun at 23,755 xg for 10 min. The supernatant was transferred to a fresh tube and spin dried at 30°C for 20 min. Precipitate was resuspended in methanol (80 µl) and water (40 µl) and analyzed by liquid chromatography mass spectrometry as described in **Section 2.9**.

For the purposes of quantification of drug in the blood samples, standard curves were constructed by spiking blank blood samples with known concentrations of pazopanib. Extractions of standard curve samples were carried out in the same way as the samples from the pharmacokinetic protocols.

2. 13 Histology

After overnight fixing in Gurr Histological Fixative (Prolab), tissue samples were processed overnight in a Shandon Citadel 1000 (Thermo Scientific) before being embedded into wax blocks using a Shandon Histocentre 3 embedding centre (Thermo Scientific). Tissues were sectioned (10 μM) from wax blocks using a Shandon Finess 325 microtome (Thermo), and stained with Haematoxylin and Eosin as follows:

Sections were deparaffinised and stained by the following method:

- 100% Xylene (Sigma) 5 min
- 100% Xylene 5 min
- 100% EtOH 2 min
- 100% EtOH 2 min
- 95% EtOH 2 min
- 95% EtOH 2 min
- 75% EtOH 2 min
- 50% EtOH 2 min
- ddH2O 2 min
- Haematoxylin (Sigma) 5 min
- Running tap water 10 min
- 80% EtOH 2 min
- Eosin (Sigma) 10-20 sec
- 95% EtOH 2 min
- 95% EtOH 2 min
- 100% EtOH 2 min
- 100% EtOH 2 min
- 100% Xylene 2 min
- 100% Xylene 2 min

Samples were allowed to dry for 5-10 minutes before mounting coverslips with DPX (Sigma). Slides were viewed under high power 2-3 days later using an Axio Scope A1 microscope (Zeiss). Magnifications are indicated in each figure. Snap frozen tissue was sectioned (5 μm) using an otf 5000 cryostat (Bright Instruments, Cambridgeshire, UK). Tissue processing, embedding and sectioning was carried

out by Cheryl Wood (Molecular Pharmacology Group, Medical Research Institute, Ninewells Hospital and Medical School).

2.14 Periodic Acid Schiff Staining

A Periodic Acid Schiff (PAS) staining kit was purchased from Sigma and carried out according to the manufacturers instructions.

2.15 Oil Red O Staining

Oil Red O staining was carried out on snap-frozen tissue sections courtesy of Dr Shaun Walsh of the Pathology department, Ninewells Hospital and Medical School.

2.16 *In Vivo* Tumour Growth Studies

Wild-type and humanised 3A4/3A7/hCAR/hPXR animals were divided into groups and induced with Aroclor 1254 or corn oil as control animals. CMT 93 and B16 cells were cultured as described in section 2.3. When cells reached approximately 70 % confluency, cells were harvested and resuspended in PBS at a concentration of $6x10^6$ cells/ml. Mice were anaesthetised using isoflurane and anaesthesia was maintained during injection of the cells using a face mask. 150 µl of the cell suspension was injected subcutaneously (s.c.) into the left and right flank of each mouse. Mice were monitored daily until the development of palpable tumours, at which stage, animals were administered with either 100 mg/kg pazopanib (p.o) or the equivalent volume of vehicle (cremaphore 8 %, ethanol 15 %, water), and the dosing regimen was continued daily until tumours reached a maximum geometric

mean diameter (GMD ($\sqrt[3]{lxbxh}$)) of 12.5 mm, tumours became ulcerated, or mice showed signs of morbidity or diminished movement. Tumours were measured daily for the duration of the tumour growth protocol. Once the tumours reached the maximum acceptable tumour GMD, tumours were excised from both flanks, and livers were harvested. All excised tissues were halved for snap-freezing or fixing.

2.17 Generation of Recombinant Enzymes

Human recombinant enzymes were generated in *E.coli* as follows:

Commercially available competent *E.coli* (Promega) were thawed on ice. Plasmid DNA (300 ng) containing the gene of interest was added to competent bacteria (100 µl) and chilled on ice for 10 min. The cells were placed in a water bath at 42°C for 90 sec and then chilled on ice for a further 20 min. The cells were plated on agar plates containing 50 µg/ml ampicillin and incubated overnight at 37°C.

The following day, colonies were scraped from the agar plate and placed into liquid broth (LB) medium (150 ml) containing antibiotic. The culture was incubated in a 2L flask under agitation at 30°C overnight. The following day the culture was divided into flasks containing of Terrific Broth (200 ml, Sigma) and 50 µg of appropriate antibiotic. The cultures were left to grow at 30°C under agitation. Samples were tested periodically throughout the day using an Ultrospec 2100 *pro,* (Amersham Biosciences) using unmodified Terrific Broth as a blank sample, until an optical density of 1 was reached at 600 nM. Once this was achieved, protein expression was induced by the addition of 1 mM aminolevulinic acid (ALA) and 1 mM Isopropyl β-D-1 thiogalactopyranoside (IPTG) overnight.

2.17.1 Harvest Culture and Generation of Spheroplasts

Cultures were transferred into 1 litre centrifuge bottles and centrifuged at 2800 xg at 4°C for 20 min in a Sorvall RC 3C Plus centrifuge and the supernatant was discarded. Pellets were resuspended in 50 ml of 2x TSE (100 mM Tris-acetate pH 7.6, 500 mM sucrose, 0.5 mM EDTA) and 50 ml of ddH_20, using a 10 ml pipette to aid homogenisation. All resuspended pellets were pooled and 0.26 mg/ml Lysozyme (Sigma) was added, and samples were rocked at 4°C for 1 hour. Bottles were balanced and centrifuged as previously described. The supernatant was discarded and the pellet resuspended in a total volume of 100 ml of spheroplast re-suspension buffer (100 mM Potassium phosphate pH7.6, 6 mM magnesium acetate, 20 % (v/v) glycerol) and stored in aliquots of 25 ml at -70°C until further processing.

Frozen aliquots were thawed in lukewarm water and 100mM (2 ml) PMSF was added to each tube, along with one complete cocktail protease inhibitor tablet (Roche) dissolved in 1 ml of H_2O. Samples were sonicated for 4 rounds of 4x10 second bursts with placement on ice for 10 sec in between. The sonicated samples were decanted into 250 ml plastic centrifuge bottles and spun at 12,000 xg for 20 min at 4°C and the supernatant was retained. Supernatant was decanted into ultracentrifuge tubes and balanced. Samples were spun at 180,000 xg for 1 h and the resultant supernatant was discarded. The pellet was resuspended in 1x TSE buffer (50 mM Tris-acetate pH 7.6, 250 mM sucrose, 0.25 mM EDTA) and hand homogenised using a Dounce homogeniser (Wheaton, USA). Aliquots were stored at -80°C.

2.17.2 Cytochrome P450 Quantification

CYP content in bacterial cells and membranes was assayed as described by Omura and Sato (Omura and Sato 1964) using a Varian Cary 4000 spectrophotometer. 2x P450 Spectrum Buffer (1 ml; 200 mM Tris-HCL pH7.4, 20 mM CHAPS, 40 % (v/v) glycerol, 2 mM EDTA) was added to 10 µl of microsomal sample and diluted with 1 ml of dH_20. The sample was reduced by the addition of a few grains of sodium hydrosulfite (dithionite), and the sample divided between a reference and a sample cuvette. Samples were measured in a Spectrophotometer at wavelength between 400 and 500 nM, with scale set at -0.02- 0.02 to acquire a baseline measurement. The sample cuvette was removed and bubbled with carbon monoxide for 40 sec, and the sample was rescanned. A peak was seen at 420 nm and 450 nm and the P450 concentration was measured using the following equations:

$$\frac{x}{0.091} = nmol\ p450\ in\ 1\ cuvette$$

$$nmol\ p450\ per\ \mu l = \frac{nmol\ in\ cuvette}{0.5 \times volume\ mics\ in\ assay} \times 1000 = pmol/\mu l$$

Where 'x' denotes the amplitude of P450, and 0.091 is the extinction coefficient for P450.

A typical reduced carbon monoixide spectrum can be seen in **Figure 2.3.**

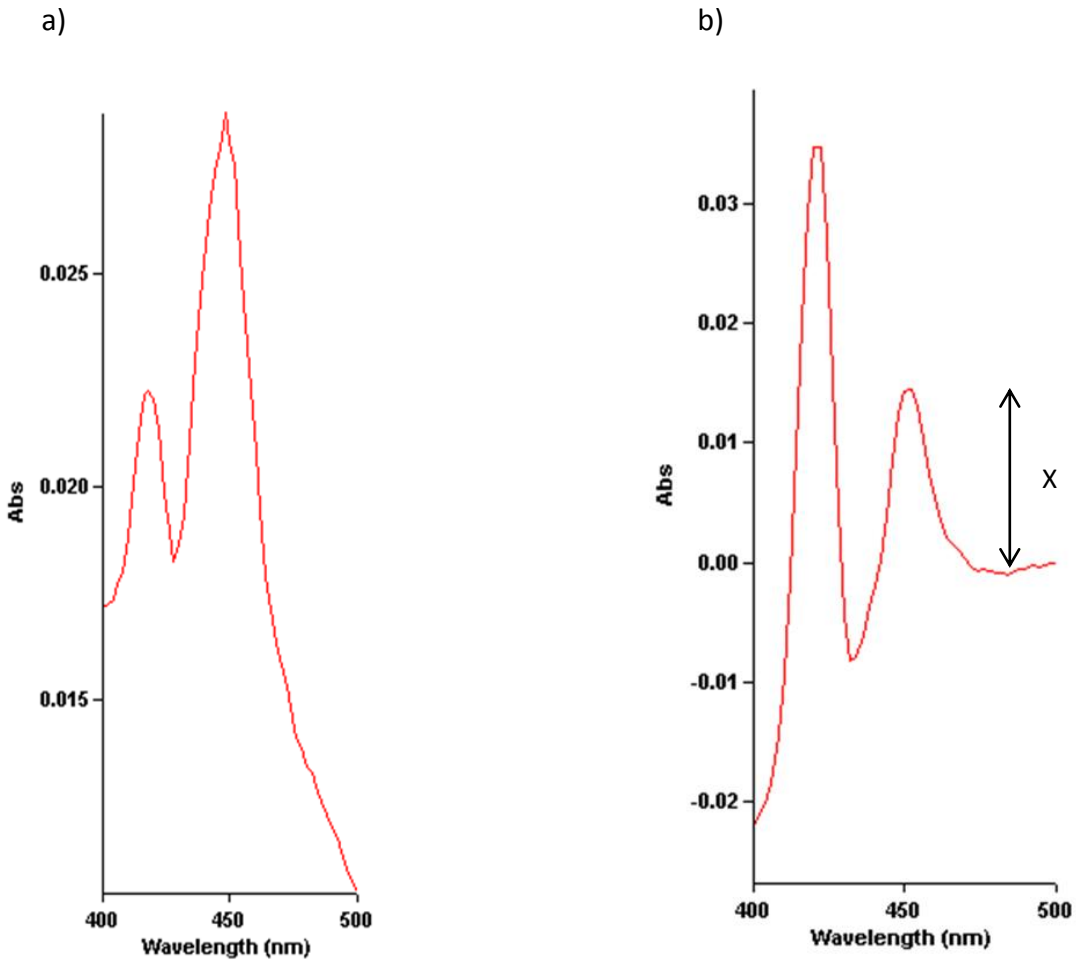

Figure 2.3. Cytochrome P450 Spectrum Traces

Representative traces obtained from a) whole bacterial cell preparations expressing human CYP3A4. b) processed bacterial membranes expressing human CYP3A4 where 'X' denotes the amplitude of P450.

Final P450 concentrations of recombinant enzymes derived from *E. Coli* are detailed in **Table 2.2.**

Enzyme	P450 Concentration (pmol/µl)	Enzyme	P450 Concentration (pmol/µl)
CYP 1A1	7.2 pmol/µl	CYP 2C19	8.2 pmol/µl
* CYP 1B1	3.1 pmol/µl	CYP 2C9	14 pmol/µl
CYP 1A2	20.3 pmol/µl	CYP 2D6	19.7 pmol/µl
CYP 2A6	3 pmol/µl	CYP 2E1	10.4 pmol/µl
* CYP 2B6	7.6 pmol/µl	* CYP 3A4	18.2 pmol/µl
CYP 2C8	22.5 pmol/µl	Cyp 3a11 (murine)	37 pmol/µl

Table 2.2. P450 concentrations of recombinant enzymes expressed in *E.coli.* Starred items were generated from constructs kindly donated by Lesley McLaughlin (Molecular Pharmacology Group, Medical Research Institute, Ninewells Hospital and Medical School). All other items were taken from stocks previously generated by Lesley McLaughlin.

2.18 *In Vitro* PXR Assay

A 96-well format human PXR nuclear receptor activation assay kit was purchased from Puracyp (Carlsbad, CA). This assay system utilizes DPX2™ human hepatoma cells. These cells harbor the human PXR gene, as well as a luciferase reporter gene linked to two promoters of human CYP3A4. The assay was carried out in accordance to the manufacturer's instructions by Dr A. K. McLeod (Molecular Pharmacology Group, Medical Research Institute, Ninewells Hospital and Medical School).

2.19 Western Blotting

2.19.1 Sodium Dodecyl Polyacrylamide Gel Electrophoresis (SDS-PAGE)

Sodium dodecyl sulfate polyacrylamide Gel electrophoresis allows proteins to be separated according to their molecular mass. Protein ladders containing proteins of known sizes were run adjacent to test samples so that the molecular weights of proteins of interest could be identified. Protein samples (10 μg) were separated by SDS-PAGE using BioRad Protean equipment.

2.19.2 SDS-PAGE Gels

SDS-PAGE gels were poured to make a 10 % running gel and 4 % stacking gel, as detailed in **Table 2.4**. Electrophoresis was carried out using a Tris/Glycine/SDS running buffer (**Table 2.5**) at a constant voltage of 100 V for 1 h.

2.19.3 Transfer of Proteins to Nitrocellulose Membrane

Following electrophoresis through the gel, the proteins were transferred electrophoretically to Protran® nitrocellulose membrane (Whatman®, Dassel, Germany). Sandwiched gels were then placed into a cassette holder and placed into a transfer tank containing ice cold transfer buffer (**Table 2.5**) and an ice block. Proteins were transferred at 100 V at room temperature for 90 mins.

Upon completion of the transfer stage, membranes were stained with Ponceau S (0.1 % w/v, 5 % acetic acid; Sigma) to verify equal protein loading. A typical Ponceau S stained membrane is shown in **Figure 2.4**. Ponceau S is a sodium salt of a diazo

dye that is designed for rapid (5 min) staining of protein bands on nitrocellulose or polyvinylidene difluoride (PVDF) membranes, both of which may be used for Western blotting. Ponceau S staining on nitrocellulose and PVDF is reversible by washing the stained membrane with Tris-buffered saline (**Table 2.5**). Proteins bound to the stained and destained membrane can then be immunologically detected using appropriate antibodies.

2.19.4 Immunoblotting

In order to minimize non-specific binding of antibody to the nitrocellulose membrane, the membranes were blocked using a 10 % w/v solution of non-fat milk powder (Marvel ™) in TBS-T for 1h at room temperature with gentle agitation. Membranes were subsequently washed in TBS-T before being incubated in the relevant primary antibody overnight at 4°C on a Stuart roller mixer (Fisher Scientific, UK) to allow antibody binding. The following morning, the membranes were washed 3 times for 5 minutes each time. The relevant horseradish peroxidase-conjugated mouse or rabbit secondary antibody was then incubated with the membrane at a dilution of 1:10000 in TBS-T, 5 % w/v Marvel™. A summary of antibodies can be found in **Table 2.3.**

Antibody	Dilution	Supplier	Raised in	Reference/Cat. Number
CH32 (CYP3A/CYP3a)	1:1000	In House	Rabbit	(Forrester, Henderson et al. 1992)
CYP1A1	1:10,000	In House	Mouse	
CYP2B	1:2000	In House	Rabbit	
CYP2C9	1:2000	In House	Rabbit	
POR	1:2000	In House	Rabbit	(Smith, Tew et al. 1994)
CYP2D6	1:1000	Sigma Aldrich	Rabbit	Cat. Num. AV41675

Table 2.3. Summary of antibodies, their dilution, and supplier.

2.19.5 Development

The bound protein-antibody complex was detected using the Immobilon Western enhanced chemiluminescence (ECL) system (Millipore). This is based on a horseradish peroxidase (HRP) chemiluminescent reaction whereby luminol reagent is oxidized by peroxidase. The oxidized luminol emits visible light as it decays to a basal state. Freshly made ECL solution (1 ml, as per manufacturer's instructions) was applied to each membrane for 40 sec prior to developing. The membranes were then visualized using a LAS-3000 luminescent image analyzer (Fujifilm).

Ingredient	10% Resolution Gel (10ml)	Stacking Gel (4ml)
H_2O	5.3 ml	2.7 ml
30% acryl-bisacrylamide mix	2 ml	0.67 ml
1.5M Tris (pH8.8)	2.5 ml	0.5 ml (pH 6.8)
10% SDS	0.1 ml	0.04 ml
10% ammonium persulfate	0.1 ml	0.04 ml
TEMED	0.008 ml	0.004 ml

Table 2.4. Recipes for 10 % resolution gel (10 ml) and stacking gel (4 ml) sufficient for two blots.

Buffer	Composition (10X Concentrated Stock)
Electrophoresis Buffer	520 mM Tris Base, 533 mM Glycine, 34.7 mM SDS
Transfer Buffer	250 mM Tris Base, 1.87 M Glycine
TBS	1.5 M NaCl, 500 mM Tris Base (p.H to 7.9)

Table 2.5. Recipes for buffers and solutions for Western blotting.

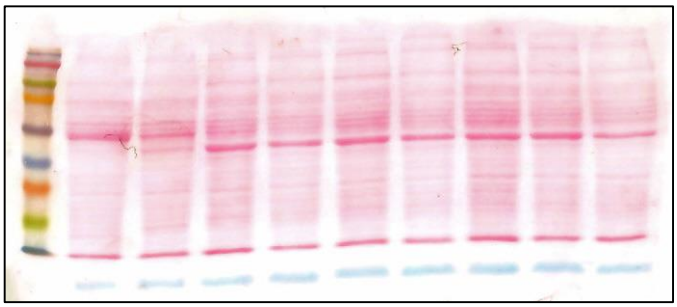

Figure 2.4. Typical Ponceau S - stained membrane.

Following transfer of proteins to nitrocellulose membranes, membranes were stained in Ponceau S (5 min), then rinsed in distilled H_2O. Proteins stained red, and even loading could be confirmed.

.

Chapter 3

Enzyme Kinetics and Microsomal Stability

3.1. Enzyme Kinetics

Predictions of the pharmacokinetics of drugs in man, volume of distribution and clearance, are often extrapolated from animal data and traditionally were based on body weight or surface area. This technique is known as 'allometric scaling'. Allometric scaling is a mathematical, empirical approach for inferring physiological data from one species to another, using factors such as organ, or body weight to 'scale' values (Obach, Baxter et al. 1997).

A general function for the scaling of pharmacokinetic parameters can be written as shown below:

$$Y = aW^b$$

Where *Y* is the parameter in question, *W* is the body or organ weight, and *a* and *b* are the coefficient and exponent of the allometric equation respectively. This may be log transformed and expressed as shown below:

$$\log Y = \log a + b \log W$$

Where log *a* is the y-intercept, and *b* is the slope.

These are the basic principles of allometric scaling and such a method is not always applicable for all drugs. Many studies have utilised modified versions of these principles to attempt to normalise and correct for a particular experimental set up, however there is no real consensus within the scientific community on these equations (Mahmood 1999). While allometric scaling and dose selection based on body weight have proven popular methods to carry out dose extrapolations, it does not allow for the consideration of species differences in biological metabolic

pathways, oxygen consumption, basal metabolic rates and other physiological parameters.

Understanding of *in vitro* enzyme kinetics and drug metabolism, is of fundamental importance if the drug in question is to be accurately adapted to the *in vivo* situation. Understanding the time-course, or kinetics, of an enzymatic reaction facilitates understanding of the underlying metabolic mechanism taking place. In order to evaluate enzyme kinetics, it is necessary to fit the enzymatic data to mathematical models which describe the hypothesized mechanisms. The solutions of these equations, based upon the "goodness of fit" of the data, allow the hypotheses to be accepted or excluded (Marangoni 2002). The equations used to fit enzymatic kinetics depend on the nature of the enzyme in question.

3.1.1 Michaelis-Menten Kinetics

For the majority of enzymes, the rate of catalysis, defined as the number of moles of product formed per second, rises with substrate concentration until a saturation point is reached. In 1913, Leonor Michaelis and Maud Menten proposed a basic model to account for these kinetic characteristics. The important feature of this model is that a specific enzyme-substrate (ES) complex is a necessary intermediate in catalysis. The model proposed, which is the simplest one that accounts for the kinetic properties of many enzymes, is:

$$E + S \overset{K1}{\leftrightarrow} ES \overset{k2}{\rightarrow} E + P$$

In which the enzyme 'E', reacts with its substrate 'S' at a rate constant of k_1 to form an enzyme-substrate complex 'ES'. From here, the ES complex undergoes a reaction

and dissociates into enzyme and product 'P', at a rate constant of k_2. When reactions which obey Michaelis-Menten kinetics are plotted, traces such as described in **Figure 3.1** are produced.

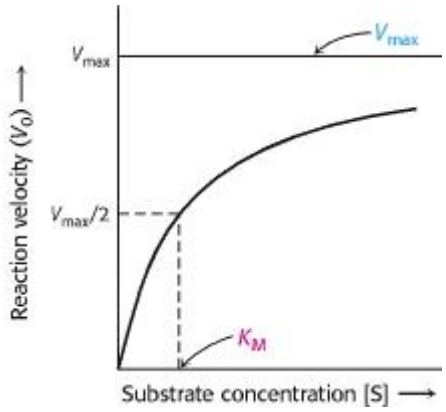

Figure 3.1 Michaelis- Menten Enzyme Kinetics

The reaction velocity (V_0) is a function of the substrate concentration (S). V_{max} is the maximum rate of reaction for an enzyme, and it occurs when all active sites of the enzyme are occupied with substrate. At this point, the enzyme is considered to be saturated. The Michaelis-Menten constant for the reaction refers to the substrate concentration required to achieve $V_{max}/2$ (Berg 2002).

3.1.2. Allosteric Enzyme Kinetics

The Michaelis-Menten model for enzyme kinetics is suitable for most enzymes in the presence of a single substrate. However, enzymes which are subject to allosteric modulation require a model which can accommodate their more complex kinetics. Allosterism refers to the modulation of an enzymes catalytic activity by a second substrate which binds to a different active site than the isosteric site, *iso* meaning 'same', and *'allo'* meaning 'other'. Enzymes may possess more than one allosteric

site, with different ligand specificities. Allosteric modulation may be agonistic or antagonistic in nature. An agonistic allosteric modulator will elicit an enhancement in the catalytic activity of an enzyme by causing a conformational change in the active sites of the enzyme to enhance affinity for the substrate. An antagonistic modulator has the inverse effect, and reduces the rate of catalysis of the enzyme (Debajyoti 1978).

3.1.3 Hill Equation

One such model which may be used in describing allosteric enzyme activity is the Hill equation. The Hill equation was first defined in 1913 by A. V. Hill to describe the binding of oxygen to haemoglobin (Hill 1913). The Hill equation, similarly to Michaelis-Menten, provides a measure of the affinity of the ligand to its receptor or enzyme, while additionally offering a measure of co-operativity of allosteric binding (Weiss 1997). The measure of co-operativity is indicated by the Hill coefficient. The equation may be represented by the following:

$$\mathrm{v} = \frac{V_m\, S^h}{K_d + S^h}$$

Where K_d is the dissociation constant, h is the Hill coefficient and V_m is the maximal velocity. The nature of the binding is described by the Hill coefficient. A Hill coefficient is greater than 1 describes positive cooperative binding, while a value less than 1 describes negative cooperative binding. A value equal to 1 denotes non-cooperative binding (Sauro 2011).

3.1.4 Metabolism of Pazopanib

In vitro studies suggest that oxidative metabolism of pazopanib in human liver microsomes is mediated primarily by CYP3A4 with minor contributions by CYP1A2 and CYP2C8. Consequently, co-administration of strong inhibitors of CYP3A4, such as ketoconazole is contraindicated in patients being treated with pazopanib (Vasudev and Larkin 2011). Four metabolites of pazopanib have been described, although not as yet in detail. However, pazopanib is considered to be pharmacologically active in its parent form, with only a very minor contribution from one of its metabolites (European Medicines Agency). CYP3A4 is the most abundant P450 enzyme in the liver, constituting approximately 30 % of total P450 present, and is involved in the metabolism of up to 50 % of all clinical drugs (Bozina, Bradamante et al. 2009). CYP3A4 exhibits broad substrate specificity and is highly polymorphic amongst the human population. This has important implications when considering drug metabolising capacities and dosing regimens for individual patients. As yet, no data are available pertaining to CYP3A4 expression and the rate of metabolism of pazopanib.

3.2. Results

3.2.1 Microsomal Stability of Pazopanib *In Vitro*

To broadly assess the rate of pazopanib metabolism *in vitro*, microsomal fractions from wild-type (C57 BL/6) mouse liver, and human liver (Invitrogen) were incubated with pazopanib (0.1 µM) and NADPH (10 µM) in a final volume of 700 µl with HEPES/$MgCl_2$ buffer. Alternatively, human recombinant CYP3A4 was used (100 pmols) in place of the microsomal sample. Samples were kept on a shaker at 37°C and 100 µl of the reaction mixture was removed into 100 µl of methanol at time points of 0, 2, 5, 10, 30 and 60 min. Samples were extracted using DEE as described in the Methods section. The percentage disappearance of pazopanib over 60 min in mouse and human microsomes does not differ significantly (12.7 % and 23.6 % respectively), however, incubations containing human recombinant CYP3A4 shows a 89 % disappearance (**Figure 3.2.1**) which is consistent with the literature showing human CYP3A4 is the major enzyme implicated in pazopanib clearance (Vasudev and Larkin 2011).

a)

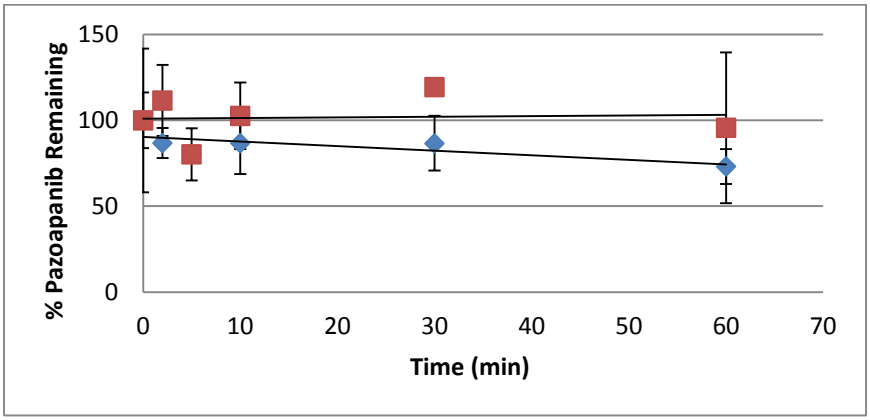

b)

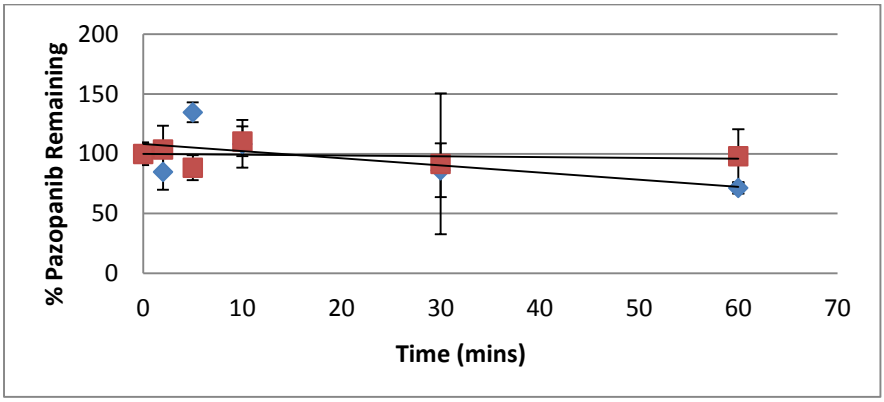

c

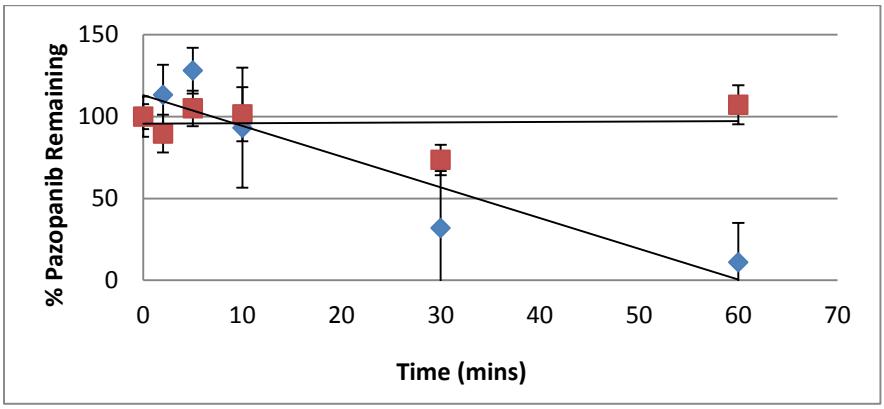

Figure 3.2.1 Pazopanib Metabolism in Mouse microsomes, Human microsomes and Recombinant CYP3A4

Time-courses showing disappearance of pazopanib (0.1 µM) in a) pooled wild-type mouse, or b) human liver microsomes (100 µg) over 60 min, compared to boiled protein control, c) time-course showing pazopanib disappearance in incubation with human recombinant CYP3A4 (100 pM). n=3 extractions per master incubation. Red squares denote boiled protein controls, blue diamonds denote live protein. Values expressed ± standard deviation (SD).

3.2.2 Optimisation of Protein Concentration in Enzyme Incubations

Modelling of enzyme kinetics is a more definitive method of predicting the extent of drug metabolism *in vivo*. To determine optimum incubation conditions to allow accurate comparisons between the kinetics of mouse and human microsomes to be drawn, protein concentration experiments were initially performed. Here, incubations were set up in triplicate, containing 0.1 µM pazopanib with 15 µg, 30 µg or 40 µg of mouse, or human liver microsomes. Samples were taken from incubation tubes at 0, 5, 10, 20, 30 and 40 min, to be extracted and analysed by LC-MS/MS. **Figure 3.3** depicts graphed data from the time courses using human liver microsomes. The coefficient of determination (R^2) values are included as an indication of the correlation between OH-pazopanib formation and time in each data set. In accordance with Pearson's correlation, as the R^2 value approached 1, the correlation between metabolite formation and P450 activity was increasingly linear and positive. Conversely, as the R^2 value approached -1 the correlation is considered increasingly linear and negative. **Figure 3.3** shows the time course containing 15 µg of microsomal protein and demonstrates the highest R^2 value of 0.92, indicating the strongest correlation of the three protein quantities. As the protein concentration in the incubations increases, the R^2 value approaches '0' indicating a decrease in the linear correlation between metabolite formation and time. As these conditions were to be used to calculate the kinetic parameters of pazopanib metabolism, the conditions yielding the highest R^2 value were adopted for subsequent experimental use.

Identical incubations were performed using mouse liver microsomes, the results of which are presented in **Figure 3.4** Similarly to the human liver microsomes, the correlation between metabolite production and time was highest at the lowest protein concentration (15 µg). Interestingly, despite having the highest R^2 value of all of the mouse protein incubations, it is still poorly correlated when compared with the 15 µg incubations using human microsomal protein (0.79 vs. 0.92 respectively). This would suggest that, in general, pazopanib is better metabolised by human liver microsomes than by mouse liver microsomes, as evidenced in **Figure 3.5, 3.6** and **3.7.**

a)

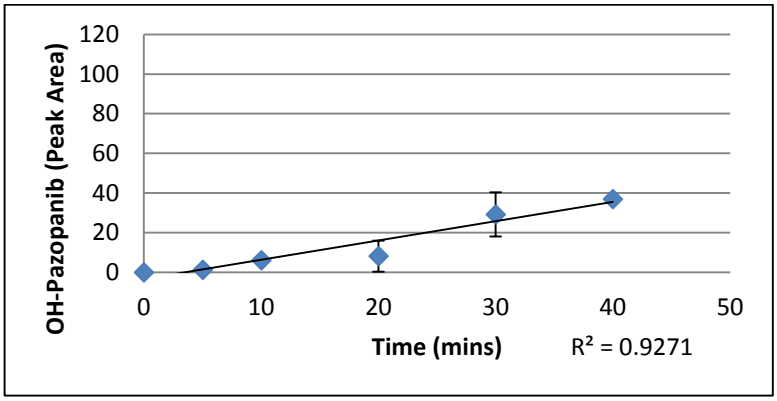

b)

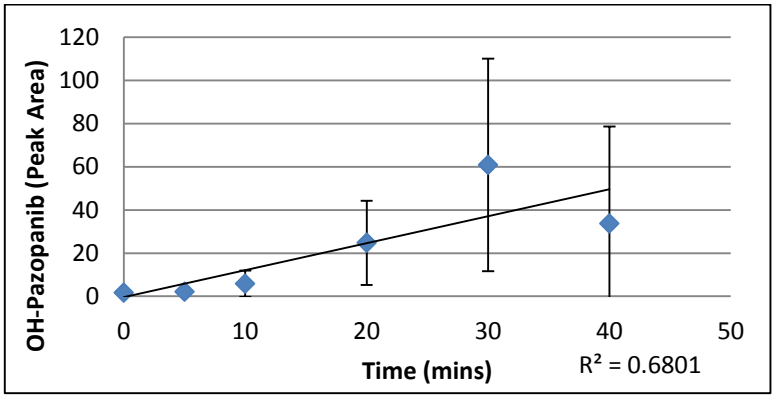

c)

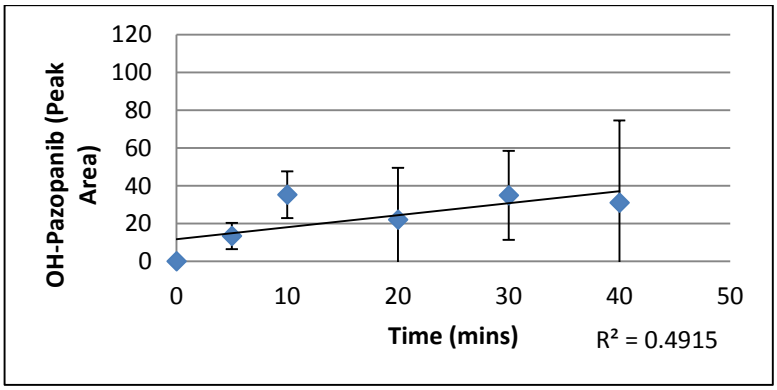

Figure 3.3. Correlation of OH-pazopanib formation with protein concentration

Graphs showing linear correlation between the formation of OH-pazopanib in pooled human liver microsome incubations over 40 min with a) 15 µg, b) 30 µg, c) 40 µg of protein. R^2 values were calculated in Microsoft Excel as a representation of the linearity of the data points. n=3 incubations per protein concentration. Values expressed ± SD.

a)

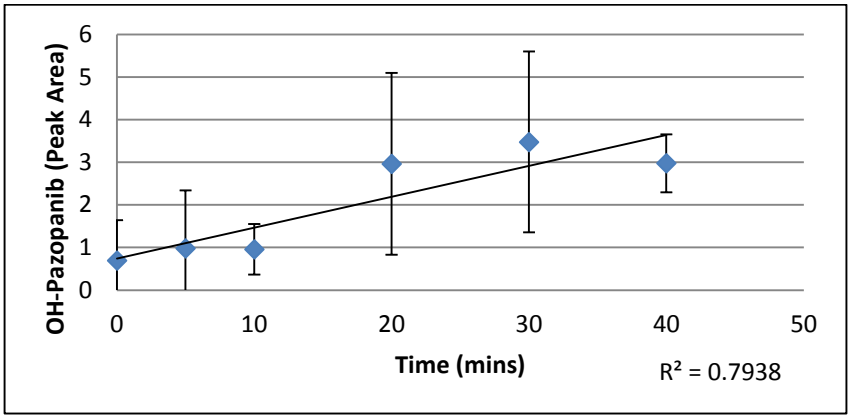

b)

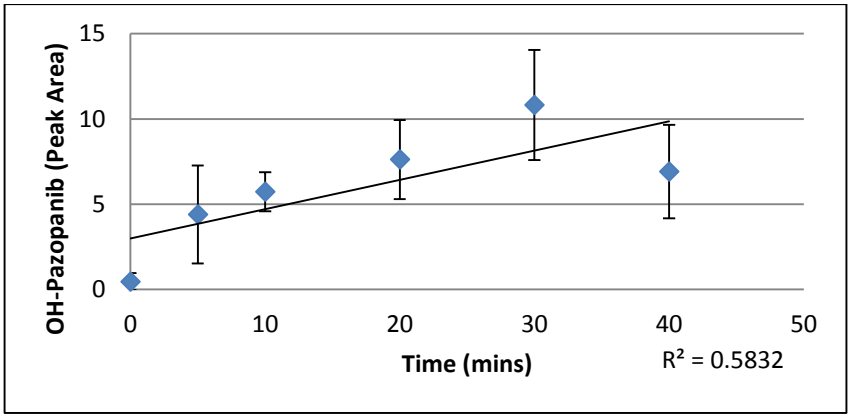

c)

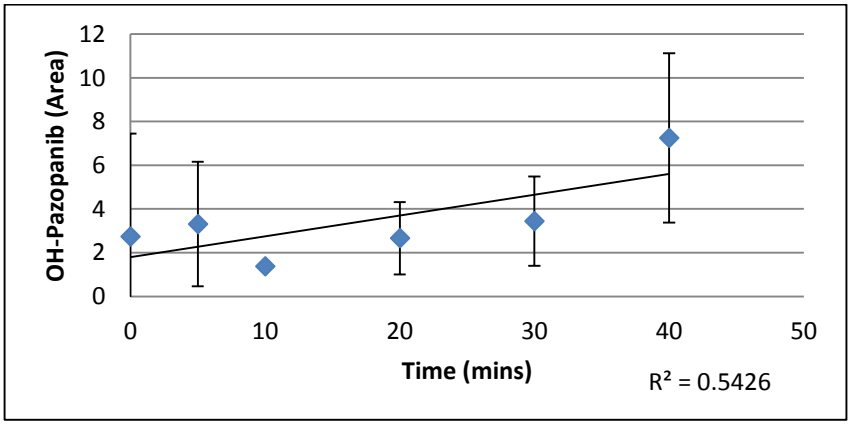

Figure 3.4 Correlation of OH-pazopanib formation with protein concentration

Graphs showing linear correlation between the formation of OH-pazopanib in mouse liver microsome incubations over 40 min with a) 15 µg, b) 30 µg and c) 40 µg of protein. R^2 values were calculated in Microsoft Excel as a representation of the linearity of the data points; n=3 incubations per protein concentration. Values expressed ± SD.

3.2.3. Optimisation of Duration of Enzyme Incubations

Similarly to the protein optimisation method, the optimal duration of incubations was determined by plotting OH-pazopanib formation against protein concentration at each of the five time points. As with the protein concentration optimisation, the time point displaying the strongest correlation between metabolite formation and protein concentration would be adopted for use. Data from incubations with human liver microsomes or mouse liver microsomes are shown in **Figure 3.5** and **3.6** respectively, graphed separately to show correlations at 5, 10, 20, 30 and 40 min. The strongest correlation between metabolite formation and time in both human and mouse microsome preparations was observed at 20 min (0.99 vs 0.96 respectively).

3.2.4 Enzyme Kinetics

In order to establish V_{max} and K_m values for human and mouse liver microsomes, incubations were set up in triplicate, containing 20 µg of human or mouse liver microsomes over a range of pazopanib concentrations between 0.5 and 40 µM. Incubations were terminated by the addition of 100 µl of methanol and extracted as described in the Methods. Data were plotted and analysed in GraFit 5 (Erithacus Software), using the Hill allosteric enzyme model (**Figure 3.7**). The V_{max} value calculated from human microsome incubations was found to be approximately 3.5x higher than the mouse incubations (1805 vs 512 peak area/min/mg respectively), suggesting that the maximum rate of pazopanib metabolism is much higher in humans than in the mouse. The K_m value of 8.9 µM in human microsomes compared to 5.2 µM in the mouse microsomes is not dissimilar, suggesting that pazopanib has a similar affinity for both human and mouse microsomes.

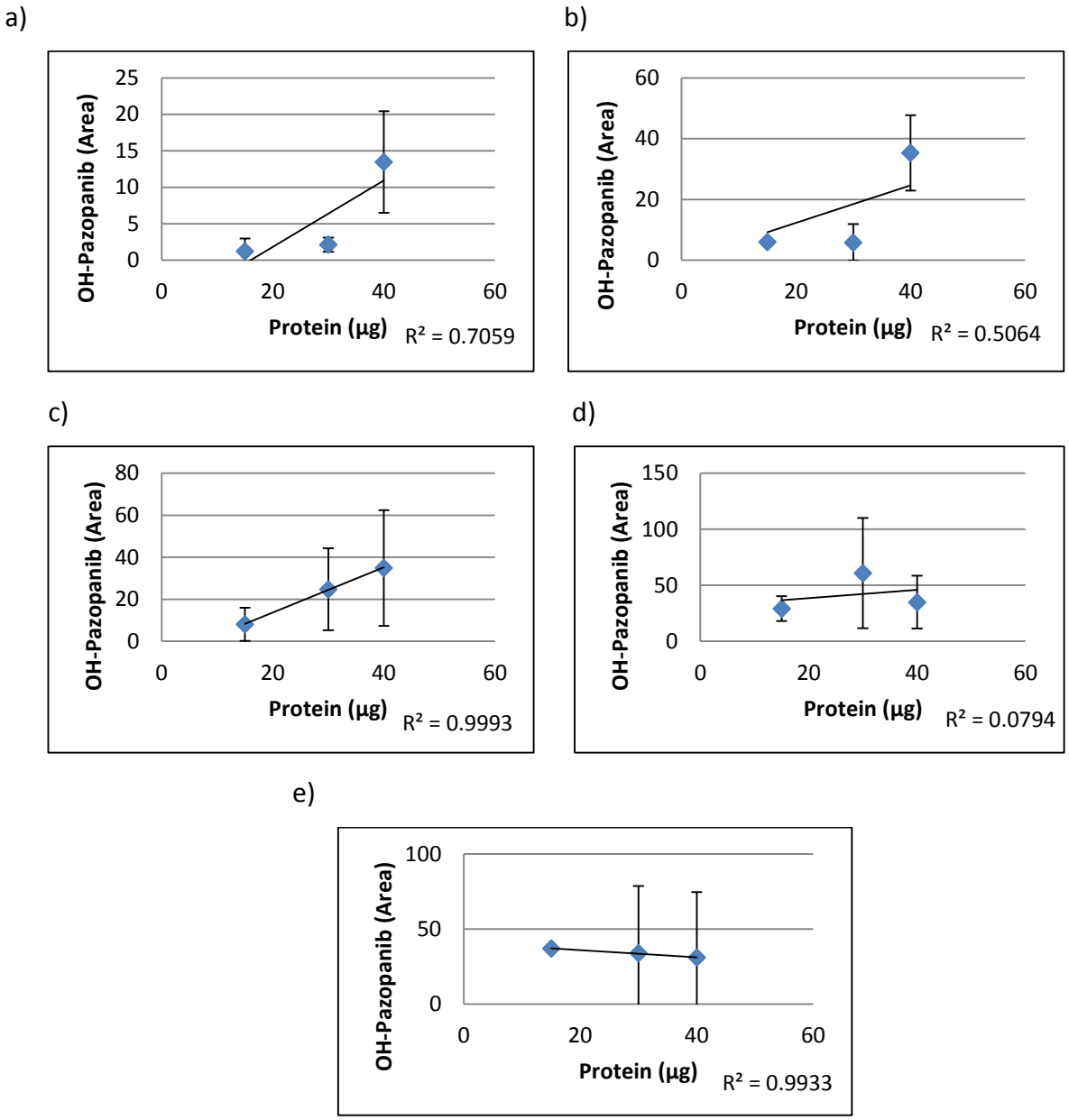

Figure 3.5 Correlation of OH-pazopanib with protein concentration at various time points

Graphs showing linear correlation between the formation of OH-pazopanib in pooled human liver microsome incubations at a) 5 min, b) 10 min, c) 20 min , d) 30 min, e) 40 min. R^2 values were calculated in Microsoft Excel as a representation of the linearity of the data points; n=3 incubations per time point. Values expressed ± SD.

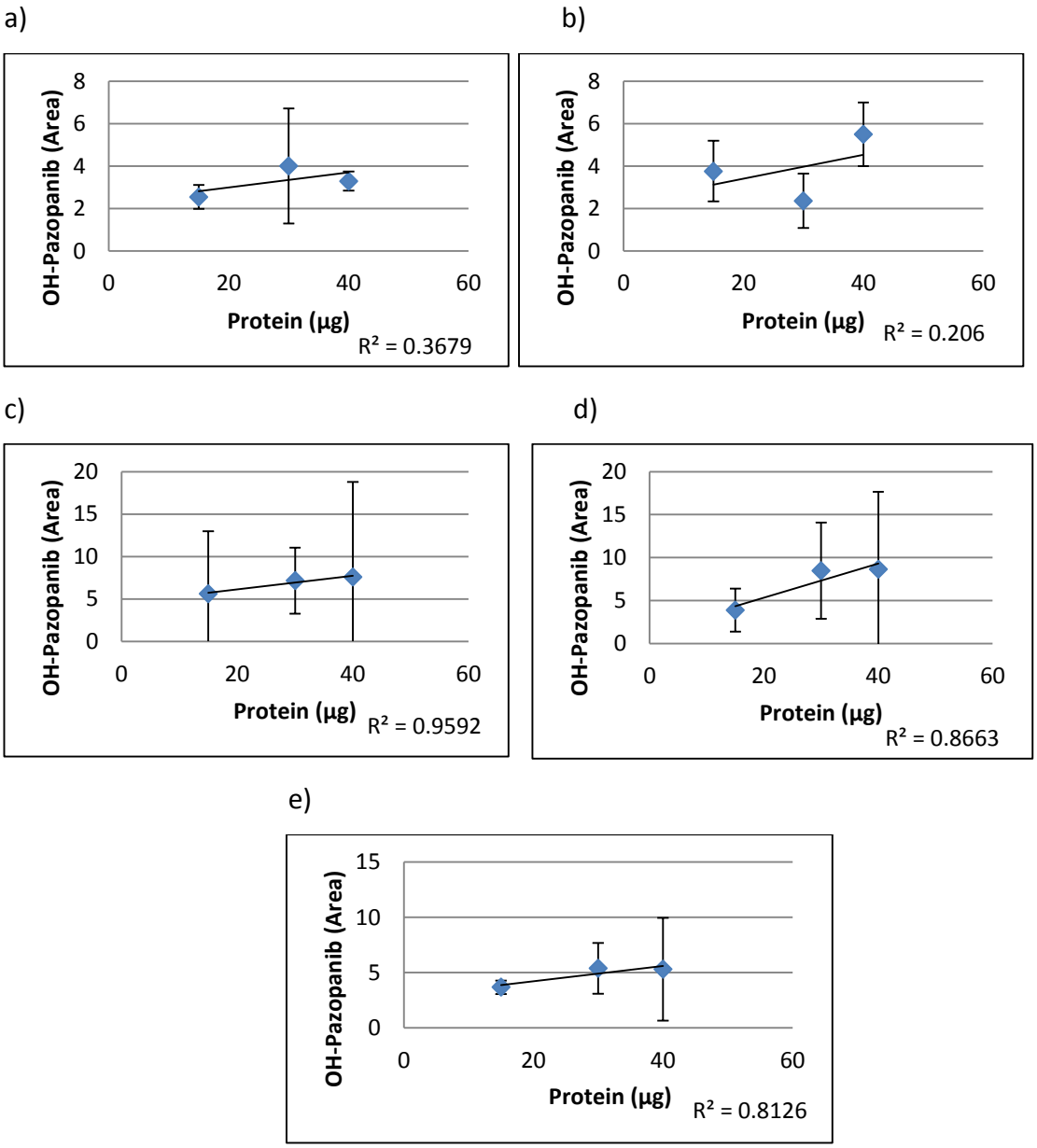

Figure 3.6 Correlation of OH-pazopanib with protein concentration at various time points

Graphs showing linear correlation between the formation of OH-pazopanib in pooled mouse liver microsome incubations at a) 5 min, b) 10 min, c) 20 min, d) 30 min, e) 40 min. R^2 values were calculated in Microsoft Excel as a representation of the linearity of the data points; n=3 incubations per time point. Values expressed ± SD.

a)

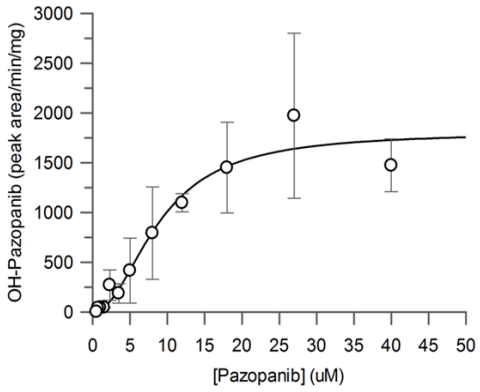

Parameter	Value	Std. Error
V max	1805.34	183.92
K m	8.91	1.50
Hill Coefficient	2.06	0.53

b)

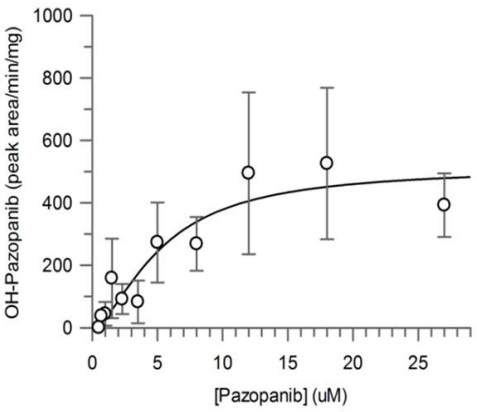

Parameter	Value	Std. Error
V max	512.86	129.56
K m	5.29	2.71
Hill Coefficient	1.63	0.66

Figure 3.7. Enzyme kinetics for pazopanib metabolism differs in human and mouse liver microsomes.

Various concentrations of pazopanib were incubated with a) commercially available pooled human liver microsomes (20 µg) or b) wild-type mouse liver microsomes (20 µg) for 20 min. Incubations were carried out in triplicate. Samples were extracted and analysed by MS-MS to measure peak area of OH-pazopanib metabolite. Data was analysed using GraFit 5. Values expressed ± SD.

From the V_{max} and K_m values, the intrinsic clearance (CL_{int}) of drug may be calculated as follows:

$$Intrinsic\ Clearance = \frac{Vmax}{Km}$$

(Kumar, Samuel et al. 2002)

From the V_{max} and K_m values show in **Figure 3.7** the intrinsic clearance based upon the equation above in human and mouse microsomes is 202.6 µmols/min/mg and 96.9 µmols/min/mg respectively.

3.2.5 Human Liver Microsome Panel Validation

A panel of 14 human liver microsomes from individual donors were purchased from BD Gentest (Woburn, MA) in order to carry out correlation studies between P450 enzyme activity, and pazopanib metabolism (see Appendix 1 for details of individual human microsome samples). The level of detection of OH-pazopanib metabolite was used as an indication of metabolic turn over. Initially, the panel of microsomes were validated using, midazolam, a known and established CYP3A4 substrate (Wandel, Bocker et al. 1994). Midazolam is metabolised almost exclusively by CYP3A4 (Kronbach, Mathys et al. 1989) and two major hydroxylated metabolites are produced; 1-OH midazolam, and 4-OH midazolam. The production of these metabolites was plotted against the activity of each of the cytochrome P450 enzymes in each liver sample. Microsomes (20 µg) were incubated with midazolam (50 µM) for 10 min (**Figure 3.8**), and correlations are listed in **Table 3.1.** In keeping with the literature, CYP3A4 showed the highest correlation with both 1-OH and 4-OH metabolite production (0.92, 0.97 respectively). Correlations were also seen with other cytochrome P450 enzymes including CYP2A6 (1-OH; 0.91, 4-OH; 0.92), CYP2C8 (1-OH; 0.83, 4-OH; 0.75) and CYP2B6 (1-OH; 0.65, 4-OH; 0.64), however, as these enzymes are not implicated in midazolam metabolism, this was considered to be a due to the activity of this particular panel of microsomes.

3.2.6 Pazopanib Metabolite Correlations in Human Liver Microsome Panel

Having validated the panel of human liver microsomes using midazolam as a test substrate, it was accepted that the panel would be useful in identifying enzymes implicated in the metabolism of pazopanib. Similarly to midazolam, pazopanib (14 µM) was incubated with individual liver microsome samples (20 µg) for 30 min. OH-pazopanib formation was plotted again cytochrome P450 activities in **Figure 3.9**. Strongest correlation was noted with CYP3A4 (0.98), as was expected. As was the case in the midazolam incubations, correlations were also seen with a number of other cytochrome P450s, including CYP2A6 (0.84), and considerably weaker correlations with CYP2B6 (0.37) and CYP2C8 (0.27). These correlations are common in the midazolam experimental set, as well as the pazopanib set. Correlations are summarised in **Table 3.2.**

a)

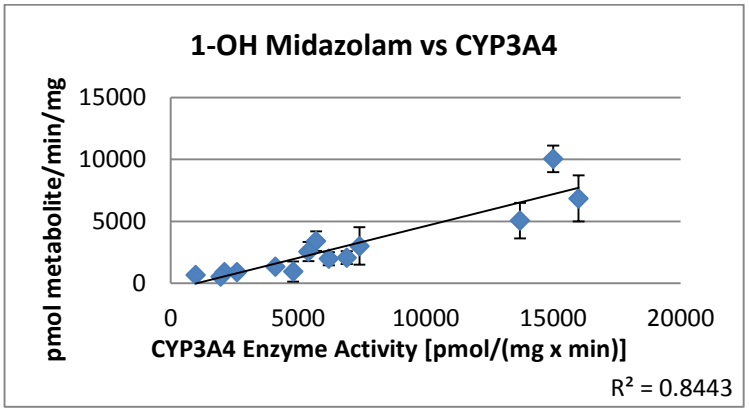
1-OH Midazolam vs CYP3A4
pmol metabolite/min/mg
15000
10000
5000
0
0
5000
10000
15000
20000
CYP3A4 Enzyme Activity [pmol/(mg x min)]
R² = 0.8443

b)

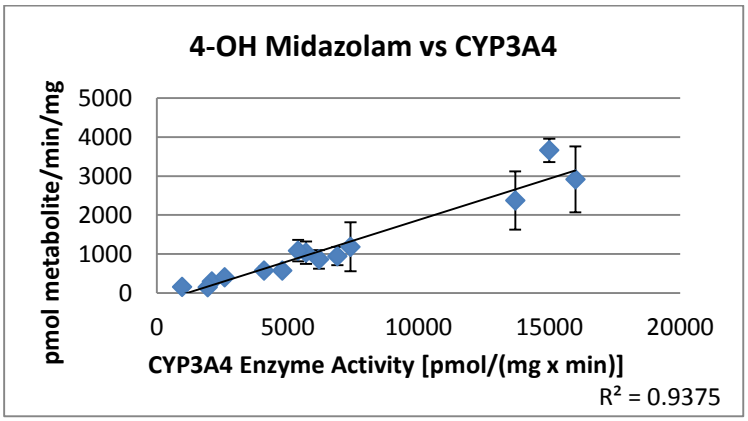
4-OH Midazolam vs CYP3A4
pmol metabolite/min/mg
5000
4000
3000
2000
1000
0
0
5000
10000
15000
20000
CYP3A4 Enzyme Activity [pmol/(mg x min)]
R² = 0.9375

c)

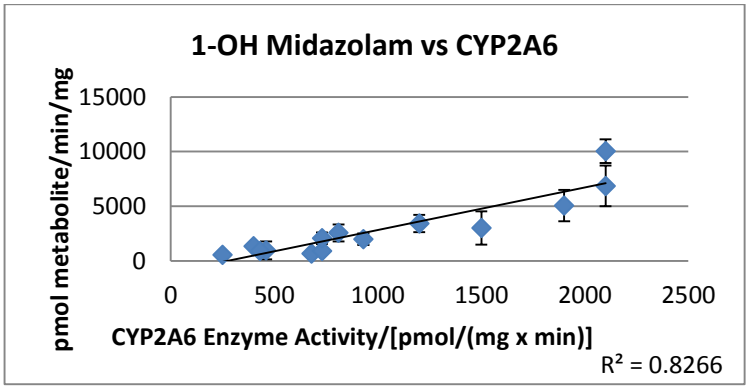
1-OH Midazolam vs CYP2A6
pmol metabolite/min/mg
15000
10000
5000
0
0
500
1000
1500
2000
2500
CYP2A6 Enzyme Activity/[pmol/(mg x min)]
R² = 0.8266

d)

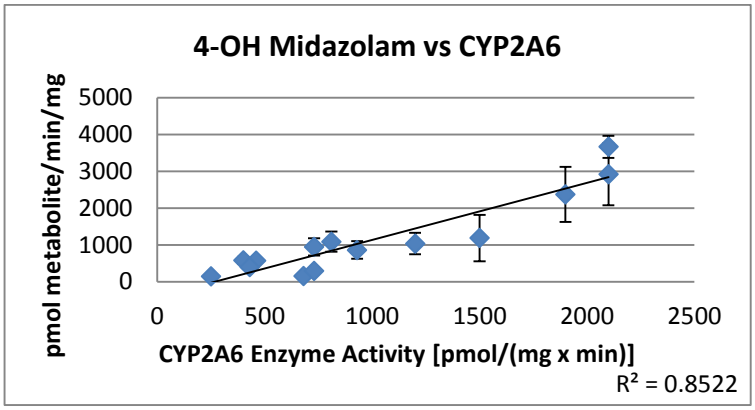
4-OH Midazolam vs CYP2A6
pmol metabolite/min/mg
5000
4000
3000
2000
1000
0
0
500
1000
1500
2000
2500
CYP2A6 Enzyme Activity [pmol/(mg x min)]
R² = 0.8522

e)

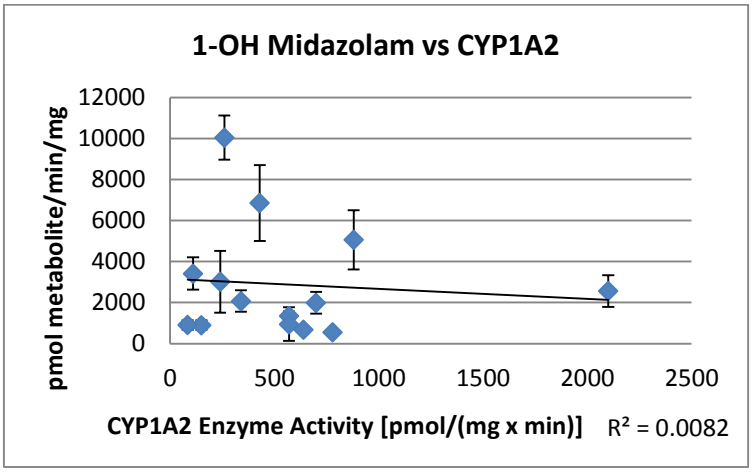
1-OH Midazolam vs CYP1A2
pmol metabolite/min/mg
12000
10000
8000
6000
4000
2000
0
0
500
1000
1500
2000
2500
CYP1A2 Enzyme Activity [pmol/(mg x min)]
R² = 0.0082

f)

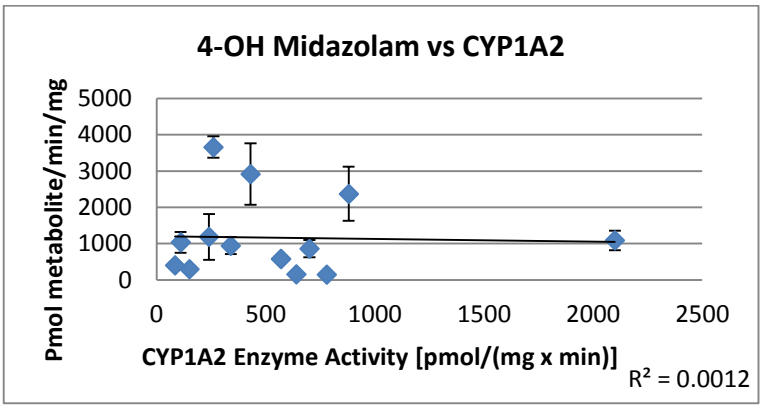
4-OH Midazolam vs CYP1A2
Pmol metabolite/min/mg
5000
4000
3000
2000
1000
0
0
500
1000
1500
2000
2500
CYP1A2 Enzyme Activity [pmol/(mg x min)]
R² = 0.0012

g)

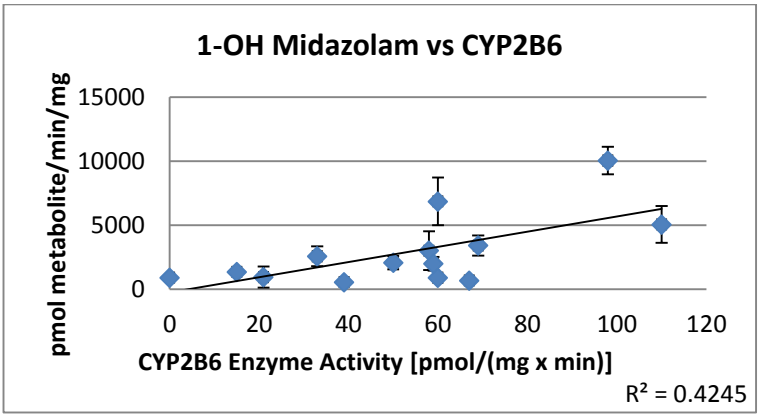
1-OH Midazolam vs CYP2B6
pmol metabolite/min/mg
15000
10000
5000
0
0
20
40
60
80
100
120
CYP2B6 Enzyme Activity [pmol/(mg x min)]
R² = 0.4245

h)

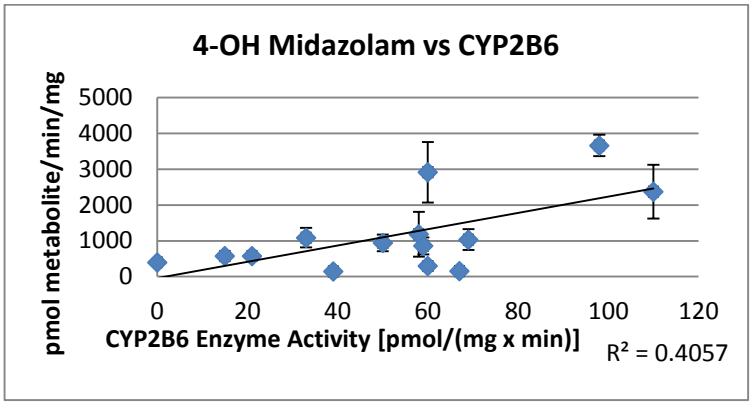
4-OH Midazolam vs CYP2B6
pmol metabolite/min/mg
5000
4000
3000
2000
1000
0
0
20
40
60
80
100
120
CYP2B6 Enzyme Activity [pmol/(mg x min)]
R² = 0.4057

i)

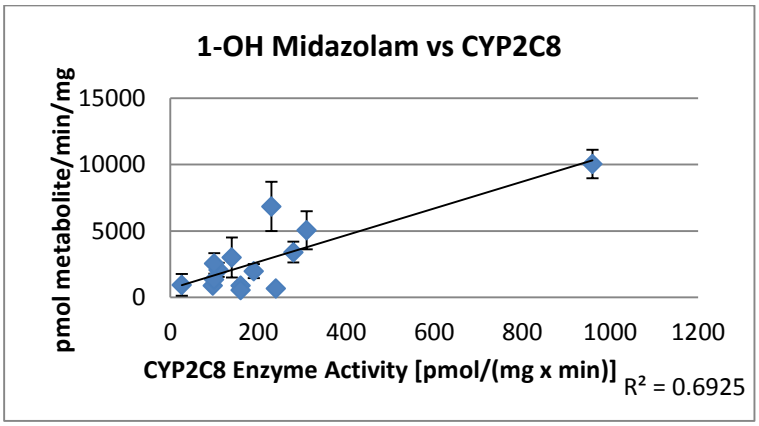
1-OH Midazolam vs CYP2C8
pmol metabolite/min/mg
15000
10000
5000
0
0
200
400
600
800
1000
1200
CYP2C8 Enzyme Activity [pmol/(mg x min)]
R² = 0.6925

k)

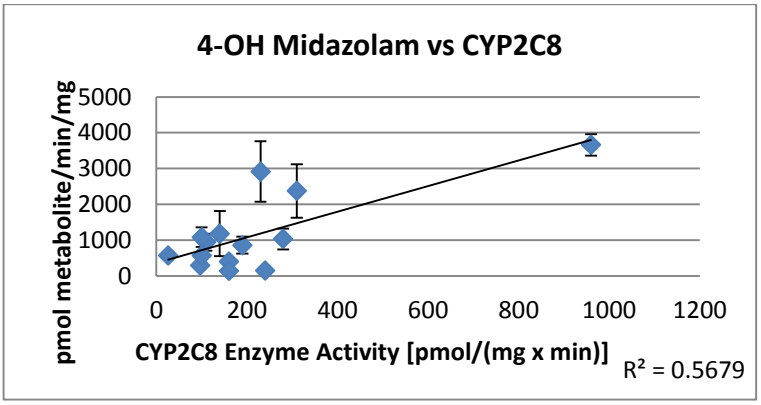
4-OH Midazolam vs CYP2C8
pmol metabolite/min/mg
5000
4000
3000
2000
1000
0
0
200
400
600
800
1000
1200
CYP2C8 Enzyme Activity [pmol/(mg x min)]
R² = 0.5679

k)

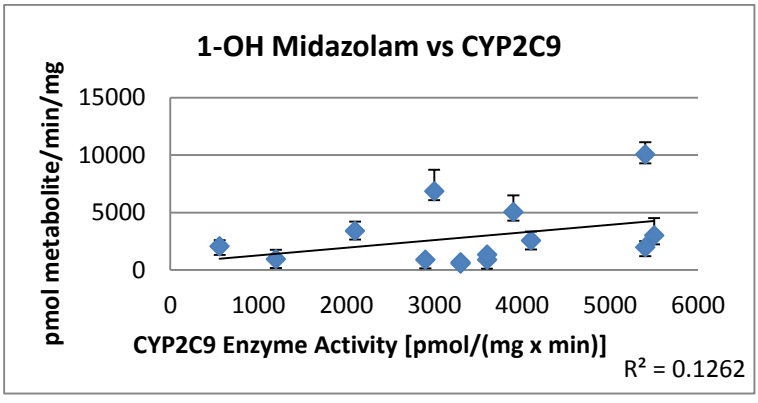
1-OH Midazolam vs CYP2C9
pmol metabolite/min/mg
15000
10000
5000
0
0
1000
2000
3000
4000
5000
6000
CYP2C9 Enzyme Activity [pmol/(mg x min)]
R² = 0.1262

l)

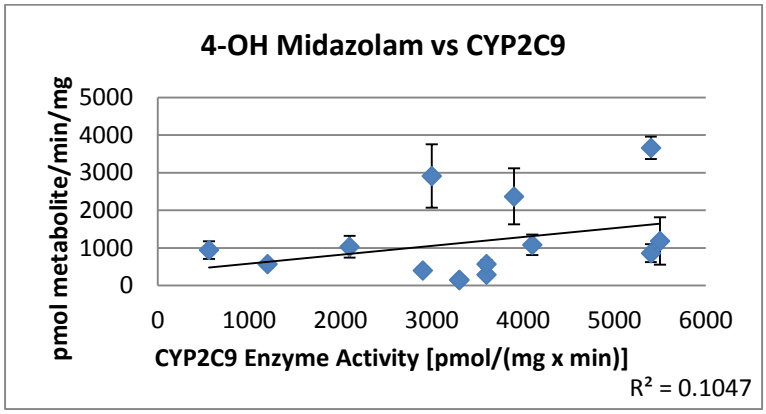
4-OH Midazolam vs CYP2C9
pmol metabolite/min/mg
5000
4000
3000
2000
1000
0
0
1000
2000
3000
4000
5000
6000
CYP2C9 Enzyme Activity [pmol/(mg x min)]
R² = 0.1047

m)

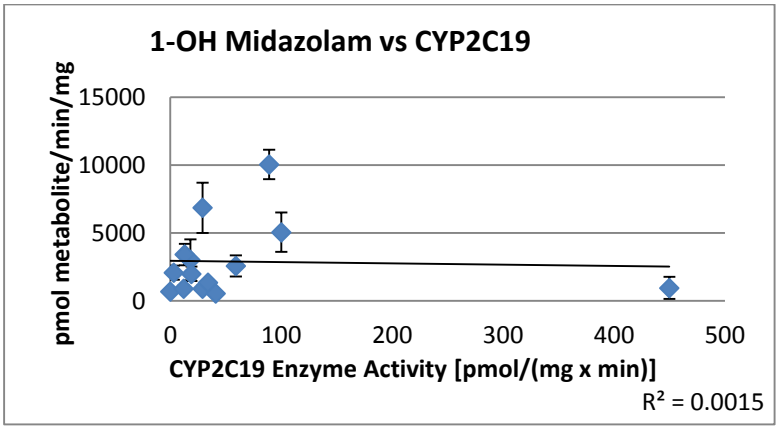
1-OH Midazolam vs CYP2C19
pmol metabolite/min/mg
15000
10000
5000
0
0
100
200
300
400
500
CYP2C19 Enzyme Activity [pmol/(mg x min)]
R² = 0.0015

n)

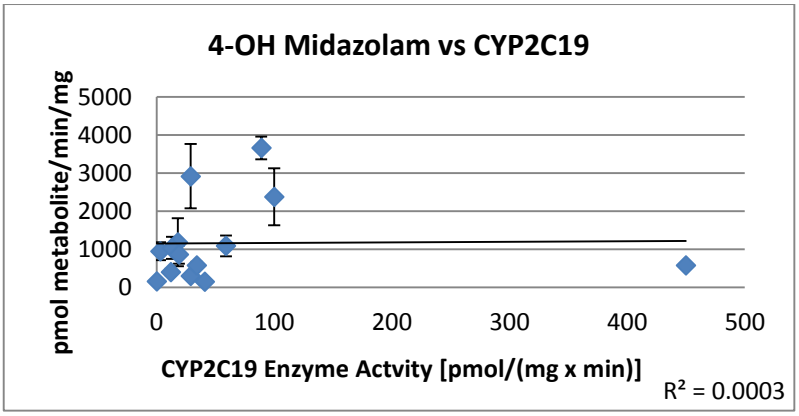
4-OH Midazolam vs CYP2C19
pmol metabolite/min/mg
5000
4000
3000
2000
1000
0
0
100
200
300
400
500
CYP2C19 Enzyme Actvity [pmol/(mg x min)]
R² = 0.0003

o)

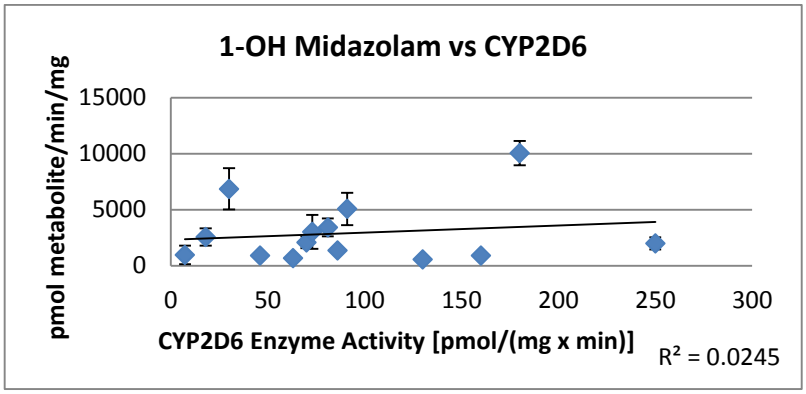
1-OH Midazolam vs CYP2D6
pmol metabolite/min/mg
15000
10000
5000
0
0
50
100
150
200
250
300
CYP2D6 Enzyme Activity [pmol/(mg x min)]
R² = 0.0245

p)

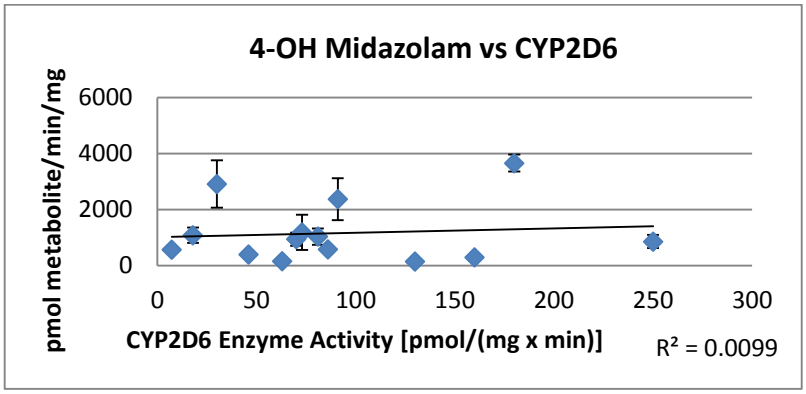
4-OH Midazolam vs CYP2D6
pmol metabolite/min/mg
6000
4000
2000
0
0
50
100
150
200
250
300
CYP2D6 Enzyme Activity [pmol/(mg x min)]
R² = 0.0099

q)

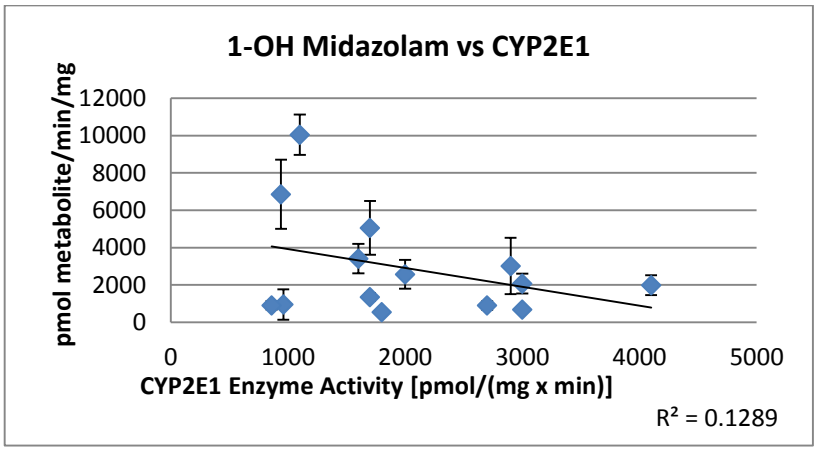
1-OH Midazolam vs CYP2E1
pmol metabolite/min/mg
12000
10000
8000
6000
4000
2000
0
0
1000
2000
3000
4000
5000
CYP2E1 Enzyme Activity [pmol/(mg x min)]
R² = 0.1289

r)

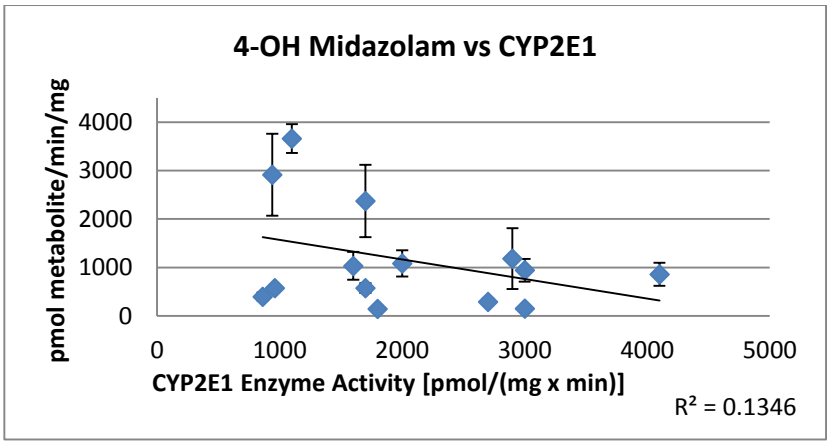
4-OH Midazolam vs CYP2E1
pmol metabolite/min/mg
4000
3000
2000
1000
0
0
1000
2000
3000
4000
5000
CYP2E1 Enzyme Activity [pmol/(mg x min)]
R² = 0.1346

s)

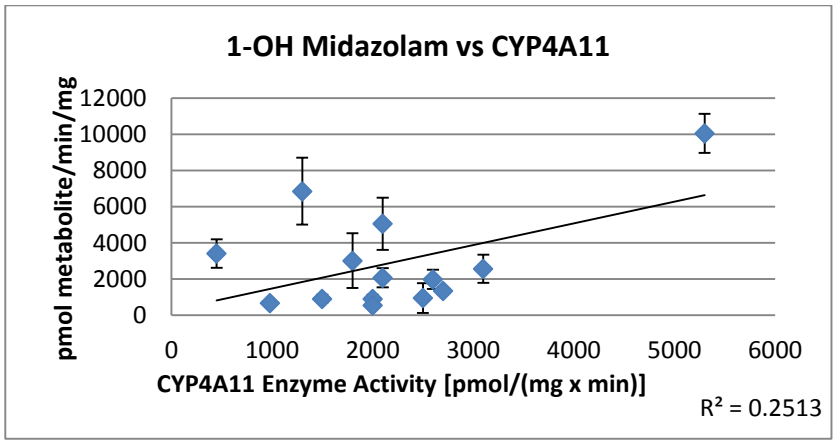

t)

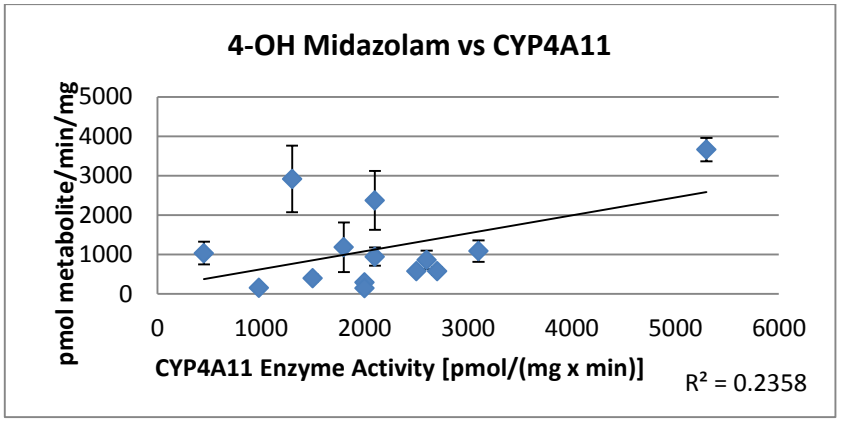

Figure 3.8. Correlation of 1-OH Midazolam and 4-OH Midazolam with P450 enzyme activity

Graphs showing linear correlation between the formation of 1-OH Midazolam and 4-OH Midazolam and CYP450 enzyme activity in a panel of human liver microsomes. Midazolam (50 µM) was incubated with individual human liver microsomes (20 µg), for 30 min in a total volume of 100 µl. Incubations were halted by the addition of acetonitrile (100 µl) and extracted. 1-OH midazolam and 4-OH-midazolam formation was measured by LC-MS/MS. R^2 values were calculated in Microsoft Excel as a representation of the linearity of the data points; n=3 incubations per liver sample. Values expressed ± SD.

Enzyme	1-OH Midaz R2	Correlation	4-OH Midaz R2	Correlation
CYP3A4	0.8443	0.9189	0.9375	0.9682
CYP2A6	0.8266	0.9092	0.8522	0.9231
CYP2C8	0.6925	0.8322	0.5679	0.7536
CYP2B6	0.4254	0.6515	0.4057	0.6369
CYP4A11	0.2513	0.5013	0.2358	0.4856
CYP2C9	0.1262	0.3553	0.1047	0.3235
CYP2E1	0.1289	-0.3590	0.1346	-0.3669
CYP2D6	0.0245	0.1567	0.0099	0.0993
CYP1A2	0.0082	-0.0907	0.0012	-0.0347
CYP2C19	0.0015	-0.0381	0.0003	0.0160

Table 3.1. Table of R^2 values and correlation between 1-OH midazolam and 4-OH midazolam formation in relation to P450 activity.

Enzyme contribution to metabolite formation ranked in descending order. R^2 values and correlation were calculated in Microsoft Excel; n=3 incubations per liver sample.

3.2.7 Pazopanib Metabolism in a Panel of Human Recombinant P450s

To verify that unexpected correlations between enzyme activity and pazopanib metabolism were a function of the microsome panel, and not necessarily applicable *in vivo*, pazopanib was incubated with a panel of recombinant human cytochrome P450s. Recombinant human P450s were generated in *E.coli* as described in the Methods. Pazopanib (14 µM), was incubated with 100 pM of each recombinant enzyme, in triplicate. The results displayed in **Figure 3.9.1.** show that CYP3A4 is predominantly responsible for the metabolism of pazopanib with non-significant contributions from CYP1A1, CYP1A2 and CYP2C8. This is generally in keeping with the literature, which states that pazopanib is predominantly metabolised by CYP3A4, with minor contributions from CYP1A2 and CYP2C8. The predominant murine Cyp3a isoform, Cyp3a11, appears to metabolise pazopanib with a similar capacity to the lesser contributing human enzymes.

a)

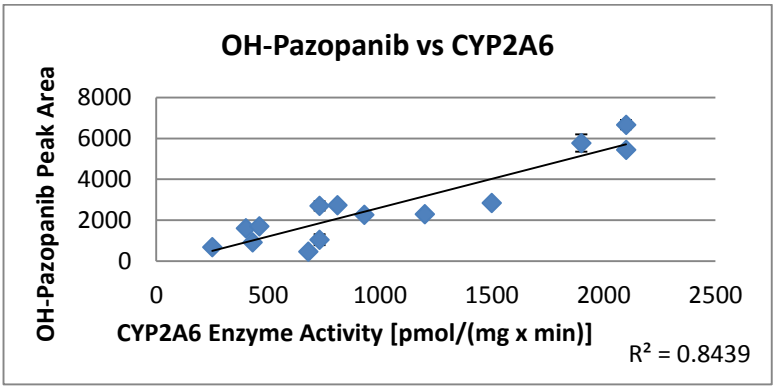
OH-Pazopanib vs CYP2A6
OH-Pazopanib Peak Area
8000
6000
4000
2000
0
0
500
1000
1500
2000
2500
CYP2A6 Enzyme Activity [pmol/(mg x min)]
R² = 0.8439

b)

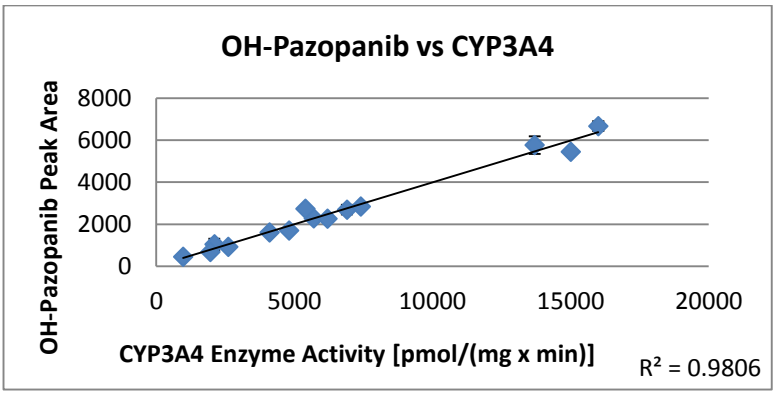
OH-Pazopanib vs CYP3A4
OH-Pazopanib Peak Area
8000
6000
4000
2000
0
0
5000
10000
15000
20000
CYP3A4 Enzyme Activity [pmol/(mg x min)]
R² = 0.9806

c)

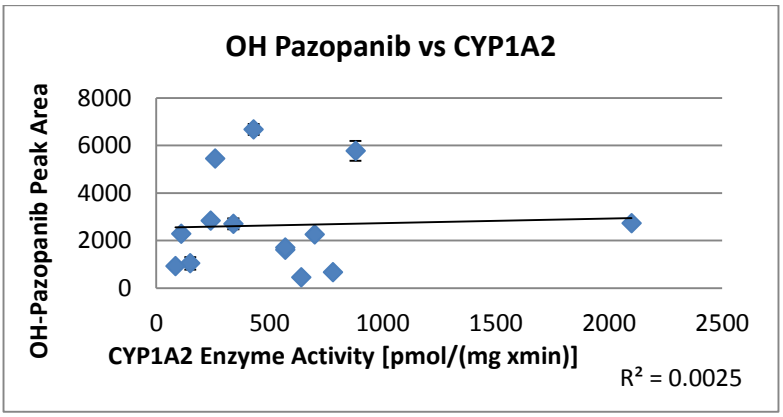
OH Pazopanib vs CYP1A2
OH-Pazopanib Peak Area
8000
6000
4000
2000
0
0
500
1000
1500
2000
2500
CYP1A2 Enzyme Activity [pmol/(mg xmin)]
R² = 0.0025

d)

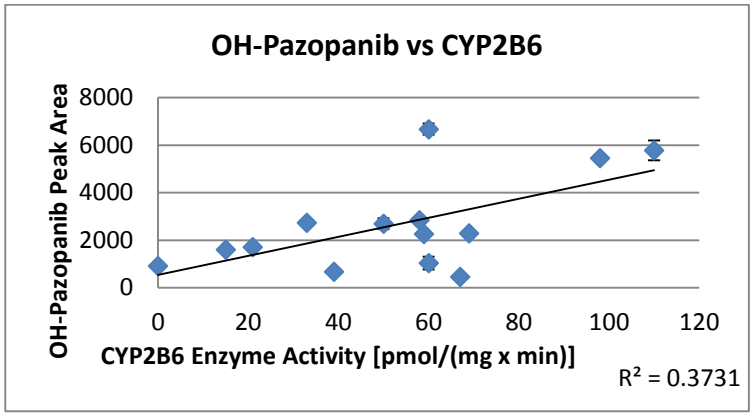
OH-Pazopanib vs CYP2B6
OH-Pazopanib Peak Area
8000
6000
4000
2000
0
0
20
40
60
80
100
120
CYP2B6 Enzyme Activity [pmol/(mg x min)]
R² = 0.3731

e)

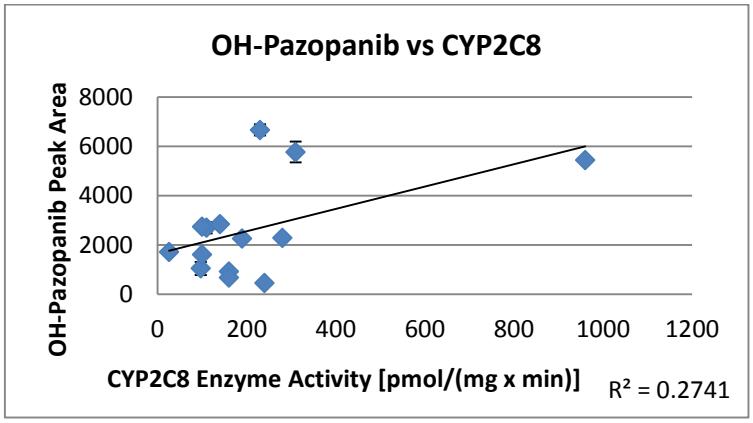
OH-Pazopanib vs CYP2C8
OH-Pazopanib Peak Area
8000
6000
4000
2000
0
0
200
400
600
800
1000
1200
CYP2C8 Enzyme Activity [pmol/(mg x min)]
R² = 0.2741

f)

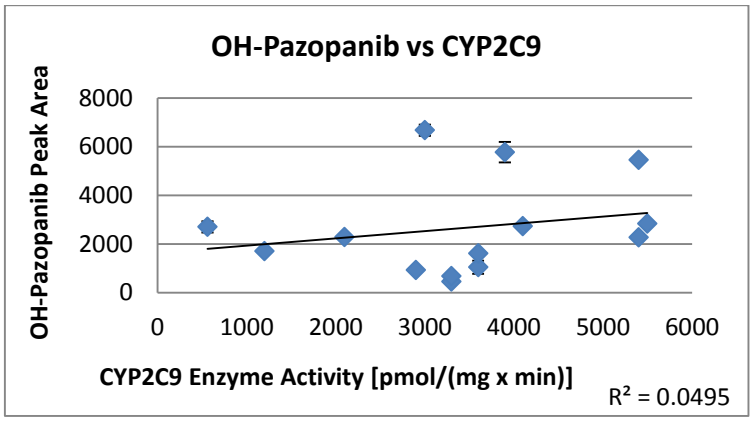
OH-Pazopanib vs CYP2C9
OH-Pazopanib Peak Area
8000
6000
4000
2000
0
0
1000
2000
3000
4000
5000
6000
CYP2C9 Enzyme Activity [pmol/(mg x min)]
R² = 0.0495

g)

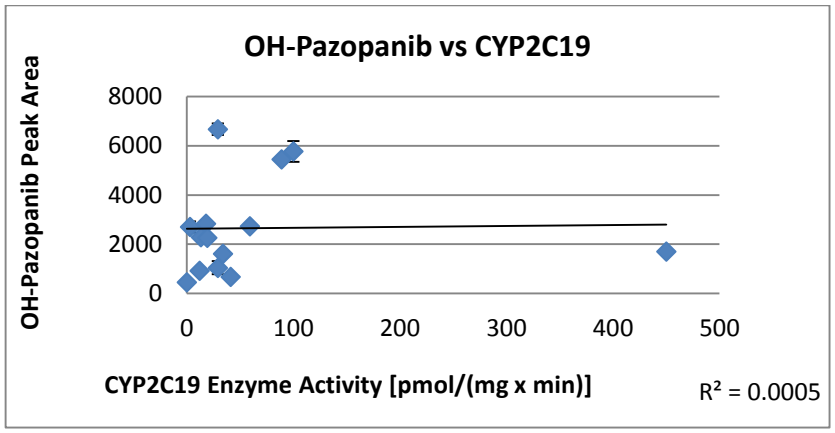
OH-Pazopanib vs CYP2C19
OH-Pazopanib Peak Area
8000
6000
4000
2000
0
0
100
200
300
400
500
CYP2C19 Enzyme Activity [pmol/(mg x min)]
R² = 0.0005

h)

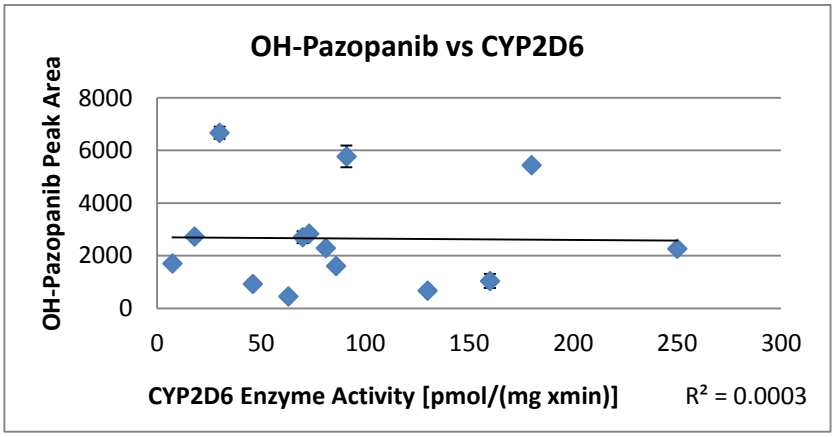
OH-Pazopanib vs CYP2D6
OH-Pazopanib Peak Area
8000
6000
4000
2000
0
0
50
100
150
200
250
300
CYP2D6 Enzyme Activity [pmol/(mg xmin)]
R² = 0.0003

i)

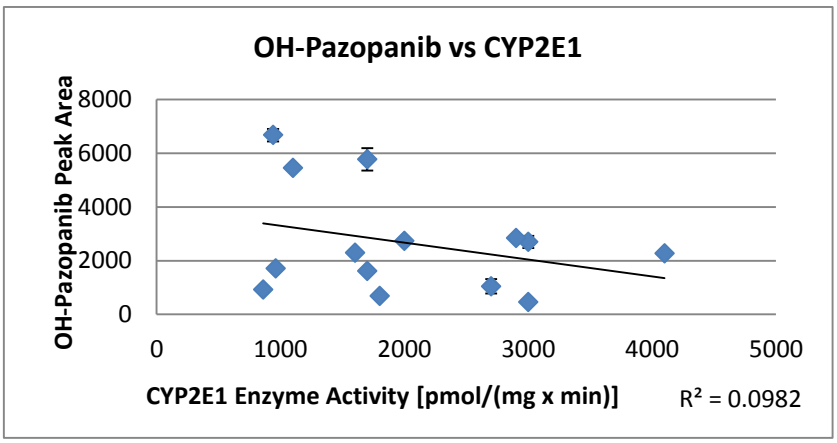
OH-Pazopanib vs CYP2E1
OH-Pazopanib Peak Area
8000
6000
4000
2000
0
0
1000
2000
3000
4000
5000
CYP2E1 Enzyme Activity [pmol/(mg x min)]
R² = 0.0982

j)

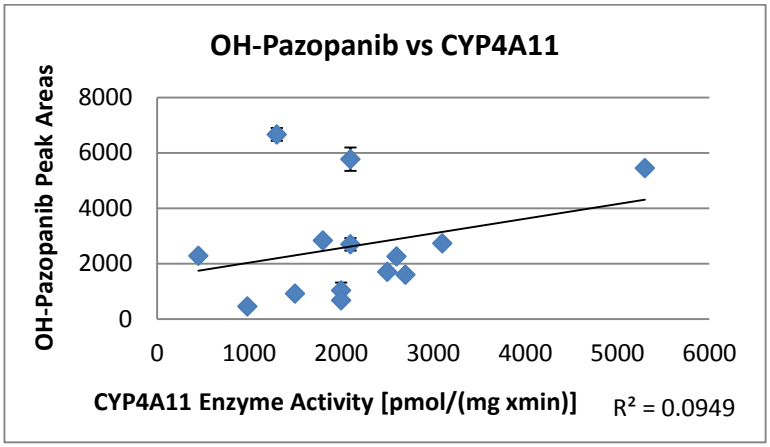

Figure 3.9. Graphs showing linear correlation between the formation of OH-Pazopanib and enzyme activity in a panel of human liver microsomes

Pazopanib (14 µM) was incubated with individual human liver microsomes (20 µg), for 20 min in a total volume of 100 µl. Incubations were halted by the addition of methanol (100 µl) and extracted. OH-Pazopanib formation was measured by LC-MS/MS. R^2 values were calculated in Microsoft Excel as a representation of the linearity of the data points; n=3 incubations per liver sample. Values expressed ± SD.

Enzyme	OH-Paz R2	Correlation
CYP 3A4	0.9806	0.9903
CYP 2A6	0.8439	0.9186
CYP 2B6	0.3731	0.6108
CYP 2C8	0.2741	0.5235
CYP 2E1	0.0982	-0.3134
CYP 4A11	0.0949	0.3081
CYP 2C9	0.0495	0.2225
CYP 1A2	0.0025	0.0502
CYP 2C19	0.0005	0.0218
CYP 2D6	0.0003	-0.0169

Table 3.2. Table showing the R^2 figures and corresponding correlation of metabolite formation versus P450 in human liver microsomes.

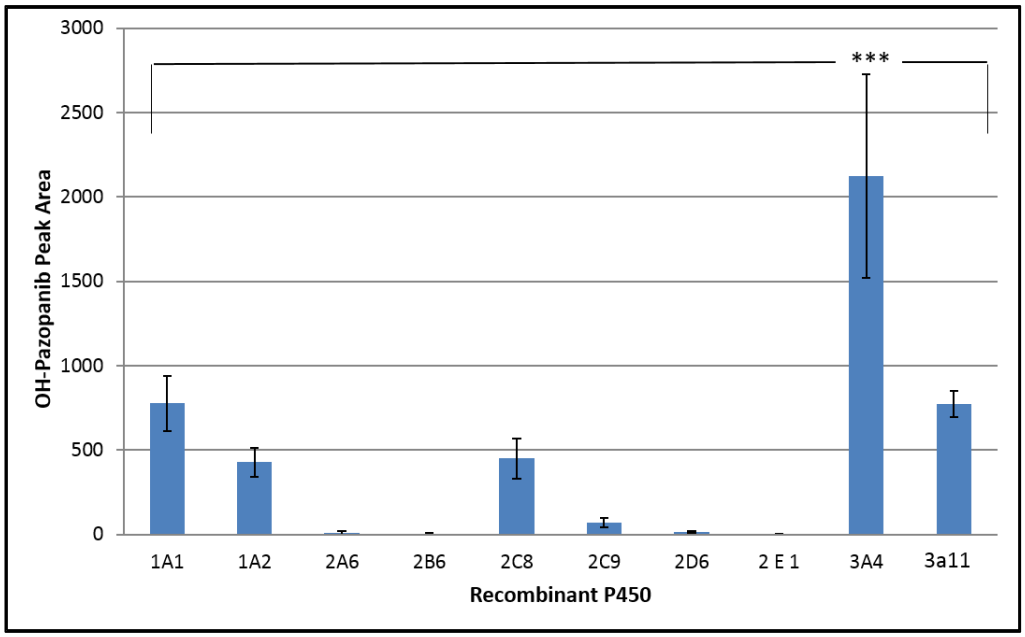

Figure 3.9.1. OH-Pazopanib formation in a panel of recombinant P450s

Human CYP3A4 is the predominant enzyme responsible for the metabolism of pazopanib. Pazopanib (14 µM) was incubated in triplicate with a panel of human recombinant CYPs (100 pM), and the predominant murine Cyp3a isoform; Cyp3a11. OH-pazopanib formation was measured by LC-MS/MS. *** *P*>0.001. Values expressed ± SD.

3.2.8. *In Vitro* Metabolism of Pazopanib in Transgenic Mouse Microsomes

Transgenic mice expressing human CYP3A4 are better models for modelling drug metabolism of CYP3A4 substrates *in vivo*, compared with wild-type mice. In order to validate the use of humanised CYP 3A4/3A7 mice for *in vivo* studies, microsomal stability experiments were carried out using microsomes derived from wild-type, un-induced hCYP3A4/3A7, induced hCYP3A4/3A7 mice, and commercially available human liver microsomes, purchased as a pool, from Invitrogen. Induced mice were treated with pregnenolone-α-carbonitrile (PCN) dissolved in corn oil for three days, at a dose of 10 mg/kg by oral gavage, while un-induced animals received corn oil prior

to being sacrificed on day 4. Livers were harvested and snap-frozen and stocks of microsomes were prepared as described in **Section 2.4.2**. **Figure 3.9.2** shows the level of expression of CYP3A/Cyp3a in these liver microsomes. The expression of CYP3A in human liver and induced hCYP3A4/3A7 mouse liver microsomes are comparable with one another, whereas the band in the wild-type mice is likely to be Cyp3a11, the most abundant mouse Cyp3a isoform in the liver. As expected, the un-induced animals express no CYP3A as the use of an inducing agent is required to drive expression of the transgene, and these animals lack endogenous Cyp3a11 as a result of the genetic manipulations, which involves the excision of the major murine Cyp3a cluster in the genome. This shows that induced hCYP3A4/7 mice express the human P450 protein at a level which approximates that found in human liver.

Pazopanib (14 µM) was incubated with protein (20 µg) and 10 µl of 10 µM NADPH at 37°C for 30 min and OH-pazopanib was measured using LC-MS/MS (**Figure 3.9.2 b**). OH-Pazopanib formation in wild-type and un-induced hCYP3A4/3A7 mouse liver microsomes does not differ; however, when hCYP3A4/3A7 mice are induced with PCN, the formation of OH-pazopanib is significantly increased compared to the un-induced hCYP3A4/3A7, and wild-type mice, to levels which are comparable to the human microsomes (P <0.001). These data show that the capacity of the hCYP3A4/3A7 mouse microsomes to metabolise pazopanib, can be elevated to levels comparable with human microsomes when animals are pre-treated with an inducing agent.

a)

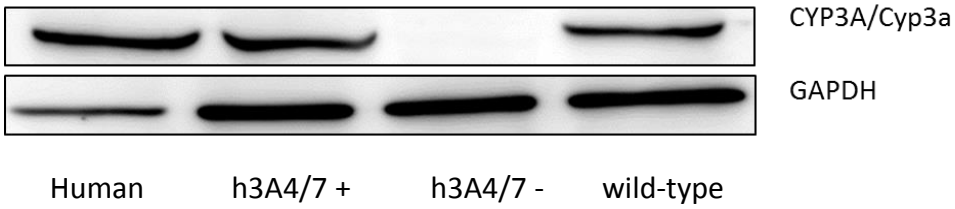

b)

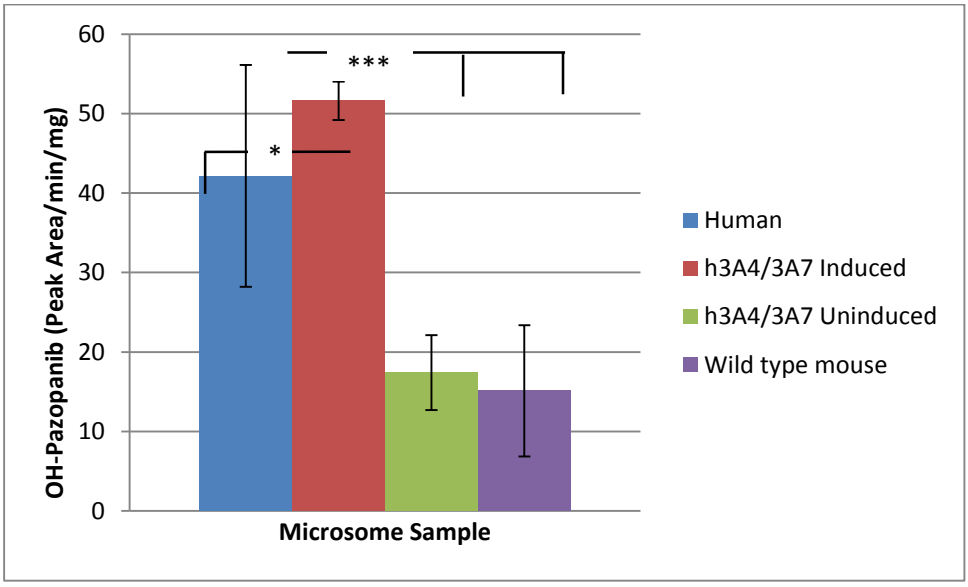

Figure 3.9.2. OH-pazopanib formation in humanised mouse, and human liver microsomes.

Metabolic capacity of induced humanised CYP3A4/3A7 mouse microsomes is more similar to metabolism in human liver microsomes than wild-type mouse. a) Western blots showing Cyp3a/CYP3A levels in liver microsomes of human, induced humanised CYP3A4/3A7 mice, un-induced humanised CYP3A4/3A7 mice, and wild-type mice. CH32 antibody can detect both human and mouse CYP3a/Cyp3a respectively b) OH-pazopanib formation in microsome incubations with pazopanib (14 µM) using human, induced humanised CYP3A4/3A7 mice, un-induced humanised 3A4/3A7 mice, and wild-type mouse microsomes (20 µg) for 30 min. All mouse microsomes are pools of 3 animals, pooled human microsomes were from Invitrogen. Incubations were extracted in triplicate. Values expressed ± SD.

3.3 Discussion

3.3.1 Summary

This chapter describes a species difference in the microsomal stability of pazopanib in human and mouse liver microsomes. The higher rate of metabolism seen in human microsomes compared to the mouse may have significant implications on the relevance of pre-clinical trials in animals, for extrapolation to the human situation. Furthermore, transgenic mice expressing human CYP3A4/3A7 better mimic human microsome metabolism of pazopanib *in vitro,* compared to wild-type mice.

3.3.2 Microsomal Stability of Pazopanib in Mouse and Human Microsomes.

Little difference was noted between total disappearance of pazopanib in mouse and human microsomes, which may be attributable to the sensitivity of the LC-MS/MS assay, or constraints of the experimental set-up, such as the availability of NADPH, oxygen, duration of incubation and so forth. However, varying these parameters had a negligible effect on the outcome of these incubations. An alternative method of assessing drug metabolism *in vitro,* is the measurement of metabolite formation. Metabolite analysis is an important consideration when an animal model is being tested for later extrapolation to humans. It is rare that a metabolite would be formed in humans but not test animals, however the metabolite may be present at significantly higher levels in humans compared to animal models. Furthermore, the rate at which it is produced may be much more rapid. This is of particular importance as often drugs may form toxic intermediate compounds and metabolites. Possibly one of the most well described examples of drug metabolism resulting in a toxic

product is *N*-acetyl-*p*-benzoquinoneimine (NAPQI), formed by CYP-mediated metabolism of acetaminophen in the liver (Bender, Lindsey et al. 2004). Given that pazopanib is known to cause hepatotoxicity in a small number of patients, but not mice, it was of interest to compare the production of OH-pazopanib formation in mouse and human microsomes.

3.3.3 Michaelis-Menten Enzyme Kinetics in Mouse and Human Microsomes

The traditional method for determining V_{max} and K_m for a metabolic reaction is the initial formation rate of metabolite method (IFRMM), where the Michaelis-Menten equation is fitted to the initial rates of formation of metabolite under linear conditions of substrate concentration, protein and time. This method is suitable when the metabolite of the parent compound has been identified and is measurable. Being based upon initial formation rates allows for relatively short incubation lengths compared to other methods of kinetic modelling (Sjogren, Lennernas et al. 2009). IFRMM is not generally appropriate for high throughput screens of new compounds however, as many compounds will undergo extensive metabolism to several metabolites, which are often unknown. An alternative approach often utilised in drug discovery and development is the substrate depletion method, which is based on the disappearance of the parent compound in question without requiring the metabolite(s) to be characterised. Linearity optimisation experiments are not usually carried out when performing substrate depletion methodologies and arbitrary values are used for time and protein are used (Jones and Houston 2004). Linearity is necessary for scaling intrinsic clearance from microsomal incubations to the whole liver, making substrate depletion an inappropriate method for such extrapolation.

Additionally, the substrate depletion method tends to require approximately 20 % substrate disappearance in order to distinguish any depletion from baseline variability. This creates the requirement for longer incubation times and high protein content which in turn may create limitations in this approach, including oxygen availability and end product inhibition. Owing to the almost negligible depletion observed in early disappearance studies, IFRMM was employed to construct kinetic curves for both mouse and human liver microsomes, from incubations carried out under the same optimal, linear conditions. The minimal disappearance of pazopanib in early experiments may be due to the limits of detection of the analysis, as well as the limitations of the assay itself. It would appear from the IFRMM method and resultant kinetic curves, that while the K_m for both the mouse and human liver microsomes are very similar, the V_{max} is substantially greater in the human liver microsomes, and consequently, the intrinsic clearance is considerably greater than in the mouse liver microsomes.

3.3.4 Human Recombinant Enzymes

This chapter makes use of a panel of human recombinant enzymes to compare the relative capacity of human enzymes to metabolise pazopanib. Human recombinant enzymes are used routinely in high throughput assays during the development of new chemical entities (NCEs), to predict clearance, and the potential for drug-drug interactions. This method offers the advantage of allowing enzymes to be studied individually (Baranczewski, Stanczak et al. 2006).

Pazopanib is described in FDA reports as being metabolised primarily by CYP3A4, with minor contributions from CYP1A1 and CYP2C8. Pazopanib is thought to be broken down into three main metabolites. These metabolites are not well described in the

literature however; one is reported to inhibit the proliferation of VEGF-stimulated umbilical vein endothelial cells with potency similar to pazopanib. The remaining metabolites are reported to be 10- to 20- fold less active (European Medicines Agency). Data described in this chapter confirm that pazopanib is a good substrate for human CYP3A4, and while mouse microsomes are capable of metabolising pazopanib, the major Cyp3a isoform in the mouse, Cyp3a11, does not contribute significantly.

3.3.5 Humanised Mouse Microsomes

One aim of this research is to investigate the utility of humanised mice as models to address the disparity between mouse models and human data. Having established a species difference in microsomal metabolism of pazopanib *in vitro,* between mouse and human liver microsome preparations, it was of interest to assess whether or not liver microsomes from humanised CYP3A4/3A7 mice better reflected the metabolism of pazopanib by human liver microsomes compared to the wild-type microsomes. This was addressed using liver microsomes pooled from humanised CYP3A4/3A7 mice, with and without induction, alongside human and wild-type mouse liver microsomes. These data show that following induction, the expression of CYP3A4 in the transgenic mouse microsomes is on par with that seen in the human liver microsome pool. The band in the wild-type lane is likely to be representative of Cyp3a11, the predominant murine Cyp3a isoform. Interestingly, despite Cyp3a11 being expressed at a level approximating the level of CYP3A4 in the human liver microsomes and the humanised mouse microsomes, metabolite formation in these incubations does not differ significantly from the un-induced humanised mouse liver

microsomes, which lack any CYP3A. These data show, that in *in vitro* microsome stability assays, murine Cyp3a does not contribute to the metabolism of pazopanib, whereas human CYP3A4 does.

Chapter 4

In Vivo Pharmacokinetic and Toxicological Studies

4.1 Introduction

Understanding the behavior of clinically used drugs in terms of their absorption, distribution, metabolism and excretion (ADME), is of paramount importance to pharmacological research and development. Understanding the pharmacokinetic and pharmacodynamic properties of a drug forms the basis of safety testing, efficacy predictions and importantly, the extrapolation of animal studies to the human situation. Each of the four components of ADME affects the overall pharmacology of a drug and must be considered individually in order to obtain a comprehensive understanding of the mechanism by which the drug works, and to allow for optimum dosing strategies (Caldwell, Gardner et al. 1995).

4.2 Absorption

The absorption of a drug is the process by which the drug enters the body's systemic circulation. The rapidity at which this occurs depends largely on the route of administration of the drug, for example, a drug which is administered by intravenous injection is incorporated into the circulation immediately, and with 100% bioavailability, whereas a drug which is administered orally must pass through the stomach in order to reach the gastrointestinal tract and liver, often resulting in a lower dose of the drug reaching its site of action. While the gastrointestinal tract is the main site of drug absorption, absorption through the skin and via the lung may also occur. Regardless of the site of absorption, all drugs must pass across cell membranes to reach the systemic circulation. The way in which this occurs depends on the chemical properties of the drug. For example, small lipophilic compounds may cross cell membranes by passive diffusion, such is the case for drugs such as

nifedipine and amitriptyline which have low solubility in water, but readily diffuse across the gastrointestinal (GI) tract. Upon absorption from the GI tract, drugs may be subjected to metabolism in the gut wall itself, before being transported to the liver via the hepatic portal vein. The liver is the main site for detoxification and metabolism in the body, and all nutrients, toxins, and drugs absorbed by the intestine are transported to the liver to undergo metabolism and detoxification prior to entering the systemic circulation. This is known as “first-pass elimination”. The extent to which a drug is subjected to first-pass elimination is a major determinant of how much of the given dose of drug will enter the circulation and reach its target, and consequently, the amount of active drug remaining in the body may be considerably lower than the initial dose (Pond and Tozer 1984). Many drugs are either weak acids, or bases, and therefore are present in solution in both an ionized and non-ionized form. Non-ionized molecules are lipid soluble, and will readily diffuse through the intestinal wall. Ionized molecules however are poorly lipid soluble and will be retained in the lumen of the intestine.

$$AH \longleftrightarrow A + H^{+}$$

Non-ionized Ionized

The equilibrium of non-ionized and ionized forms of a drug is dependent on the intrinsic ionization constant (pK_a) of the drug, and on the pH gradient across the membrane (Ellis and Blake 1993). The relationship between pK_a, pH, and ionization can be described by the Henderson-Hasselbach equations for acids and bases:

$$pH = pKa + \log\frac{[R]}{[RH]}\ (acid)$$

$$pH = pKa + \log\frac{[B]}{[BH]}\ (base)$$

(Craig 2004)

4.3 Distribution

Understanding the distribution of a drug is an important factor when estimating the efficacy of a given dose. If a drug is to be efficacious, it must be able to reach its site of action, or, target tissue in the body. Upon entry into the systemic circulation, the distribution of a drug throughout the body is dependent on a number of factors, including tissue haemodynamics, lipophilicity, plasma protein binding, diffusion into lipid membranes and the function of active drug transporters. Drug distribution describes the relationship between measurable systemic concentrations of drug, and the amount of drug in the body. It is an indication of the extent of drug distribution and is therefore a theoretical parameter, rather than a physiological volume (Grover and Benet 2009).

When considering drug distribution, it is important to take into account the potential for a given drug to diffuse out of the plasma and into surrounding tissues, creating a "drug reservoir". Drug reservoirs have the potential to prolong the duration of action of a drug. If the drug reservoir is in equilibrium with the plasma concentration of the drug, the stored drug may be released from its storage tissue to maintain this equilibrium as the plasma concentration falls, thus maintaining the initial plasma concentration for longer. This is well described with regards to the anaesthetic agent

thiopental. Thiopental is a highly lipophilic anaesthetic, given prior to surgery via an intravenous bolus injection. Due to the high blood flow to the brain, thiopental has a very short onset of action, leading to rapid induction of anaesthesia. However, thiopental binds poorly to brain lipids and as the plasma concentrations falls as thiopental diffuses into tissues, the concentration in the brain falls in order to maintain concentration equilibrium with the plasma. This leads to loss of anaesthesia by redistribution rather than by metabolism. If thiopental is administered repeatedly, it will diffuse into poorly perfused tissues such as adipose tissue, creating a reservoir. If this occurs, the action of thiopental may be greatly prolonged as the drug is released slowly from the adipose stores upon termination of administration, and the recovery period is significantly prolonged (Hemmings and Hopkins 2006).

4.4 Metabolism

The majority of drugs which enter the body will undergo some form of metabolism prior to excretion. The routes by which metabolism may occur are vast and varied and are influenced by innumerable external and endogenous factors making the term “drug metabolism”, one of the most complex aspects of ADME to define. The primary site of xenobiotic metabolism is the liver however, extra-hepatic tissues, often the site of absorption or secretion of a drug (e.g. lungs, kidneys and intestine) are also involved in drug metabolism. Typically, xenobiotic metabolism is a biphasic process, whereby a drug undergoes a primary metabolic process which in turn creates a substrate for secondary metabolism, as discussed previously in Chapter 1.

While metabolism may be an integral step in the ultimate excretion of a drug, it may also serve as an activation step in the conversion of an inactive “pro-drug”, to a

pharmacologically active metabolite. This is true for the oestrogen receptor antagonist, tamoxifen, which is used in the treatment of oestrogen-positive breast cancer. Tamoxifen undergoes extensive oxidative metabolism by the cytochrome P450 enzymes, resulting in the formation of several pharmacologically active metabolites, some of which have been found to exert a greater anti-oestrogen effect than the parent compound. The plasma concentrations of tamoxifen and its metabolites vary considerably among patients. This is considered to be a result of variations in P450 activity which lead to altered rates of metabolism, and ultimately altered systemic exposure to tamoxifen and its metabolites (Desta, Ward et al. 2004). Variation in metabolic capacity and routes may have significant effects on the efficacy of a drug.

4.4.1 Species Differences in Metabolism

Variation in drug metabolism by both Phase 1 and Phase 2 enzymes between species has been recognized for many years and has become an area of increasing interest with the advent of simpler assay systems, such as isolated liver cells and hepatocytes, which allow for closer interrogation of drug metabolism mechanisms. Variation in drug metabolism between species may be described as quantitative, wherein the same metabolic pathways are active as in the human but at a different rate, or, qualitative, wherein different metabolic routes than the human are instigated (Gibson).

Species differences in metabolism may be attributable to variations in transcription factors. For example, species differences in CAR and PXR activators are well recognized, and they are attributable to structural variances in the ligand binding

domains of these receptors in different species. These are important considerations when extrapolating data obtained from rodent safety studies to human trials (Graham and Lake 2008). One example of such species variation is seen in the metabolism of the tranquilizer, diazepam. Diazepam metabolism in humans and in canines is primarily by N-demethylation and C-3 hydroxylation, however in rats, C-3 and 5-phenyl hydroxylation are the main pathways (Hucker 1970). It is also known that the anticonvulsant activity of diazepam is more persistent in mice than in rats. In the brain, diazepam levels are similar in both species, however the concentrations of N-demethyl diazepam and oxazepam appear to accumulate in mouse brain, and not in the rat. This metabolite accumulation is considered to be responsible for the prolonged effect of diazepam in mice compared to rats (Marcucci, Fanelli et al. 1970).

4.4.2 Sex Differences in Drug Metabolism

Disparity in drug metabolism between the sexes is another confounding factor when attempting to establish a paradigm for the metabolism of new drugs. Male and female animals, including humans display differences in drug metabolizing enzyme expression and regulation.

One of the first reports of gender differences in the response to xenobiotics was described by Nicholas and Barron in 1932. Their work reported different responses to various doses of sodium amytal in male and female rats. Their study showed that the dose of sodium amytal required to achieve anesthesia in female rats was half of that required to elicit the same effect in the male (Nicholas and Barron 1932).

As well as physical factors such as body weight and composition, the hormonal and genetic control of drug metabolism is a major determinant to drug responses. Early

studies concerning hormonal control of drug metabolizing enzymes found that differences between P450 activities in male and female rats could be abolished by castration. Furthermore, the higher P450 activity of the male animals could be restored in castrated animals with testosterone administration (Kato and Onoda 1970). Initially it was thought that gonadal hormones elicited their effect on hepatic drug metabolizing enzymes by acting directly on the liver itself. This was challenged by several studies which found that the gonadal hormones only exerted effects on hepatic enzymes in the presence of an intact pituitary gland. A study by Eden in 1979, described differences in growth hormone secretion patterns in adult male and female rats. In the male, growth hormone (GH) is secreted in a pulsatile manner, with 'bursts' of hormone secretion occurring approximately every three hours. The female however releases growth hormone at a tonic, low level, resulting in a constant level of GH in the blood at a lower level than the peak concentrations seen in males (Eden 1979). A later study by Mode *et al.* showed that by administering a constant low dose of growth hormone to hypophysectomised female rats, that a feminisation of liver enzyme expression occurred. Similarly, oestrogen treatment of male rats also produced a shift toward female liver enzyme expression (Mode, Gustafsson et al. 1982).

More recently, human studies have found that drug metabolizing enzymes are expressed at different levels between males and females. In a study by Wolbold *et al.* surgically acquired liver samples obtained from male and female patients were tested for CYP3A4 expression. CYP3A4 levels were found to be two-fold higher in females compared with males. This was reflected in a 50 % increase in the rate of N-

dealkylation of verapamil (a CYP3A4 substrate) in microsomal incubations (Wolbold, Klein et al. 2003).

4.4.3 Age-Related Variations in Drug Metabolism

There are several factors which contribute to variation in drug metabolism capacity with age, including liver size, hepatic blood flow, protein binding, and the amount of drug metabolizing enzymes present. Both Phase 1 and Phase 2 drug metabolizing enzymes, including the cytochromes P450s are differentially expressed throughout all stages of life, from gestation to adult life. In foetal liver, the total P450 content is approximately 30-60 % of that found in adult liver. For this reason, neonates are generally at greater risk of drug toxicity than infants and adults due to their impaired ability to metabolize drugs. The hepatic P450 content and drug metabolizing capacity of newborn infants approaches adult levels at the age of around ten years old (Choonara 2005). Age-related variation in drug metabolizing capacity can have significant toxicological consequences, as was demonstrated by the so called 'grey baby syndrome', following chloramphenicol treatment in newborns. 'Grey baby syndrome' was identified in infants whose mothers had received chloramphenacol in the late stages of pregnancy, and in neonates receiving the drug after birth. The resultant condition is characterized by vomiting, anorexia, respiratory distress, hypotension, grey discolouration of the skin, and death. This syndrome was found to occur due to neonatal immaturity of the hepatic glucuronide pathway by which chloramphenacol is metabolized, meaning the drug accumulates in the infant at toxic levels (Hughes *et al.* 2001).

Advancing age is not generally associated with any significant alterations in the level of phase 1 or 2 enzymes in the liver, however hepatic metabolism is affected by a decrease in hepatic blood flow by approximately 40 %, compared with the average adult. Drug metabolism in the elderly is also highly impacted by polypharmacy, with elderly individuals consuming on average four times the quantity of prescribed drugs compared to younger individuals (McLean and Le Couteur 2004).

4.5 Excretion

Excretion of a drug from the body is via two major routes; biliary and renal, and is heavily influenced by drug transporters. Small contributions towards excretion of drugs may occur in saliva, sweat, breast milk and the lungs, however, these are most often negligible, with the exception of exhalation of volatile anesthetics (Preckel and Bolten 2005). With the primary function of metabolism being the transformation of a drug to a more polar, water-soluble form, the primary route for the excretion of most drugs is by renal filtration. The kidneys receive approximately 25 % of the total systemic circulation in humans, and so are constantly exposed to drugs and xenobiotics which are present in the blood. Filtration of blood through the glomerulus and the movement of glomerular filtrate through the nephron is the process during which reabsorption of non-toxic substances such as water, glucose and amino acids occur, while waste material is carried to the collecting ducts for excretion in urine. Large molecules such as albumin, to which many drugs bind with some degree of affinity are not filtered at a glomerular level, and therefore only unbound drug is able to be removed from the circulation by glomerular filtration (Verbeeck and Musuamba 2009). In addition to passive filtration, the nephron is able to selectively transport molecules in and out of the tubular lumen via a myriad of

drug transporters. These transporters include organic anion transporters (OAT) 1-4, P-glycoprotein (Pgp) of which there are two subclasses; multidrug resistance protein (MDR) 1 and 2, peptide transporter 1 and 2, and organic cation transporters 1 and 2. These transporters exhibit broad substrate specificity, with many xenobiotics serving as substrates for one or more type of transporter. This means that the process of active transport of molecules in the kidney is subject to competition and inhibition, which can lead to drug-drug interactions with multiple substrates (Shitara, Sato et al. 2005).

Biliary excretion is the second major route of elimination, however, research into the mechanisms by which it occurs in humans has been somewhat confounded by difficulties in obtaining bile from healthy patients. Bile sampling is an invasive procedure and so is usually limited to post-operative patients who have undergone surgery for existing hepatobiliary dysfunction. Consequently, faecal elimination is used as a measure of non-urinary drug elimination (Ghibellini, Leslie et al. 2006). Bile is secreted from hepatocytes in an osmotic process and is released into canaliculi running between adjacent cells. Canalicular bile is drained into bile ductules and ducts before being further concentrated in the gall bladder, where it is stored in the fasting state prior to release into the small intestine in the fed state. Organic solutes including bile salts, phospholipids and cholesterol are secreted by hepatocytes into the bile, where they form micelles which may be reabsorbed in the intestine (Trauner and Boyer 2003). In addition to organic solutes drugs and their metabolites may also be excreted into the bile. Similarly to the kidney, the liver contains a vast array of uptake and efflux transporters which are localized to the apical and the basolateral membranes of both hepatcoytes and cholangiocytes. As the liver is both a major site

of drug metabolism, as well as excretion of xenobiotics, it is therefore at high risk of prolonged exposure to toxic compounds and metabolites and consequential tissue damage. Similarly to bile salts and cholesterol, xenobiotics which enter the bile may be reabsorbed in the intestine and undergo enterohepatic cycling, which re-introduces the compound back into the liver (Roberts, Magnusson et al. 2002). Furthermore, xenobiotics may cause disruption to the bile formation process and result in drug-induced cholestasis, where bile cannot flow from the hepatic ducts to the gallbladder or intestine. This may also result in liver injury as drugs and metabolites can linger for extended periods of time, during which they may be re-up taken into hepatocytes, causing further injury (Padda, Sanchez et al. 2011).

4.6 Results

4.6.1. Establishing the Role of Cyp3a in the Metabolism of Pazopanib *In Vivo.*

In order to acquire a general understanding of the contribution of Cyp3a in the mouse to pazopanib metabolism *in vivo,* adult male wild-type (n=4) and Cyp3ac knock-out mice (n=4) were administered pazopanib at a dose of 20 mg/kg pazopanib *per os.* (*p.o*.). A pharmacokinetic experiment was carried out as described in Chapter 2 and the data are shown in **Figure 4.1**. Interestingly, despite pazopanib being a known CYP3A4 substrate, the deletion of the murine Cyp3a cluster has no significant effect on the pharmacokinetic profile of pazopanib *in vivo,* suggesting that murine Cyp3a is not implicated in pazopanib metabolism in the mouse.

a)

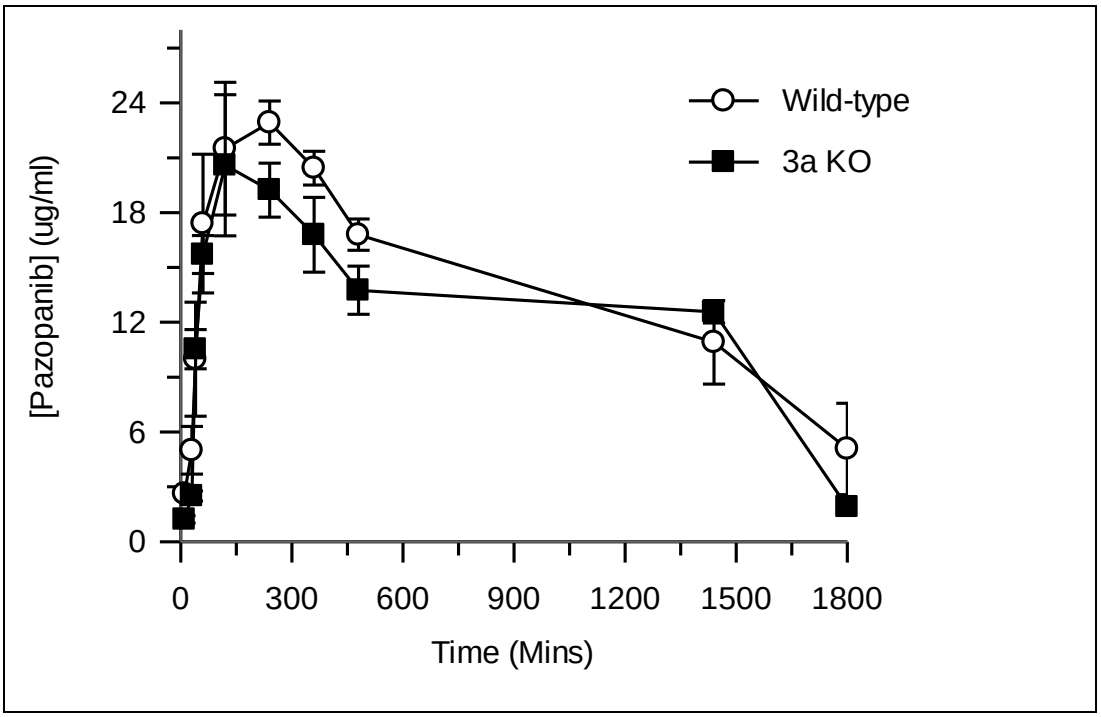

b)

Genotype	**Half Life (Mins)**	**Cmax (µg/ml)**	**AUClast (min*µg/ml)**	**AUCinfin (min*µg/ml)**	**Clearance (ml/min/kg)**
WT	1037 ± 136.6	24.5 ± 6	24642 ± 4298	39321 ± 29692	0.7 ± 0.3
Cyp3a KO	478 ± 127.8	22 ± 7.6	18084 ± 3861	19488 ± 3665	1.1 ± 1.8

Figure 4.1. The deletion of the murine Cyp3a cluster has no effect on the pharmacokinetic profile of pazopanib compared to wild-type mice. a) Pharmacokinetic profile of pazopanib in wild-type, indicated by open circles (n=4) and Cyp3a cluster knock-out mice, indicated by black boxes (n=4). Pazopanib (20 mg/kg) administered by oral gavage b) raw data summarizing pharmacokinetic parameters calculated in Winonlin. No significant differences in pharmacokinetic parameters were noted between the groups. Values expressed ± SEM.

4.6.2. Investigation into Hepatic P450 Contribution to Pazopanib Metabolism in the Mouse

The apparent non-involvement of Cyp3a in the metabolism of pazopanib in the mouse raised the question; which, if any cytochrome P450s are implicated in the hepatic metabolism of pazopanib in the mouse? The HRN mouse was utilized in an attempt to address this question. Adult male wild-type (n=4) and HRN mice (n=5) were dosed with pazopanib at a dose of 20 mg/kg (*p.o*.) and the pharmacokinetic profiles of pazopanib were analyzed. The data are displayed in **Figure 4.2.** If a drug undergoes extensive hepatic metabolism, it would be expected that the exposure to the drug in HRN mice, which lack functional P450 enzymes in the liver, would be greatly increased due to the inability of these mice to metabolize the drug. However, it can be seen in **Figure 4.2.** that once again there is no significant difference between the pharmacokinetic profile of pazopanib in wild-type and HRN mice. Taken together with data from Cyp3ac knock-out mice, this implies that in the mouse, hepatic P450s play a negligible role in the metabolism of pazopanib.

a)

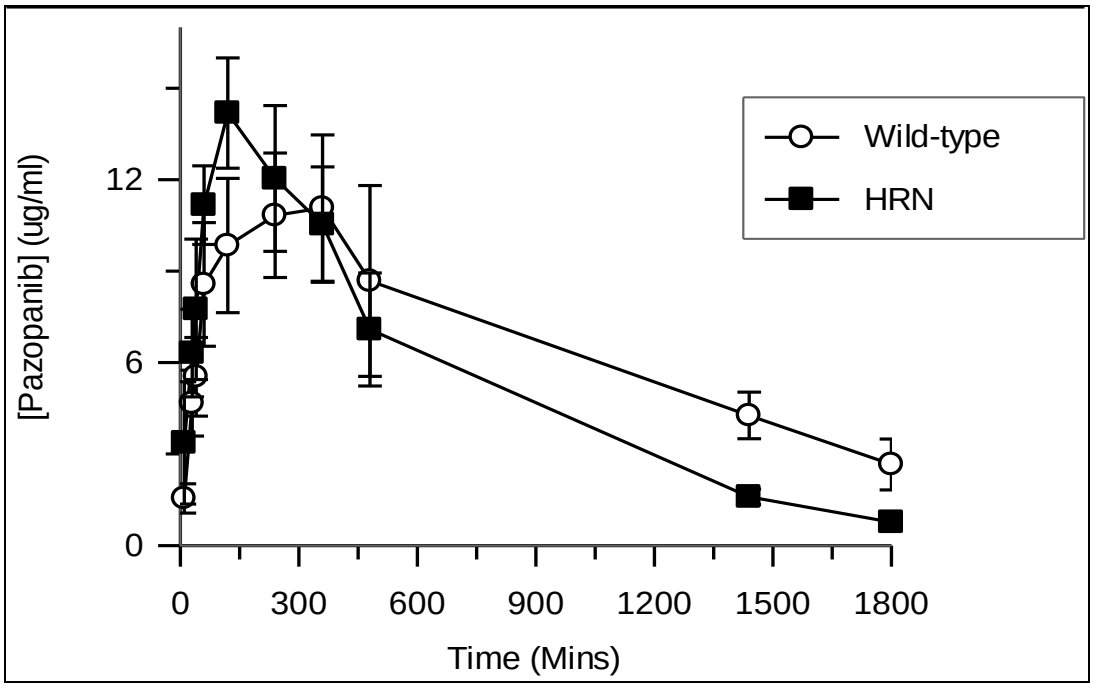

b)

Genotype	**Half Life (Mins)**	**Cmax (µg/ml)**	**AUClast (min*µg/ml)**	**AUCinfin (min*µg/ml)**	**Clearance (ml/min/kg)**
WT	772 ± 270.3*	11.5 ± 5.5	12274 ± 6316	15276 ± 7645	1.5 ± 0.6
HRN	385 ± 114.8*	14.8 ± 3.9	10451 ± 2218	10933 ± 2193	1.9 ± 0.4

Figure 4.2. Inactivation of hepatic P450 enzyme activity has a marginal effect on the pharmacokinetic profile of pazopanib compared to wild-type mice. a) Pharmacokinetic profile of pazopanib in wild type (n=5) and HRN (n=5) mice. Pazopanib (20 mg/kg) administered by oral gavage. b) raw data summarizing pharmacokinetic parameters calculated in WinNonLin. Half-life was found to differ between groups (t-test, $P<0.05$). Values expressed ± SEM.

4.6.3 Pharmacokinetic Profiling of Pazopanib in Induced Wild-Type Mice

In Chapter 2, **Figure 3.7** describes differences in the rate of pazopanib metabolism between mouse and human microsomes *in vitro*, which suggests a species variation in the metabolism of pazopanib exists between mice and humans. In order to assess the potential significance of human CYP3A4 in the clearance of pazopanib, pharmacokinetic experiments were carried out using wild type, h3A4/3A7 and h3A4/3A7/hCAR/hPXR mice. The mice were induced prior to the pharmacokinetic dosing using the drugs and dosing schedule carried out by Hasegawa *et al.* (Hasegawa, Kapelyukh et al. 2011). Each inducing agent had a corresponding wild type control. A western blot showing the levels of induction in wild-type, humanised CYP3A4/3A7 and humanised CYP3A4/3A7/hCAR/hPXR animals using PCN and rifampicin can be seen in **Figure 4.**6. Little differences were observed in OH-pazopanib pharmacokinetics among the treatment groups, however the pattern of OH-pazopanib formation in wild-type and h3A4/3A7/hCAR/hPXR animals when induced, is consistent with an increase in metabolism of pazopanib. It is relatively complex to interpret these OH-pazopanib profiles *in vivo*, as there is no information available on Phase 2 reactions involved in the metabolism of pazopanib.

Wild-type mice were dosed with vehicle (corn oil), or rifampicin at 10 mg/kg for 3 days or, PCN at 10 mg/kg (*i.*p) for 2 days prior to the commencement of the PK study (n=4 all groups). Mice were then dosed with 20 mg/kg pazopanib (*p.o.*) the resultant pharmacokinetic profiles are displayed in **Figure 4.3.** Both the human-specific inducer rifampicin, and mouse-specific inducer PCN cause a non-significant reduction in maximum plasma concentration, compared with the corn oil treated vehicle control group **(Table 4.1)**. Furthermore, both inducing agents cause a non-significant

decrease in the bioavailability of pazopanib, as represented by the area under the curve (AUC), compared to the vehicle control group. PCN is a potent activator of murine PXR, and this is reflected in the Cyp3a induction seen in Western blots displayed in **Figure 4.7.**

4.6.4 Pharmacokinetics of Pazopanib in Humanised CYP3A4/3A7 mice

Having established that induction of wild-type mice had a small, albeit non-significant effect on the metabolism of pazopanib, as outlined in **Table 4.1,** the pharmacokinetic study was repeated in hCYP3A4/3A7 mice, induced with the murine PXR agonist PCN at 10 mg/kg (*i.p*) for 2 days, as was the case in the wild-type animals. Two groups of hCYP3A4/3A7 mice were used; one group received vehicle (corn oil) and one received PCN. The pharmacokinetic profiles obtained in these animals are displayed in **Figure 4.4.**

a)

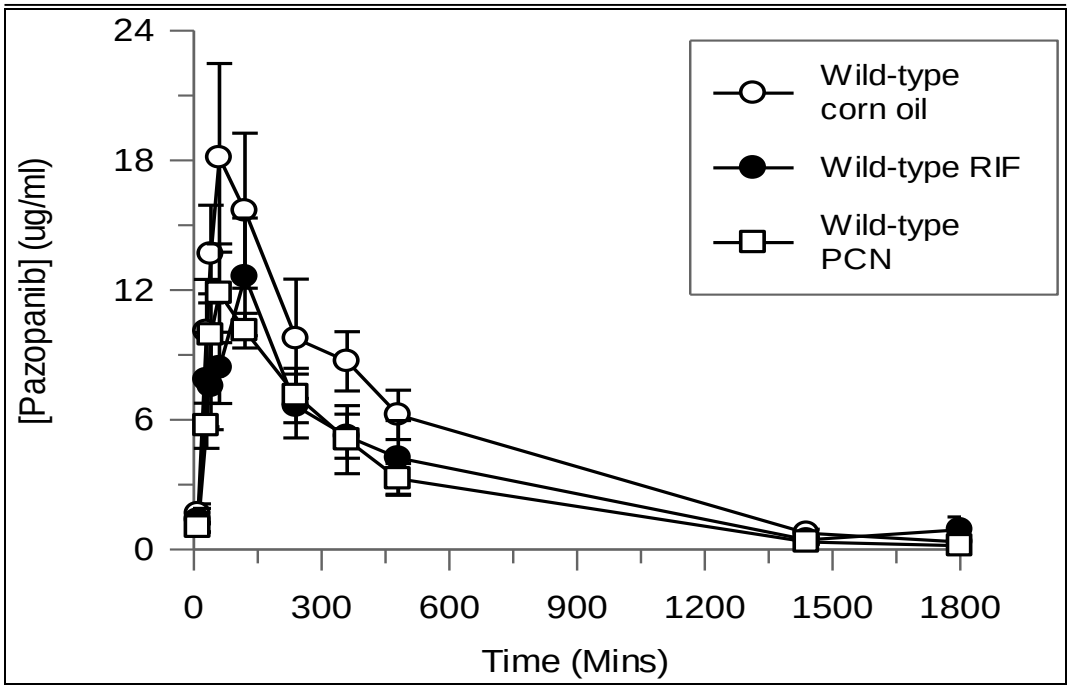

b)

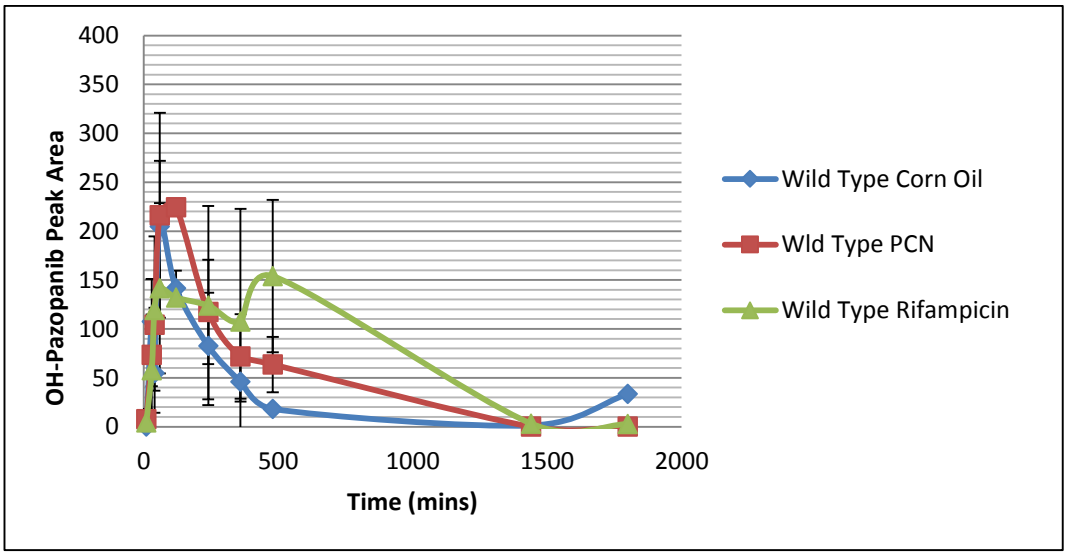

Figure 4.3. The pharmacokinetic profile of pazopanib does not change with induction with PCN or Rifampicin in wild-type mice. Pharmacokinetic data from wild type mice induced with either 10 mg/kg PCN 10 mg/kg (*i.p.*) for 2 days or 10 mg/kg rifampicin (*i.p.*) for 3 days. Pazopanib (20 mg/kg) administered by oral gavage, n=4. Statistical analysis of pharmacokinetic parameters (t-test) showed no significant difference between groups b) OH-pazopanib formation in wild-type mice differs slightly between inducing treatments over PK time course. CMax -* Corn Oil vs PCN. $P<0.05$, N=2. Values expressed mean ± SEM

a)

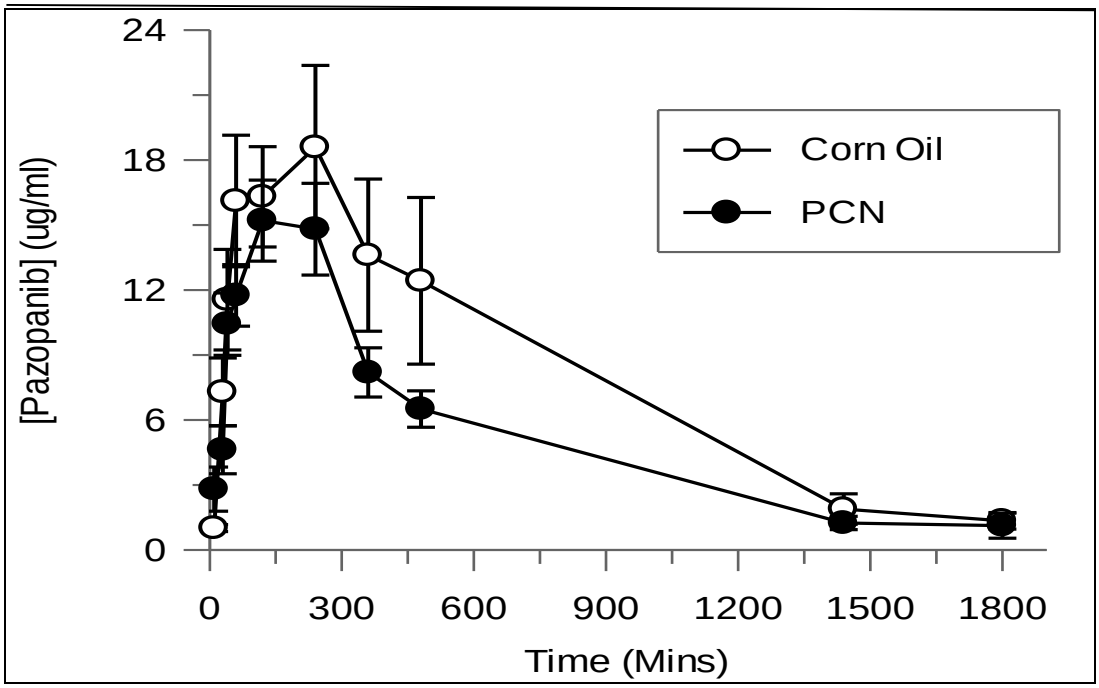

b)

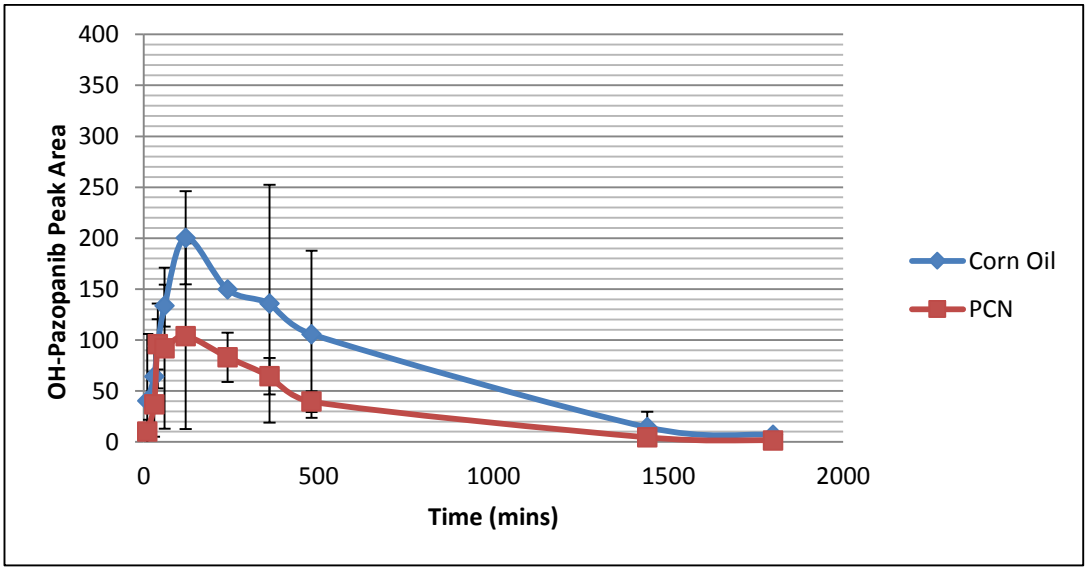

Figure 4.4. Induction of hCYP3A4/3A7 mice with PCN does not significantly alter pazoapnib pharmacokinetic parameters. Pharmacokinetic data from h3A4/3A7 mice induced with 10 mg/kg PCN (*i.p.*) for 2 days, vs corn oil. Pazopanib (20 mg/kg) administered by oral gavage, n=6. Pharmacokinetic parameters are not statistically different between treatments (t-test) b) OH-pazopanib detection does not differ between hCYP3A4/3A7 animals treated with corn oil or PCN and dosed with pazopanib. Values expressed mean ± SEM

4.6.5. Pharmacokinetics of Pazopanib in h3A4/3A7/hCAR/hPXR Mice.

The pharmacokinetics of pazopanib was non-significantly altered in un-induced and induced hCYP3A4/3A7 mice. The pharmacokinetic study was performed in h3A4/3A7/hCAR/hPXR mice induced with the human PXR ligand, rifampicin. Mice were administered rifampicin at a dose of 10 mg/kg for 3 days (*i.p.*) On day 4, mice were dosed with pazopanib at a dose of 20 mg/kg (*p.o.*) and a PK experiment was carried out previously described. Un-induced animals received corn oil as a control for rifampicin. The pharmacokinetic profiles of pazopanib and OH-metabolite in these mice are displayed in **Figure 4.5**. Statistical analysis (t test) showed clearance, half-life and area under the curve to differ significantly between induced and un-induced groups as displayed in **Table 4.1** ($P < 0.001$).

a)

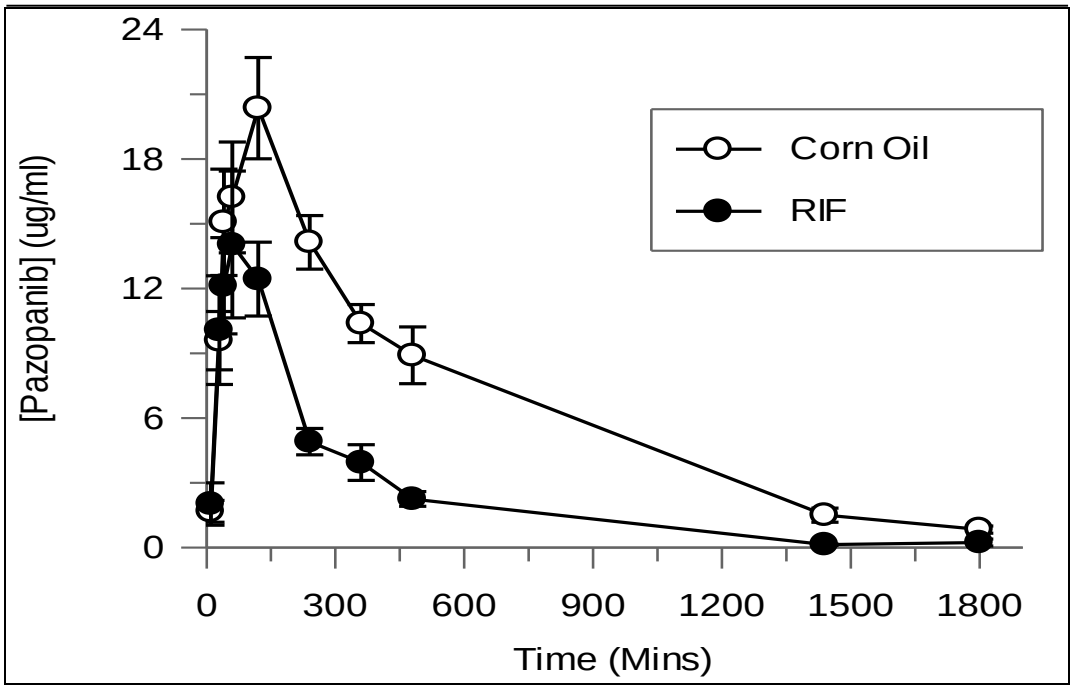

b)

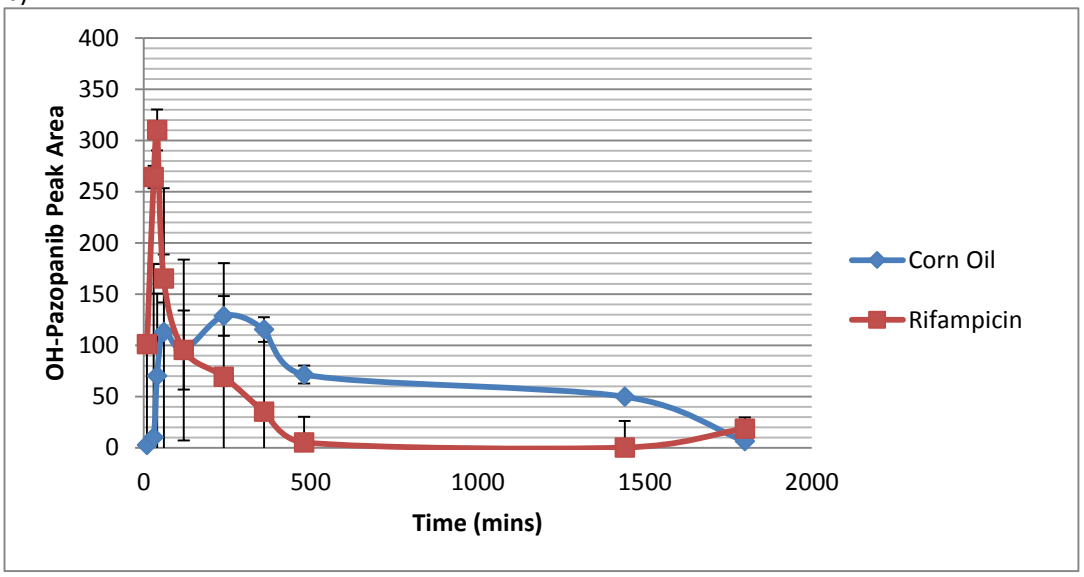

Figure 4.5. Induction of humanised CYP3A4/3A7/hCAR/hPXR mice with rifampicin significantly alters the pharmacokinetic profile of pazopanib. Pharmacokinetic data from h3A4/3A7/hCAR/hPXR mice induced with 10 mg/kg rifampicin (*i.p.*) for 3 days vs corn oil. Pazopanib (20 mg/kg) administered by oral gavage, n=6. Clearance, half-life and AUC differd significantly between treatments (t-test, $P < 0.001$) b) OH-pazopanib formation does not differ between h3A4/3A7/hCAR/hPXR animals treated with corn oil or rifampicin and dosed with pazopanib. Values expressed ± SEM.

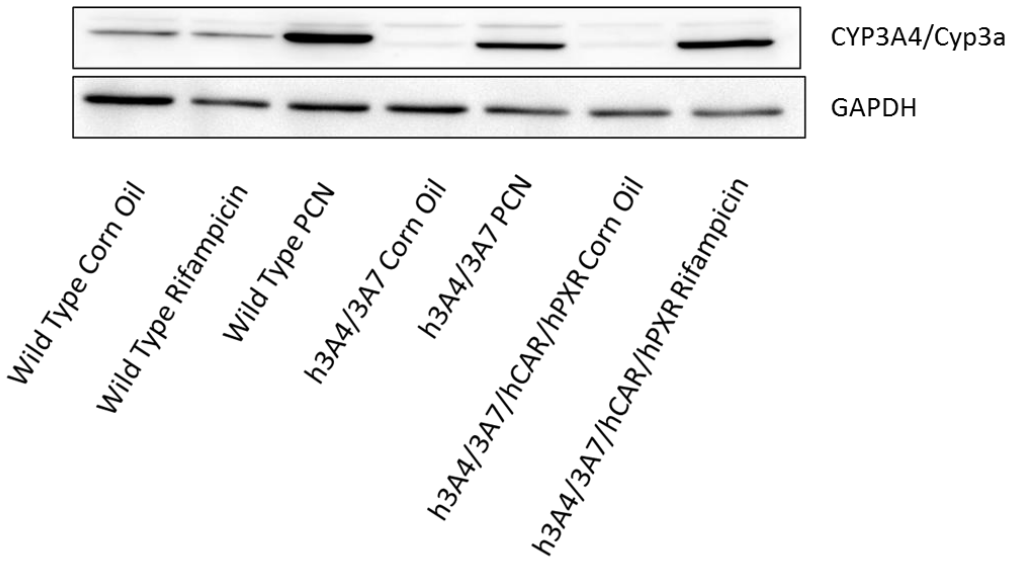

Figure 4.6. Western blots from pharmacokinetic study showing induction of murine Cyp3a, or the CYP3A4/7 transgene. Pools of 4 (wild-type), and 6 (humanized) microsomes derived from mouse livers were blotted to confirm induction of Cyp3a with PCN and CYP3A with rifampicin.

Mouse Treatment	Half Life (Mins)	Cmax (μg/ml)	AUClast (min*μg/ml)	AUCinfin (min*μg/ml)	Clearance (ml/min/kg)
WT CO	314 ± 42.3	13.7 ± 1.4	7140 ± 639	7268 ± 757	2.8 ± 0.3
WT PCN	280 .9 ± 32.6	13.7 ± 4.6	5759 ± 2344	5878 ± 2390	3.4 ± 1.6
WT Rif	300 .4 ± 69.4	13.4 ± 3.7	5770 ± 2654	5841 ± 2739	3.9 ± 1.3
h3A4/3A7 CO	366 .3 ± 81.9	21.7 ± 10.1	14221 ± 6852	14961 ± 7337	1.6 ± 0.7
h3A4/3A7 PCN	349 .3 ± 99	16.9 ± 4.6	8808 ± 2834	9203 ± 2843	2.4 ± 0.8
h3A4/3A7/ hCAR/hPXR CO	366 .3 ±49.8	21.2 ± 5.0	11704 ± 3149	12150 ± 3353	1.7 ± 0.6
h3A4/3A7/ hCAR/hPXR Rif	241 .8 ± 34.6	15.7 ± 7.7	4484 ± 1213	4508 ± 1214	4.7 ± 1.2

Table 4.1. Pharmacokinetic parameters from *in vivo* experiments

Mean pharmacokinetic data calculated using WinNonLin software. Values expressed mean ± SD. Statistics as calculated using Graphpad Instat, are described in **Tables 4.2-4.4**.

Mouse Treatment	WT CO	WT PCN	WT RIF	h3A4/3A7 CO	h3A4/3A7 PCN	h3A4/3A7/ hCAR/hPXR CO	h3A4/3A7/hCAR/ hPXR Rif
WT CO		ns	ns	ns	ns	ns	Ns
WT PCN	ns		ns	ns	ns	ns	Ns
WT Rif	ns	ns		ns	ns	ns	Ns
h3A4/3A7 CO	ns	ns	ns		ns	ns	*
h3A4/3A7 PCN	ns	ns	ns	ns		ns	Ns
h3A4/3A7/ hCAR/hPXR CO	ns	ns	ns	ns	ns		*
h3A4/3A7/ hCAR/hPXR Rif	ns	ns	ns	ns	ns	ns	

Table 4.2. Statistically significant differences between half-life in *in vivo* pharmacokinetic experiments ns= non-significant, * $P < 0.05$.

Mouse Treatment	**WT CO**	**WT PCN**	**WT RIF**	**H3A4/ 3A7 CO**	**h3A4/3A7 PCN**	**h3A4/3A7/ hCAR/hPXR CO**	**h3A4/3A7/hCAR/ hPXR Rif**
WT CO		ns	ns	ns	ns	Ns	Ns
WT PCN	ns		ns	*	ns	Ns	Ns
WT Rif	ns	ns		*	ns	Ns	Ns
h3A4/3A7 CO	ns	ns	ns		ns	Ns	***
h3A4/3A7 PCN	ns	ns	ns	ns		Ns	Ns
h3A4/3A7 / hCAR/hPXR CO	ns	ns	ns	ns	ns		*
h3A4/3A7 / hCAR/hPXR Rif	ns	ns	ns	ns	ns	Ns	

Table 4.3. Statistically significant differences between the area under the curve in *in vivo* pharmacokinetic experiments ns= non-significant, * $P< 0.05$, *** $P< 0.001$

Mouse Treatment	WT CO	WT PCN	WT RIF	h3A4/3A7 CO	h3A4/3A7 PCN	h3A4/3A7/ hCAR/hPXR CO	h3A4/3A7/hCAR/ hPXR Rif
WT CO		ns	ns	ns	ns	Ns	ns
WT PCN	ns		ns	ns	ns	Ns	ns
WT Rif	ns	ns		*	ns	*	ns
h3A4/3A7 CO	ns	ns	ns		ns	ns	***
h3A4/3A7 PCN	ns	ns	ns	ns		ns	**
h3A4/3A7/ hCAR/hPXR CO	ns	ns	ns	ns	ns		***
h3A4/3A7/ hCAR/hPXR Rif	ns	ns	ns	ns	ns	ns	

Table 4.4. Statistically significant differences between clearance of pazopanib in *in vivo* pharmacokinetic experiments ns= non-significant, * $P< 0.05$, ** $P< 0.01$, *** $P< 0.001$

4.6.6 Pazopanib and PXR Activation

GlaxoSmithKline has reported that pazopanib has shown potential to induce CYP3A4 in an *in vitro* human PXR assay (Shukla, Sakamuru et al. 2011); however, drug concentrations at which this was seen and the degree of induction achieved are not described. In an *in vitro* human PXR assay in human liver hepatocellular carcinoma derived cells (DPX2 cells) (**Figure 4.7 a)**, performed by Dr A.K. McLeod (Molecular Pharmacology Group, Medical Research Institute, Ninewells Hospital and Medical School) it can be seen that indeed, pazopanib elicits a dose-dependent activation of PXR *in vitro*, with maximum induction (approximately 8-fold compared to DMSO control) at a concentration of approximately 1 µM. This suggested that pazopanib has the potential to activate PXR *in vivo,* and therefore may have the potential to induce its own metabolism through the up-regulation of CYP3A4.

To investigate PXR activation *in vivo,* wild-type and humanised PXR mice were dosed with pazopanib or 4 days at 200 mg/kg by oral gavage. Untreated mice received an equivalent of vehicle based upon body weight. On day 4, mice were sacrificed and livers harvested for Western blot. Drugs that are strong PXR activators will cause an induction of hepatic CYP3A4/Cyp3a, however, western blots shown in **Figure 4.7 b**, show only a marginal increase in Cyp3a levels in wild-type mice, which is not reflected in the humanised PXR animals.

a)

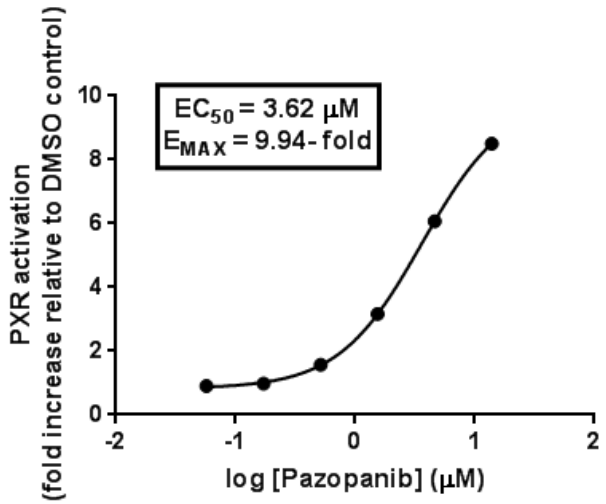

b)

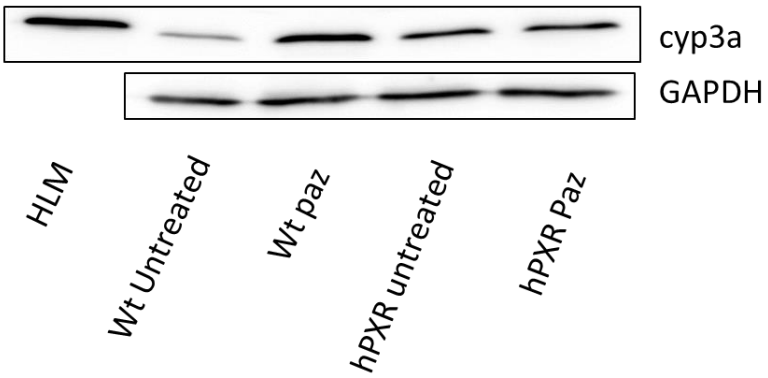

Figure 4.7. *In vitro* and *in vivo* investigations into the effect of pazopanib on PXR.

a) Graph obtained from *in vitro* DPX2 Assay and b) Western blots of pooled wild type and humanised PXR mouse liver microsomes (10 µg pooled protein per lane) showing induction of Cyp3a in wild-type mice which is not reflected in the humanised PXR mice, n=3 untreated, n=4 pazopanib treated.

4.6.7 Treatment of wild-type and humanised mice with high dose pazopanib

Having observed differences in the pharmacokinetic parameters of pazopanib in wild-type and h3A4/3A7/hCAR/hPXR mice (**Figure 4.5**), as well as a species difference in the kinetics of metabolism of pazopanib in mice and human microsomes (**Figure 3.7**), it was of interest to establish whether or not susceptibility to hepatic injury differed between the two models. Groups of hCYP3A4/3A7/hCAR/hPXR and wild-type mice were induced for three days using rifampicin, at a dose of 60 mg/kg. On the fourth day, all animals received a high dose of pazopanib (200 mg/kg) by oral gavage while control animals received an equivalent volume of vehicle (cremaphore 15 %, ethanol 8 % and water) based on body weight. Mice were monitored for 30 h post pazopanib dosing. Animals appeared healthy, and at 30 h post dosing, animals were killed and blood was taken for biochemical analysis as described in **section 2.11**. Upon harvesting the livers from these mice, it was noted that h3A4/3A7/hCAR/hPXR mice exhibited large, pale livers which were mottled in appearance. Liver to body weight ratio was used as an indication of hepatic hypertrophy, and are represented in **Figure 4.8.** h3A4/3A7/hCAR/hPXR animals treated with vehicle had slightly larger livers than wild-type animals, although this difference was not statistically significant. However, h3A4/3A7/hCAR/hPXR animals induced with rifampicin and treated with pazopanib have significantly larger livers compared to h3A4/3A7/hCAR/hPXR animals treated with vehicle (P <0.05, n=3), as well as wild-type animals treated with either vehicle or rifampicin and pazopanib (P <0.001, n=3). **Figure 4.9** shows no significant elevations in ALT levels in wild-type mice following high dosing with pazopanib compared with controls (75.4 ± 6.8 U/l rifampicin and pazopanib, 37.8 ± 14.3 U/l pazopanib, 30.5 ±

13.6 U/I vehicle). This is largely consistent with findings outlined by the FDA and GlaxoSmithKline, which describe repeated high dosing of pazopanib in wild-type mice as having negligible effects on blood biochemistry in these animals (GlaxoSmithKline 2013). h3A4/3A7/hCAR/hPXR animals treated with rifampicin and pazopanib and which exhibited enlarged, pale livers however also displayed elevated levels of ALT compared to wild-type animals which received the same dosing regimen (117.8 ± 34 U/I h3A4/3A7/hCAR/hPXR rifampicin and pazopanib, 41.2 ± 1.9 U/I pazopanib, 43.6 ± 4.0 U/I vehicle, *P* <0.01, n=3), as well as wild-type and h3A4/3A7/hCAR/hPXR animals which received pazopanib alone, or vehicle (*P* <0.001, n=3 all groups). No changes were seen in total bilirubin levels in any group.

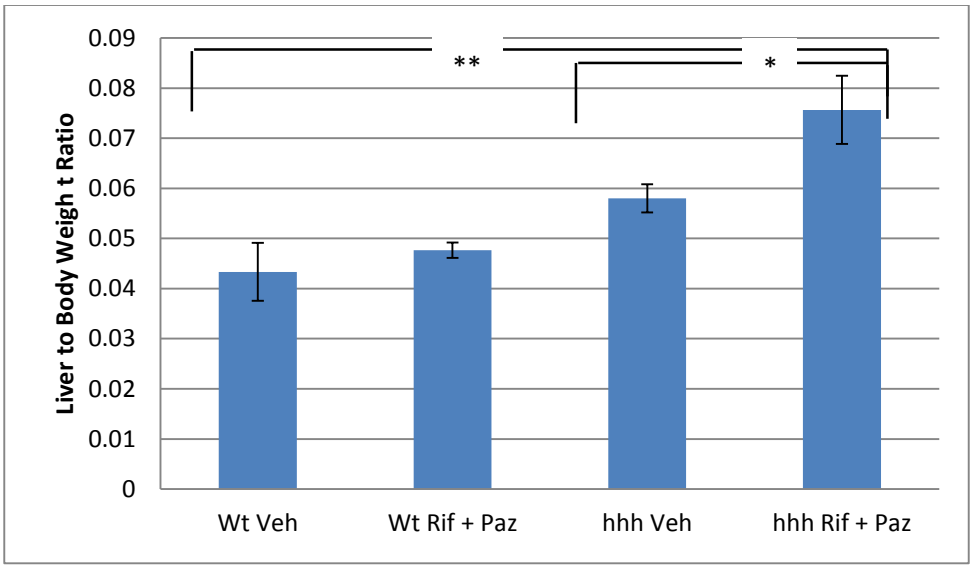

Figure 4.8. Liver to body weight ratios of wild-type and h3A4/3A7/hCAR/hPXR mice treated with either vehicle, or rifampicin and pazopanib. Humanised mice (hhh) treated with rifampicin and pazopanib have significantly enlarged livers compared to wild-type animals. *= *P*< 0.05 hhh Rif + Paz vs hhh Veh, **= *P*< 0.01 hhh Rif + Paz vs WT Veh. n=3 all groups. Values expressed ± SD.

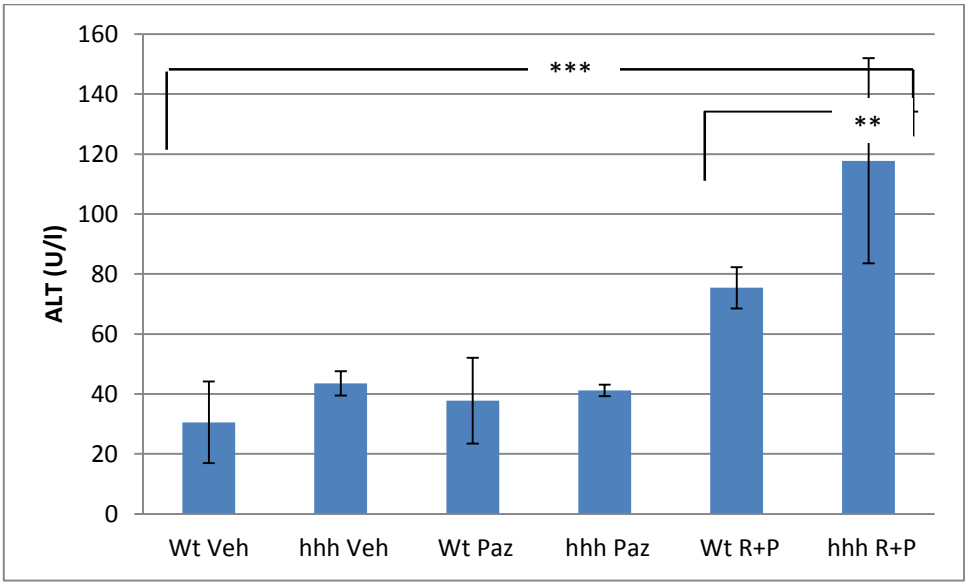

Figure 4.9. Plasma ALT levels in high dose pazopanib mice.

ALT levels were determined in blood obtained from cardiac punctures performed 30h post-pazopanib dosing. H3A4/3A7/hCAR/hPXR (hhh) mice showed significantly elevated ALT compared to animals treated with vehicle or pazopanib alone and wild-type animals. n=3 all groups. ***= hhh R+P vs Wt Veh, hhh Veh, WT Paz, hhh Paz. **= hhh R+P vs Wt R+P. Values expressed ± SD.

4.6.8 Liver Pathology

Pale, mottled and enlarged livers are often the result of excessive lipid accumulation in the hepatocytes. Initial haemotoxylin and eosin (H&E) staining appeared to show lipid-like droplets such as would be expected in fatty liver disease. **Figure 4.10** shows H&E staining on snap-frozen liver sections of vehicle treated and rifampicin and pazopanib treated wild- type h3A4/3A7/hCAR/hPXR mice. It is apparent that animals which exhibited an enlarged, pale liver phenotype, coupled with elevated ALT also

showed distinct lipid-like vacuoles in the liver. This vacuolation and ALT elevation is absent in wild-type animals (**Figure 4.11**). Furthermore, this phenotype was absent in h3A4/3A7/hCAR/hPXR animals which received vehicle and pazopanib, or rifampicin and vehicle, suggesting that induction and expression of the human CYP3A4 transgene as well as dosing with pazopanib is required to elicit the phenotype.

Having established that the phenotype is exclusive to Rif-induced and pazopanib-treated h3A4/3A7/hCAR/hPXR mice, several sections from vehicle treated and affected livers were stained in an attempt to identify the nature of the vacuolation seen in them. Oil Red O staining was carried out with the help of Dr Shaun Walsh, Ninewells Hospital and Medical School, and sections are displayed in **Figure 4.12**. Interestingly, these sections are negative for lipids, which are normally detected by red staining in affected tissue. Subsequently, Periodic Acid Schiff staining was performed on sections from the same livers, using a commercially available staining kit from Sigma (**section 2.14**) to stain for polysaccharides such as glycogen. Sections were also negative for glycogen, which stains pink to red, in colour. These sections are represented in **Figure 4.13**.

a)

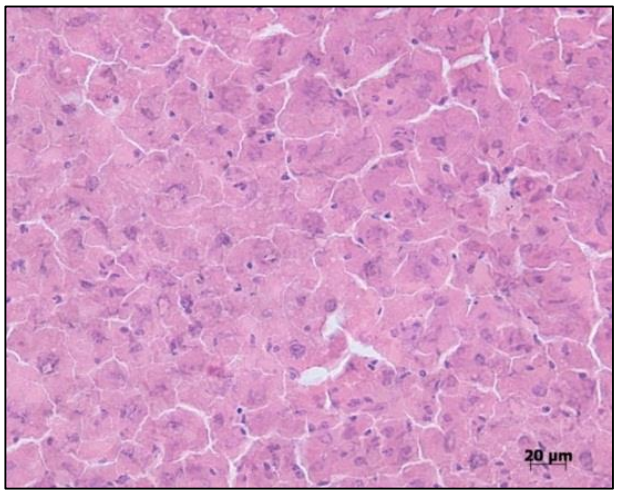

b)

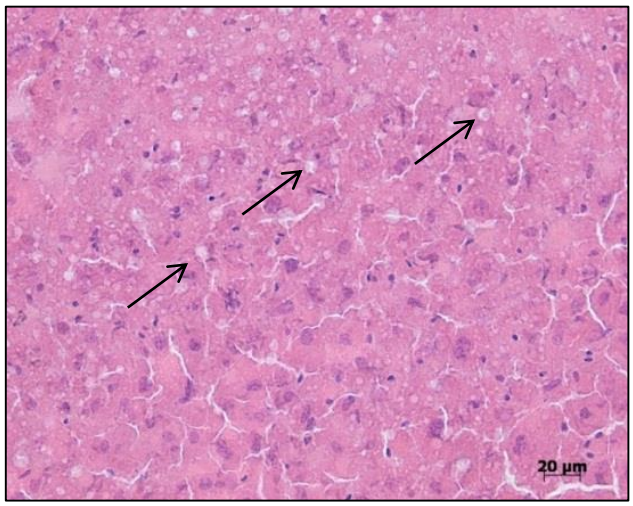

Figure 4.10: Haemotoxylin and Eosin stained liver sections from wild-type and humanised mice

Haematoxylin and Eosin staining performed on sections from snap-frozen liver of h3A4/3A7/hCAR/hPXR mice treated with a) corn oil and vehicle or b) rifampicin induced (60mg/kg, 3 days *i.p.*) and 200mg/kg pazopanib p.o. H&E was carried out as described in the methods. Arrows indicate lipid like vacuolation in the pazopanib-treated animals, which are absent in the control animals. Photomicrographs are representative of n ≥ 2, magnification x 20.

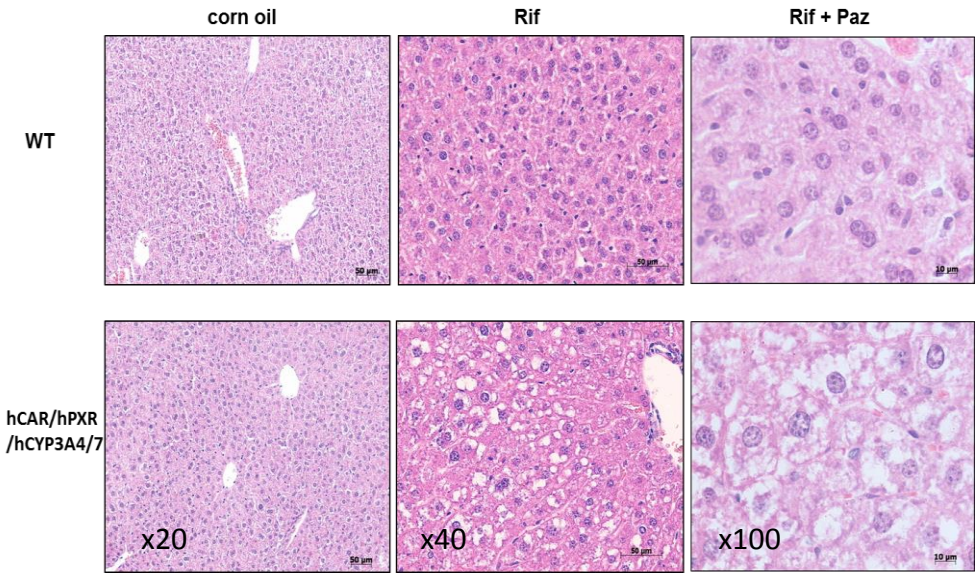

Figure 4.11. Degenerative vacuolation in livers of humanised animals.

Wild-type and h3A4/3A7/hCAR/hPXR animals treated with corn oil show no signs of liver abnormality (Dr Zoe Riches, Molecular Pharmacology Group, Ninewells Hospital and Medical School), "Rif" (60 mg/kg, *i.p*) treated wild-type animals show a normal liver phenotype while h3A4/3A7/hCAR/hPXR animals show evidence of liver abnormality. "Rif + Paz" wild-type animals treated with 60 mg/kg rifampicin (*i.p*) and 200 mg/kg pazopanib (*p.o*) appear to show little sign of liver abnormality, h3A4/3A7/hCAR/hPXR animals treated with 60 mg/kg rifampicin (*i.p*) and 200 mg/kg pazopanib (*p.o*) show extensive degeneration coupled with hepatomegaly and a mild elevation in ALT. Pictomicrographs representative n≥2.

a)

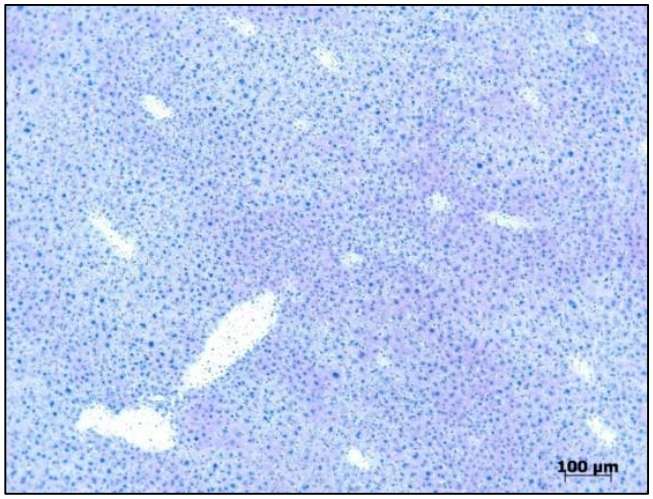

b)

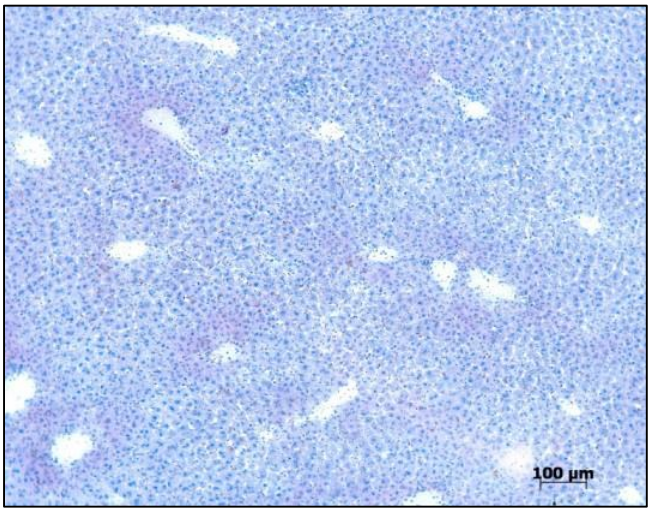

Figure 4.12. Lipid staining in vehicle treated and pazopanib treated mice.

Oil Red O staining for lipids on a) vehicle treated h3A4/3A7/hCAR/hPXR mice, and b) Oil Red O staining on h3A4/3A7/hCAR/hPXR mice induced for 3 days with 60 mg/kg rifampicin (*i.p*) and treated on day 4 with 200 mg/kg pazopanib (*p.o.*). Neither vehicle nor treated livers stained positively for lipids, Photomicrographs representative of n ≥ 2.Magnification x 40.

a)

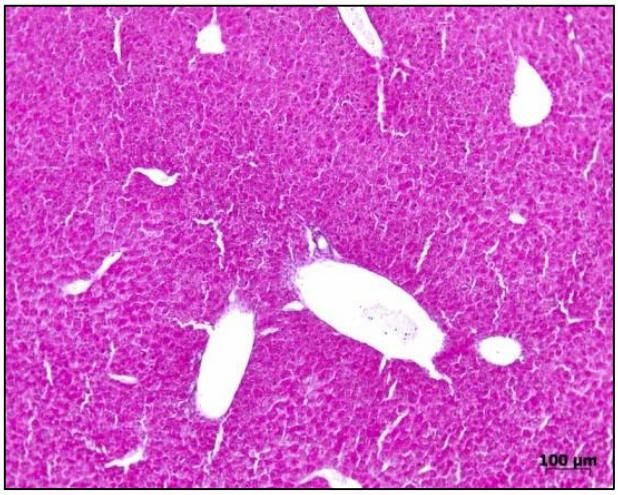

b)

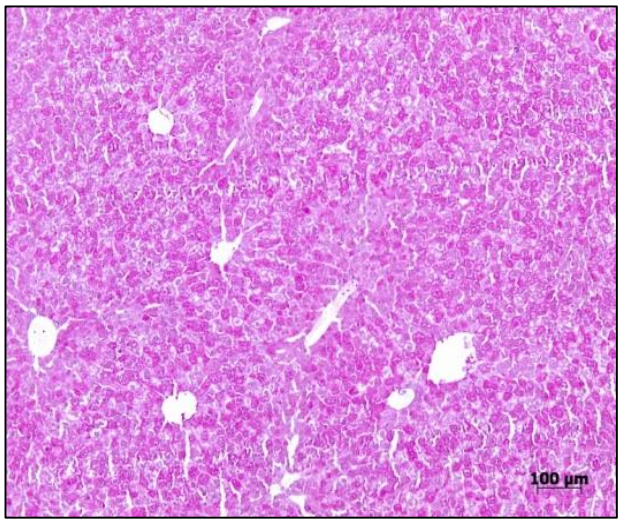

Figure 4.13. Periodic Acid Schiff (PAS) staining in vehicle treated and phenotypic mice.

PAS staining for glycogen on a) vehicle-treated h3A4/3A7/hCAR/hPXR mice and b) h3A4/3A7/hCAR/hPXR mice induced for 3 days with 60 mg/kg rifampicin (*i.p.*) and treated on day 4 with 200 mg/kg pazopanib (*p.o.*). Neither vehicle-treated or Rif-induced livers stained positively for glycogen. Photomicrographs are representative of n ≥ 2, magnification x 40.

4.6.9 Mechanism of Liver Phenotype

The pale and enlarged liver phenotype observed in h3A4/3A7/hCAR/hPXR mice when induced with rifampicin for 3 days at 60 mg/kg (*i.p*.) and dosed with 200 mg/kg pazopanib (*p.o.*) was not observed in wild type mice treated with the same drug regimen. It was then of interest to attempt to define which aspect of the humanisation of the h3A4/3A7/hCAR/hPXR mouse was the causative gene in the observed phenotype. The h3A4/3A7/hCAR/hPXR mouse is generated by crossing h3A4/3A7 mice, with hCAR/hPXR mice, as described in **Section 1.14.4**, and therefore the phenotype observed in these livers may be the product of CYP3A4/3A7 activity, or of the human nuclear receptors CAR and PXR.

Initial attempts to address this were made by dosing 3 groups of mice; h3A4/3A7/hCAR/hPXR, h3A4/3A7 and hCAR/hPXR, with 60 mg/kg rifampicin (*i.p*), for 3 days prior to the administration of 200 mg/kg pazopanib (*p.o*.). At 60 mg/kg, rifampicin induces Cyp3a in wild-type mice, and therefore it was expected to induce in all genotypes in this study. Western Blots in **Figure 4.14** however, show no induction in the h3A4/3A7 animals, for reasons that are yet to be elucidated. The groups which displayed the mottled liver phenotype are highlighted by boxes. The h3A4/3A7 mouse possesses murine CAR and PXR, and therefore PCN, the murine PXR-specific inducing agent is the drug of choice for use with this line, as opposed to rifampicin. To avoid introducing further inducing agents and controls for these experiments, a pharmacological approach was adopted to circumvent the requirement for entire new data sets using PCN. Ketoconazole is a clinically used antifungal agent, and a potent inhibitor of CYP3A4 *in vivo.* At high doses, ketoconazole has the capacity to inhibit the activity of most cytochrome P450

enzymes. The rationale behind this investigation was to inhibit the activity of CYP3A4, which is required for the production of OH-pazopanib, to ascertain whether or not the phenotype persists in the absence of the metabolite. h3A4/3A7/hCAR/hPXR mice were induced for 3 days using 60 mg/kg rifampicin (*i.p*.) on day 4, 100 mg/kg ketoconazole (*p.o.* in corn oil) or corn oil alone was administered to mice 30 min prior to the administration of 200 mg/kg pazopanib (*p.o*.). Mice then underwent a pharmacokinetic experiment as previously described and killed at 30 hr post pazopanib dosing. The traces illustrated in **Figure 4.15** shows that co-administration of ketoconazole at 100 mg/kg is sufficient to significantly alter the PK parameters of pazopanib in rifampicin-induced h3A4/3A7/hCAR/hPXR mice. Furthermore, liver to body weight ratios and ALT levels were unchanged between ketoconazole treated and control animals.

The mottled liver phenotype persists in ketoconazole treated mice (**Figure 4.16**), suggesting that this is a cytochrome P450-independent effect.

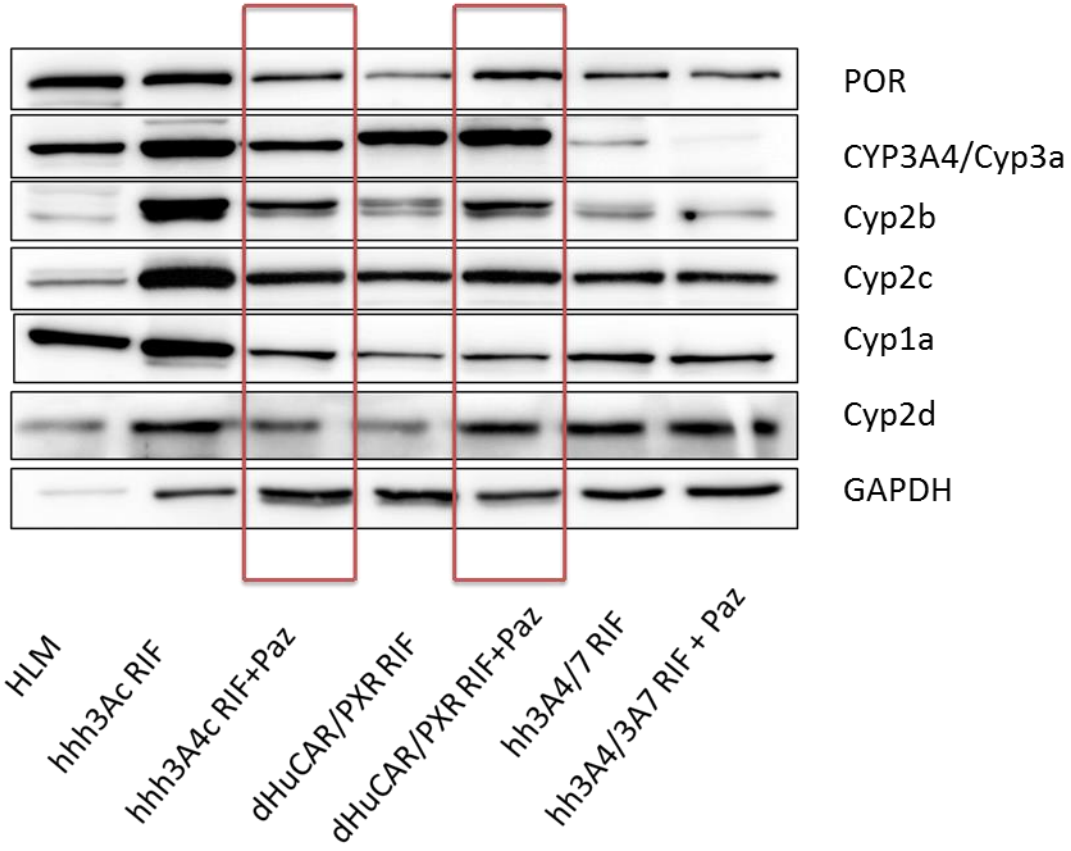

Figure 4.14. Western Blots showing levels of various cytochrome P450 enzymes in mice treated with various inducers, followed by a high dose of pazopanib.

From left to right: Human liver microsomes (HLM), h3A4/3A7/hCAR/hPXR 60 mg/kg rifampicin for 3 days (*i.p*), h3A4/3A7/hCAR/hPXR 60 mg/kg rifampicin for 3 days (*i.p*) plus 200 mg/kg pazopanib (*p.o.*) on day 4, hCAR/hPXR 60 mg/kg rifampicin (*i.p.*) for 3 days, hCAR/hPXR 60 mg/kg rifampicin (*i.p.)* for 3 days plus 200 mg/kg pazopanib (*p.o.*) on day 4, h3A4/3A7 60 mg/kg rifampicin (*i.p*) 3 days, h3A4/3A7 60/mg/kg rifampicin (*i.p.*) for 3 days plus 200 mg/kg pazopanib (*i.p*) on day 4. Animals not receiving pazopanib on day 4, received an equivalent dose of vehicle, based on body weight. Western blotting was carried out on a pool of human liver microsomes, or a pool of mouse liver microsomes (n=3 mice per lane).

a)

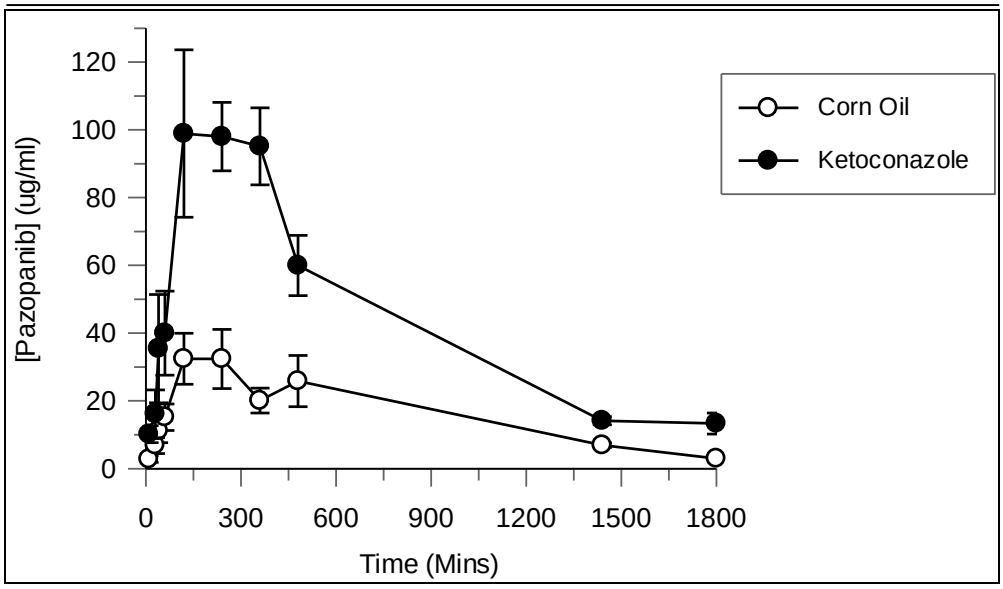

b)

Mouse Treatment	**Half Life (Mins)**	**Cmax (µg/ml)**	**AUClast (min*µg/ml)**	**AUCinfin (min*µg/ml)**	**Clearance (ml/min/kg)**
Corn Oil	452.1 ± 97.6	41.6 ± 20.1	29607.8 ± 12960.3	29978.3 ± 14087.4	8.5 ± 5.3
Ketoconazole	504.8 ± 122	124.7 ± 36.3 (***)	84109.9 ± 16083.5	94813 ± 21732.4	2.2 ± 0.6 (*)

c)

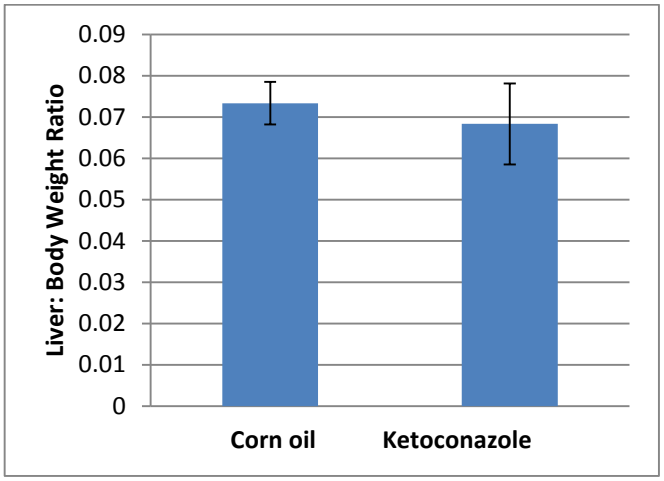

d)

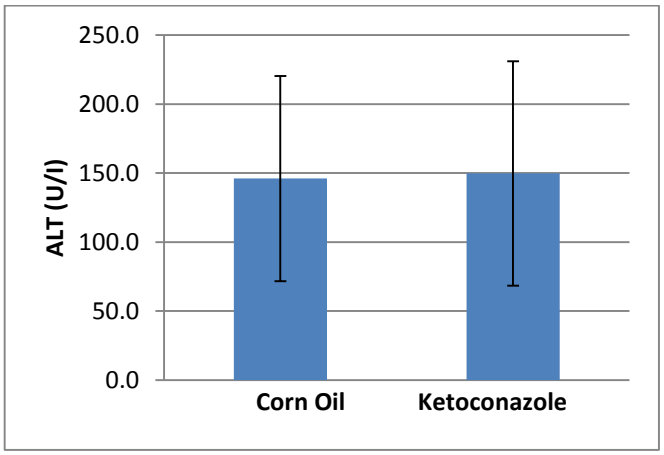

Figure 4.15. Ketoconazole significantly alters the pharmacokinetics of pazopanib in h3A4/3A7/hCAR/hPXR mice but has no effect on ALT levels or liver size.

a) Pharmacokinetic profile from h3A4/3A7/hCAR/hPXR mice induced with 60 mg/kg rifampicin (*i.p*) for 3 days and administered with 200 mg/kg pazopanib (*p.o.*). One set of mice were pre-treated with 100 mg/kg ketoconazole (*p.o.*) 30 min prior to pazopanib dosing, control mice received corn oil, n=6. Values expressed mean ± SEM b) Pharmacokinetic parameters from a) *** Cmax, AUC, and AUC infin. * Clearance. Corn oil half-life, AUC infin, and clearance n=4, due to ill-fitting parameters from two animals, which could not be calculated. All other values n=6 c) No significant differences exist between liver to body weight ratios of ketoconazole treated and control mice, n=6 d) No significant differences exist between plasma ALT in ketoconazole treated and control mice, n=3. Values expressed ± SD.

a)

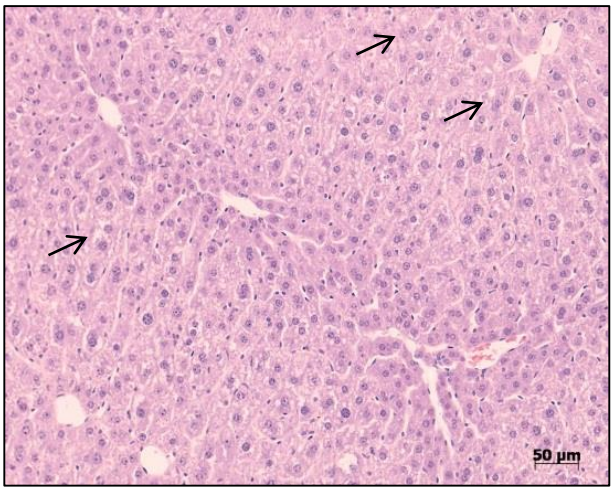

b)

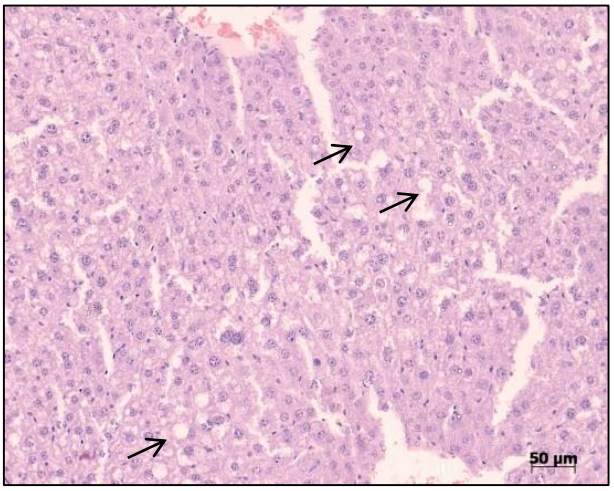

Figure 4.16. Vacuolaton persists in liver sections from ketoconazole and pazopanib treated h3A4/3A7/hCAR/hPXR mice.

a) h3A4/3A7/hCAR/hPXR mice treated with rifampicin at 60 mg/kg (*i.p.*) for 3 days followed by 200 mg/kg pazopanib (*p.o.*) exhibited the mottled phenotype b) mice induced with rifampicin and received ketoconazole at 200 mg/kg (*p.o.*) 30 min prior to the administration of pazopanib at 200 mg/kg (*p.o.*) also exhibited this phenotype 30 hr after pazopanib dosing. Arrows indicate vacoulation. Photomicrographs representative of n=2, magnification x20.

Given that this phenotype was reproducible, and its cause remained undefined, new sections were cut and stained with H&E for microscopy at a magnification of x100 in an effort to identify the structure of these lipid-like vacuoles. Interestingly, under high magnification it can be seen that these 'vacuoles' appear to be holes in the tissue as seen in **Figure 4.11.** Upon examination, the cells appear to be undergoing a degenerative process which includes the swelling and eventual collapse of the nucleus along with destruction of the cytoplasm. Interestingly, this phenotype was not as pronounced in h3A4/3A7/hCAR/hPXR mice which received pazopanib alone as it is in h3A4/3A7/hCAR/hPXR mice which were induced with rifampicin and also treated with pazopanib. The phenotype was never found in wild-type animals with any treatment combination. This suggests that rifampicin has a role in the development of this phenotype, but only in the humanised model. As the phenotype persists in humanised mice co-treated with ketoconazole, and therefore the effect is unlikely to be due to the humanisation of CYP3A4/3A7, rifampicin may be acting through human PXR on a non-CYP target to elicit this response.

4.7 Discussion

4.7.1 Summary

The data in this chapter describe a species difference in the pharmacokinetic profiles of pazopanib *in vivo* in wild-type and humanised mice. Furthermore, a difference in sensitivity to the toxic effects of pazopanib in the presence and absence of enzyme induction in these animals is explored.

4.7.2 Species Variation in the Pharmacokinetics of Pazopanib

In vitro data obtained from microsomal and recombinant CYP450 incubations described in Chapter 3 shows that murine enzymes are less efficient at metabolising pazopanib compared to human P450 enzymes. A dose of 20 mg/kg pazopanib was selected for pharmacokinetic studies based on the efficacy this dosed elicited in human xenografts of a variety of cancers as reported by Kumar *et al.* This study reported an efficacious plasma concentration of pazopanib in tumour bearing mice of 40 µM. The maximum plasma concentrations observed in the pharmacokinetic experiments detailed in this chapter range between 27 and 45 µM (Kumar, Knick et al. 2007).

It is apparent from pharmacokinetic studies in Cyp3a cluster knockout animals that Cyp3a has a negligible role in pazopanib metabolism *in vivo,* with no significant differences in pharmacokinetic parameters observed between the wild-type and Cyp3a cluster knockout animals. Further investigations using the HRN model indicate that the murine hepatic P450 system is not implicated in pazopanib metabolism, with a negligible shift occurring between the wild-type and HRN animals. Given the *in vitro* evidence suggesting that the human enzymes are more efficient at metabolising

pazopanib than the mouse, the humanised 3A4/3A7 and humanised 3A4/3A7/hCAR/hPXR animals were employed in order to assess whether this observation was reflected *in vivo.* These animals were induced as described in the Methods prior to administration of pazopanib. All inductions included a corresponding wild-type control. In keeping with the hypothesis that wild-type animals do not significantly metabolise pazopanib, neither PCN or rifampicin induction altered the pharmacokinetic parameters of pazopanib in the wild-type control group, despite induction of Cyp3a in the PCN treated animals, as shown by Western Blot. The humanised 3A4/3A7 mice show a non-significant decrease in the maximum plasma concentration and area under the curve, as well as a non-significant elevation in the rate of clearance. Despite being statistically insignificant, the trend seen in these mice suggests that the presence of human CYP3A4, induced with PCN, may play a minor role in the metabolism of pazopanib in these animals. It would be of interest to repeat this study and extend the induction protocol from two to three days to ascertain whether or not the induction of the transgene can be increased and significant changes in the pharmacokinetic parameters elicited. This experiment was repeated in the h3A4/3A7/hCAR/hPXR mouse line. Humanisation of animals for CYP3A4, and the nuclear receptors CAR and PXR, elicited a profound shift in the pharmacokinetic profile of pazopanib with a statistically significant decrease in half-life and area under the curve, and an increase in the rate of clearance, suggesting that the human CYP3A4 enzyme is significantly better at metabolising pazopanib than the mouse Cyp3a isoform, in the presence of the humanised nuclear receptors. Taken together these data suggest that while CYP3A4 is likely to contribute towards pazopanib metabolism when maximally induced in these mice, the nuclear receptors CAR and PXR may also be implicated.

4.7.3 Pazopanib and Pharmacogenomics

Pazopanib monotherapy outcome varies significantly between patients and little is known about mechanisms by which pazopanib therapy fails in certain individuals. In 2011, a study by Xu *et al.* presented evidence for genetic biomarkers which were predictive of positive pazopanib outcome. The study analysed 27 functional polymorphisms in 13 genes associated with angiogenesis or exposure and metabolism of pazopanib in 397 renal cell carcinoma patients (Xu, Bing et al. 2011) The genotypes were correlated with progression-free survival (PFS) and objective response rate (RR) in patients receiving either 800 mg/day pazopanib, or placebo. The study identified 3 polymorphisms in genes coding for interleukin 8 (IL-8) and hypoxia inducible factor 1 alpha (HIF1α) which were significantly correlated with progression-free survival, as well as 5 polymorphisms in HIF1α, PXR (nuclear receptor 1/ 2) and vascular endothelial growth factor A (VEGFA) which were significantly associated with positive RR (Xu, Bing et al. 2011). Given that our model is humanised for PXR, it was of interest to assess whether or not our mouse model reflected *in vitro* pazopanib-induced PXR activation described by the FDA. The data shown in this chapter demonstrate that pazopanib is able to activate PXR in an *in vitro* human hepatoma cell assay, which is in keeping with the literature. Chronic dosing of wild-type animals with 200 mg/kg pazopanib (*p.o.*) for 4 days, leads to a modest induction of hepatic Cyp3a in these animals. This would be expected as pazopanib is a PXR substrate, and the activation of PXR leads to an up-regulation of its target genes, including Cyp3a. Interestingly, these results are not reflected in the humanised PXR animals given the same treatment. It is worthy of note however, that these animals show higher basal levels of Cyp3a in the liver than the wild-type animals, and this may limit the inducibility of P450s in these animals.

4.7.4 Pazopanib-Induced Hepatic Failure in Humans

Pazopanib-induced liver failure occurs in approximately 0.2 % of patients receiving the drug. Fatal hepatotoxicity is associated with elevations of ALT and total bilirubin levels; however, overall elevations in ALT and total bilirubin have been observed in 53 % and 36 % of patients enrolled in clinical trials, respectively. Specific risk factors pertaining to fatal hepatotoxicity have not been identified (Keisner and Shah 2011). A recent report by Klempner *et al.* presented two case studies of patients who had succumbed to pazopanib-induced liver failure with accompanying biopsy information. Neither patient exhibited any underlying chronic liver pathology prior commencing pazopanib treatment. Both patients experienced grade 3 elevations in ALT levels by 6 weeks of pazopanib treatment, and underwent a core-biopsy at weeks 7-8. Both patients were described as exhibiting mild cholestatic hepatitis with inflammation surrounding portal tracts (Klempner, Choueiri et al. 2012).

A further aim of this research was to investigate potential differences in hepatic toxicity of pazopanib in wild-type and humanised mouse models. This was of particular interest as there is no published evidence of hepatic toxicity in pre-clinical studies using mice. The selection of the humanised 3A4/3A7/hCAR/hPXR model for these studies was made as these mice showed a significant shift in pharmacokinetic parameters when induced, and it is yet unknown whether the toxicity associated with pazopanib therapy is due to the parent compound, or a metabolite.

Livers from humanised 3A4/3A7/hCAR/hPXR animals induced with rifampicin and dosed with a high dose of pazopanib as described in **Section 4.6.9**, exhibited an enlarged, mottled liver phenotype at the time of harvest, which was not present in the wild-type animals. Sections taken from these livers showed extensive lipid-like

vacuolation when stained with haemotoxylin and eosin; however, histological stains for lipids and glycogen were negative, and confirmed by a pathologist. At a higher magnification (x 100), an unusual apoptosis-like phenotype was identified in which the nuclei in the phenotypic liver sections appear to become enlarged and collapse. This appears to be accompanied by the destruction of the surrounding cytoplasm. It can be concluded from these sections that the vacuole-like structures seen at lower magnifications are in fact 'vacant' areas in the section where cells have died. Mouse studies using rifampicin at doses of 100 mg/kg have been described and no liver damage has been reported when given as a monotherapy. However, in a study by Chowdhury *et al.* a combination therapy of isoniazid and rifampicin elicited a hepatotoxic effect through apoptosis in wild-type BALB/c mice, however neither drug was toxic when given alone. This suggests that there may be a cumulative effect of combinational therapy on liver toxicity using rifampicin (Chowdhury, Santra et al. 2006). Interestingly, the high dosing studies detailed in this chapter do not describe any liver abnormalities in wild-type mice given any treatment combination, although the humanised 3A4/3A7/hCAR/hPXR mice, when treated with rifampicin and pazopanib together, do show an abnormal liver phenotype.

4.7.5 CYP3A4 Activity and Pazopanib-Induced Liver Injury

Given that the humanised 3A4/3A7/hCAR/hPXR mouse is a multiple-humanised line, there are several aspects of this model that could be responsible for the development of this phenotype, be it the humanisation of CYP3A4/CYP3A7, or one or both of the nuclear receptors. In order to assess the role of CYP3A4 in the development of this phenotype, a pharmacological approach was adopted in which ketoconazole was co-

administered alongside rifampicin and pazopanib. Ketoconazole is a potent inhibitor of CYP3A, and exerts this inhibition by antagonising the nuclear receptors CAR and PXR, as well as the farnesol X receptor (Huang, Wang et al. 2007).

The dose of 100 mg/kg ketoconazole has been shown to abolish acetaminophen-induced hepatotoxicity in mice; however the mechanisms by with this occurs have only been speculated (Culo, Renic et al. 1995). The experiments presented in Chapter 4, however show a persistent liver phenotype in mice co-dosed with ketoconazole, suggesting that CYP3A4 is not the causative factor of this liver phenotype.

4.7.6 PXR and CAR in Liver Injury

The apparent lack of involvement of CYP3A4 suggests that the phenotype observed may be a result of the humanisation of PXR or CAR in this model, however, there is extensive evidence in the literature supporting the hypothesis that PXR is hepatoprotective against drug induced liver injury and inflammatory liver disease.

A study by Daly *et. al.* in 2010 presented evidence that patients possessing a SNP variant of PXR and as a consequence, lower levels of expression may be more susceptible to liver injury caused by flucloxacillin treatment. Patients expressing the PXR variant 'rs3814055; C-25385T' accumulated higher levels of drug in the liver, leading the formation of flucloxacillin, which in turn can result in an immune response leading to liver damage (Andrews, Armstrong et al. 2010).

There is little information in the literature regarding the role of CAR in human hepatoprotection, however several mouse studies suggest a role for CAR in the protection against bile acid toxicity. A study by Guo *et al.* showed that mice knocked out for both PXR and FXR (both bile acid sensing nuclear receptors), showed high levels of liver damage when fed a diet containing 1 % cholic acid. This toxicity was

shown to be ablated by pre-treatment of the mice with CAR activators phenobarbital (PB) or TCPOBOP. Pre-treatment of the animals with CAR activators caused a marked reduction in bile acid and bilirubin in the PXR/FXR knock-out mice, suggesting a protective roll for CAR in bile acid toxicity (Guo, Lambert et al. 2003).

Chapter 5

Syngeneic Tumour Cell Lines and Xenograft Studies

5.1 Introduction

In many xenograft studies, cell lines are selected based on a particular genotype, tumour type, or mutation. In this way it is possible to generate mouse models of specific human cancers in immunocompromised mice with which to test tailored chemotherapeutic regimens. Immunocompromised mice remain a useful model for investigating the growth patterns of human- derived tumours, as well as the efficacy of new drugs against such tumours in mice. As discussed in **Section 1.12.2** immunocompromised mice have several limitations in terms of accurately reflecting human disease, including the lack of a functional immune system, and differences in the expression and activity of cytochrome P450 enzymes, among others.

5.1.1 Discrepancies between Murine and Human Responses to Chemotherapy

It is not uncommon for anti-cancer therapies to elicit highly effective anti-cancer results in transplanted human xenografts in *nude* and *scid* mice; however these promising pre-clinical results are often followed by failure of the drug in question in clinical trials (Kerbel 2003). A study in 1989 by Giovanella *et al.* demonstrated the impressive, curative potential of the synthetic camptothecin analog, 9-AC in *nude* mice bearing human colon cancer xenografts (Giovanella, Stehlin et al. 1989). Later studies demonstrated its effectiveness against human melanoma xenografts (Pantazis, Hinz et al. 1992), and human ovarian carcinoma xenografts (Pantazis, Kozielski et al. 1993). Despite the extensive efficacy of 9-AC in *nude* mice against several human tumour types, its limited efficacy in humans led to the development of 9-AC to be halted in 1999 (Takimoto 2001). In 2001, Kirstein *et al.* analysed the

pharmacokinetics of 9-AC in paediatric solid tumour xenografts under several dosing schedules, and found that exposure of 9-AC required for maximal anti-cancer activity in the mice exceeded the maximum tolerated exposure in patients (Kirstein, Houghton et al. 2001). While xenografts in immunocompromised mice remain an essential tool for drug development, it is understandable that variations in outcome between xenograft models and human trials have led to scepticism among some researchers. This has led to the development of genetically engineered and humanised mouse models, which may better reflect the human outcome of future pre-clinical trials. Several mouse models may be employed in a study to allow a more detailed insight into the effects of the immune system, microenvironment interactions and genetics on drug pharmacokinetics and efficacy (Richmond and Su 2008).

5.1.2 Allosteric and Xenograft Tumour Growth Studies

A study by Wood *et al.* in 2000 described the pharmacological properties of an emerging tyrosine kinase inhibitor PTK787/ZK 222584 (vatalanib) in *nude* and wild-type mice. The study showed vatalanib caused a significant growth inhibition of human tumours; A-431 epidermoid carcinoma, Ls174T and HT-29 colon carcinomas and PC-3, DU145 and CWR-22 prostate carcinomas grown subcutaneously in *nude* mice. The study also utilised a syngeneic orthotopic renal cell carcinoma cell line (RENCA) in immune competent mice. Vatalanib was found to significantly reduce the rate of growth of primary tumours, as well as the incidences of metastases into the lymph nodes and lung. Furthermore, histolological analysis revealed a significant reduction in microvessel formation in primary and secondary tumours in mice treated with valatanib (Wood, Bold et al. 2000). Given the similar modes of action of valatanib

and pazopanib, it is reasonable to assume that pazopanib would be efficacious against syngeneic tumour growth *in vivo.*

5.1.3 Efficacy of Pazopanib in Tumour Growth Studies

A later study by Kumar *et al.* in 2007 described the efficacy of pazopanib against a range of human xenografts in *scid* mice. The study showed pazopanib to be efficacious against HT29 colon, A375P melanoma, PC3 prostate, Caki-2 renal, BT474 breast and H322 lung tumour xenografts, at doses as low as 20 mg/day (*p.o*). While Pazopanib is licensed for the treatment for the treatment of renal cell carcinoma, data presented in this study suggest that it has a broad anti-cancer effect *in vivo* against a variety of tumour types (Kumar, Knick et al. 2007).

The work described in this chapter attempts to assess, for the first time, whether or not pazopanib is efficacious against syngeneic, mouse- derived tumours in humanised mice, and whether or not the presence of the human transgene affected the efficacy of pazopanib compared to wild-type mice. While a renal cell carcinoma cell line would have been the primary choice for such studies, a murine renal cell carcinoma cell line was not available for use. The cells chosen were based upon successful pilot studies performed by Lesley McLaughlin (Molecular Pharmacology Group, Medical Research Institute, Ninewells Hospital and Medical School). CMT 93 cells are a mouse- derived colorectal tumour cell line, while B16 cells are a murine melanoma cell line.

5.2 Results

5.2.1 Validation of Syngeneic Cell Lines CMT 93 and B16

One aim of this research is to investigate variations in efficacy of pazopanib against tumours *in vivo*, in h3A4/3A7/hCAR/hPXR and wild-type mice. Pazopanib is an anti-angiogenic compound, and therefore elicits little cell death *in vitro*. Cytotoxicity data are displayed in **Figure 5.1.**

One further consideration when performing xenograft studies in humanised mice is the duration of transgene induction. For short term induction in pharmacokinetic studies as described earlier, rifampicin and PCN are effective inducing agents. These treatments are, however, short acting and the level of induction declines over approximately 72 h. Western blots carried out by Dr Zoe Riches (Molecular Pharmacology Group, Medical Research Institute, Ninewells Hospital and Medical School) are displayed in **Figure 5.2.a.** These Western blots show that the induction of Cyp3a/CYP3A4 in wild-type and humanised 3A4/3A7/hCAR/hPXR mice induced with either 10 mg/kg, or 60 mg/kg rifampicin (*i.p.*) for 3 days declines after 48 h after the last dose. Establishing an effective dosing regimen to maintain the expression of the transgene would require complex investigation and a great number of animals. It was therefore of interest to identify an inducing agent which would maintain a suitable level of induction of Cyp3a/CYP3A4 for a long-term protocol. Aroclor 1254 is a polychlorinated biphenyl mixture that was originally developed for industrial uses, including the manufacturing of plastics and inks, for use in capacitors, and the production of heat exchange and hydraulic fluids (Mayes, McConnell et al. 1998). Additionally, Aroclor 1254 has been shown to be a potent inducer of hepatic cytochrome P450s in mammals (Matthews, Fries et al. 1978). Its high lipophillicity

means that Aroclor 1254 is an extremely long-acting drug, and maintains CYP induction for extended time periods (Chen, Chen et al. 2003). Blots performed by Dr Zoe Riches (Molecular Pharmacology Group, Medical Research Institute, Ninewells Hospital and Medical School) confirmed that Aroclor 1254 at a dose of 500 mg/kg was sufficient to induce hepatic Cyp3a in wild type mice after 7 days (**Figure 5.2-b**). With evidence showing that it is possible to induce Cyp3a in wild-type animals using 500 mg/kg Aroclor 1254 *i.p*. an induction study was performed in h3A4/h3A7/hCAR/hPXR mice. H3A4/3A7/hCAR/hPXR mice were treated with Aroclor 1254 at 500 mg/kg *i.p.* or corn oil as a control, and culled at a series of timepoints over a period of 4 weeks. The livers were harvested and microsomes prepared as previously described. The data are displayed in **Figure 5.2-c.** and show a robust induction that persists over the 4 week period.

a)

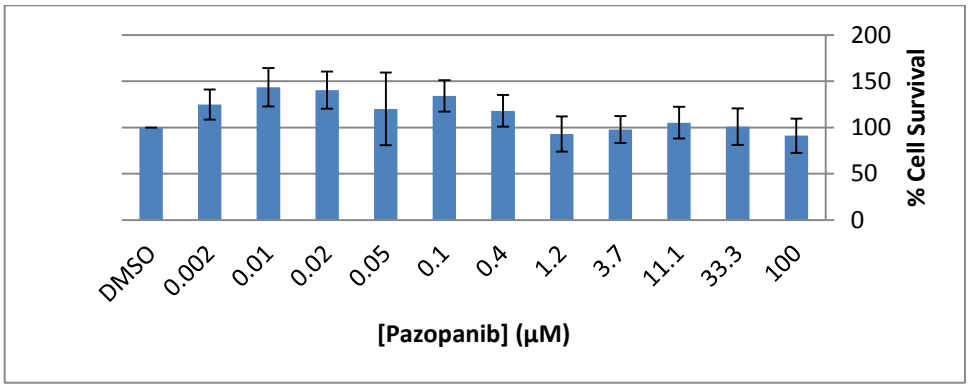

b)

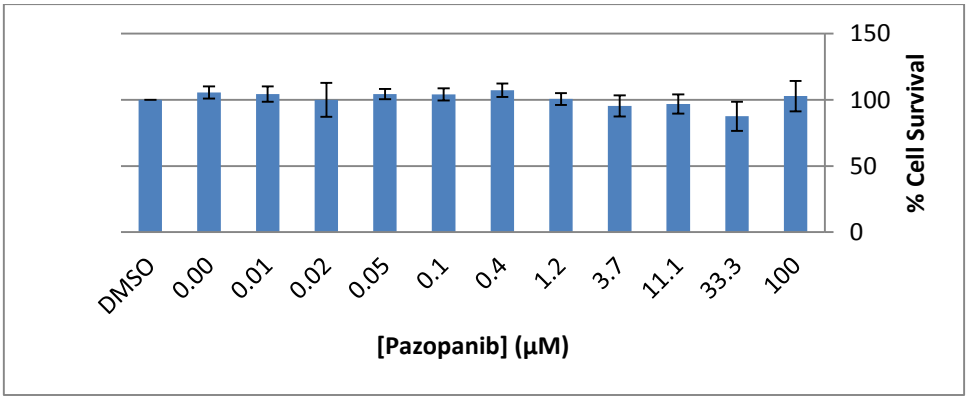

c)

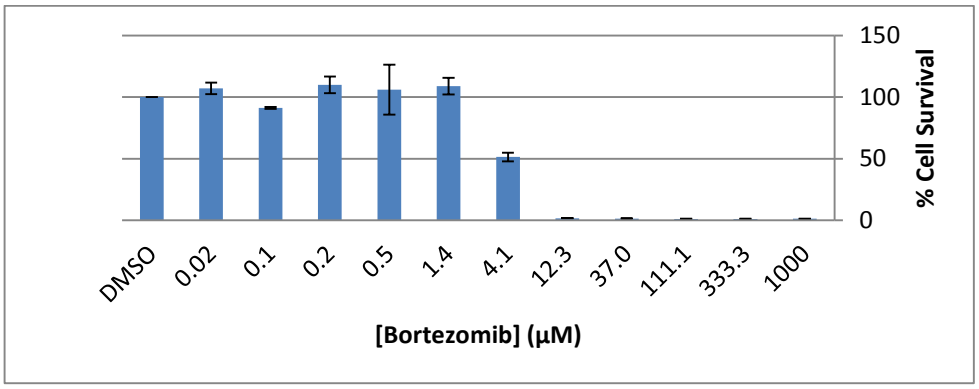

Figure 5.1. *In Vitro* Experiments to determine pazopanib efficacy against CMT 93 and B16 cells.

a) Pazopanib does not cause cytotoxic cell death in CMT 93 cells, or in B16 Melanoma cells (b), while bortezomib (c), a proteasome inhibitor and cytotoxic agent, kills efficiently *in vitro* in CMT 93 cells. Values expressed ± SD.

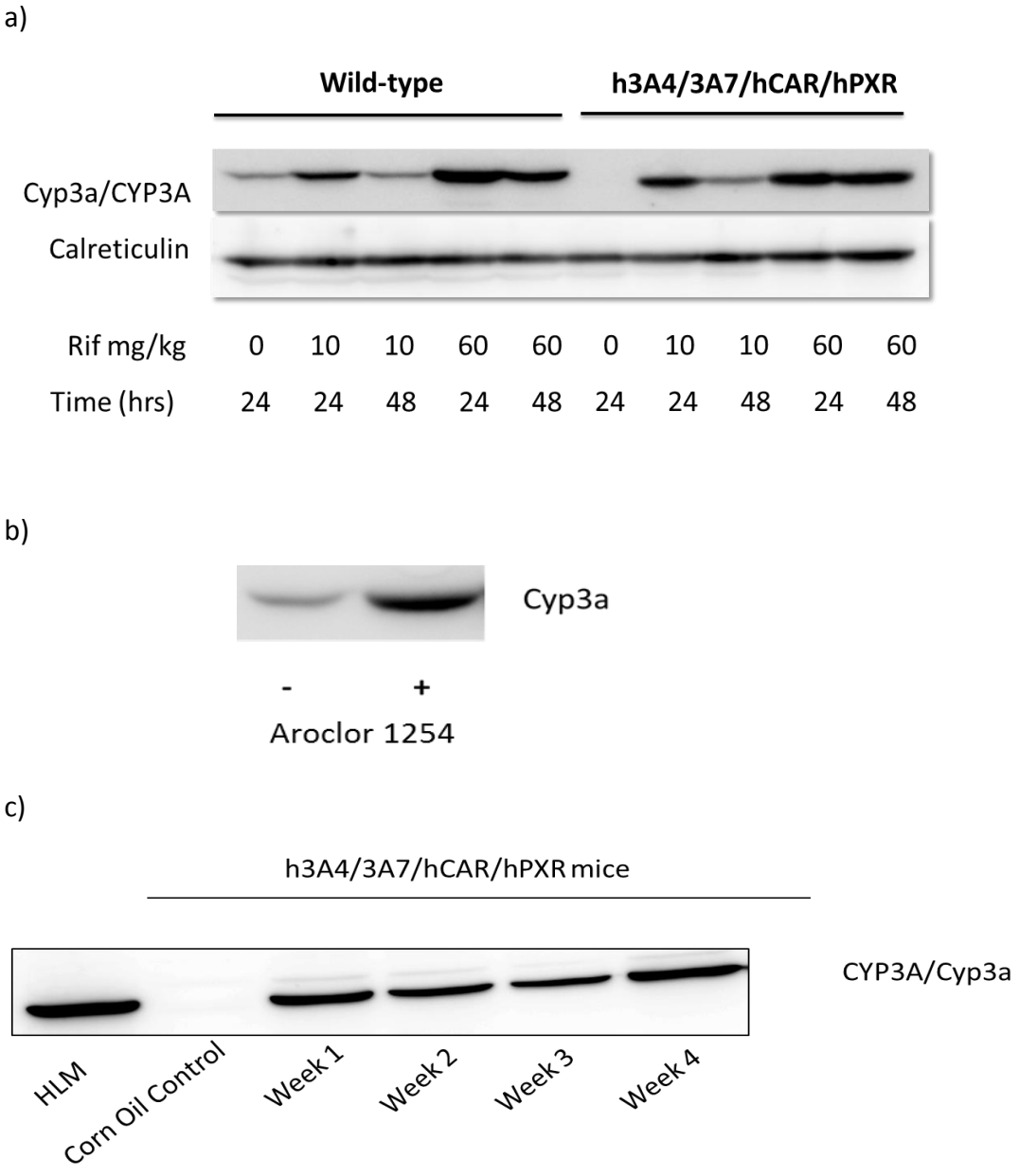

Figure 5.2. Western blots showing induction of Cyp3a/CYP3A using rifampicin and Aroclor 1254

a) Rifampicin induction of CYP3A/Cyp3a is diminished after 48 hours b) Aroclor 1254 induces Cyp3a in wild-type mice (7 days following injection) '-' indicates control treated animals, '+' indicates Aroclor 1254-treated animals. Calreticulin as a loading control c) Aroclor 1254 induced CYP3A in h3A4/3A7/hCAR/hPXR mice over a 4 week time course. Animals received a single dose of Aroclor (500 mg/kg, *i.p*), and livers were harvested weekly thereafter. n ≥ 2 animals per lane.

5.2.2 CMT 93 Pilot Study

Despite previous success in growing these cells *in vivo,* only 2 of 38 mice included in the study showed any signs of tumour development on one flank, for reasons that remain unclear. Possible explanations to account for the lack of growth include the passage number of the cells (17), or the length of time they had been in storage since their first use. Another potential contributory factor was the age of the mice used, which differed between groups and genotypes from approximately 10 weeks, to 3 months old.

5.2.3 Investigation into the Utility of the B16 Melanoma Cell Line; Growth Curves

B16 Cells are a mouse-derived melanoma cell line. These cells were injected subcutaneously in the same fashion as the CMT93 cells as previously described. Wild-type and h3A4/3A7/hCAR/hPXR mice were divided into Aroclor 1254-induced, and un-induced cohorts. The tumours developed in all mice included in the study, with 38 out of 39 mice developing tumours in both flanks. Given the aggressive nature of these cells, and the rapidity at which the tumours developed, mice were weighed and dosed, and tumours were measured daily to monitor changes. The data are displayed in **Figure 5.3.** Tumour growth was reasonably consistent among all the cohorts of mice. Average survival post inoculum differed between groups however, and data are displayed in **Figure 5.3.** It can be seen that in both wild-type and h3A4/3A7/hCAR/hPXR animals pre-treated with corn oil, pazopanib significantly improves survival compared to vehicle-treated animals. Interestingly, pre-treatment of wild-type mice with Aroclor 1254 causes a significant reduction in overall survival time compared to uninduced animals. Pre-treatment of h3A4/3A7/hCAR/hPXR

animals with Aroclor 1254 also reduces overall survival compared to corn oil treated animals; however this is not statistically significant. It would have been expected that pre-treatment of h3A4/3A7/hCAR/hPXR mice with Aroclor 1254 would have significantly increased the rate of growth of tumours, and decreased the overall survival rate of these animals due to the increased metabolism of pazopanib by the induced CYP3A4, and subsequent decrease in exposure to the parent drug. It is possible that while inducing CYP3A4 using Aroclor 1254, the induction may not be great enough to alter the pharmacokinetics of pazopanib to the degree to which efficacy would be affected. Data presented in Chapter 4, **Figure 4.5** and **Table 4.1,** show a significant decrease in exposure of h3A4/3A7/hCAR/hPXR animals to pazopanib when induced with rifampicin compared to control animals pre-treated with corn oil (4484 ± 1213 vs 11704 ± 3149 min*µg/ml respectively). It may be that while Aroclor 1254 does induce CYP3A4 to a similar extent as rifampicin, the induction may not be sufficient to affect the efficacy of pazopanib *in vivo.* It would be necessary to carry out a pazopanib pharmacokinetic study using both inducing agents in two cohorts of mice in order to compare the exposure seen using both agents.

a)

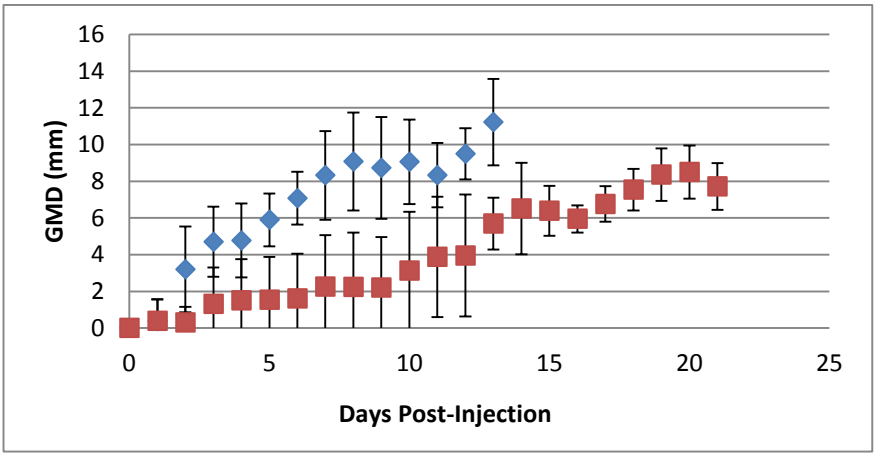

Wild-type animals treated with corn oil and vehicle (blue), or corn oil and pazopanib (red).

b)

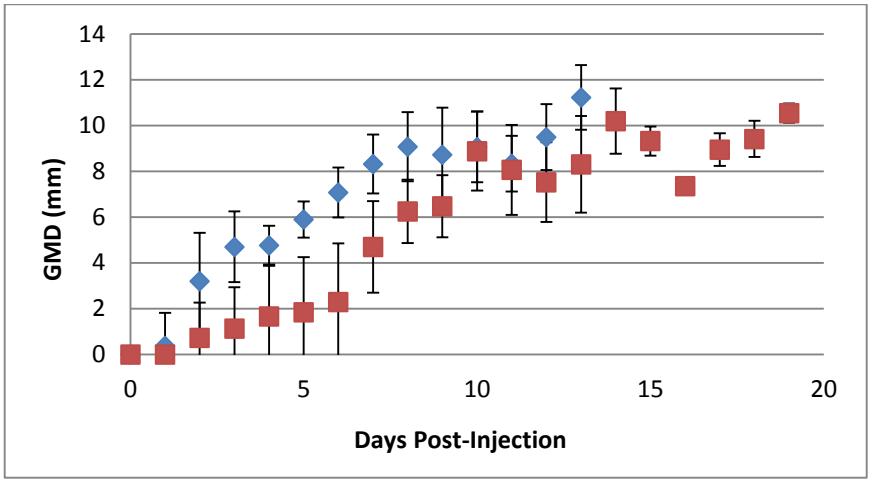

Wild-type animals treated with Aroclor 1254 and vehicle (blue), or Aroclor 1254 and pazopanib (red).

c)

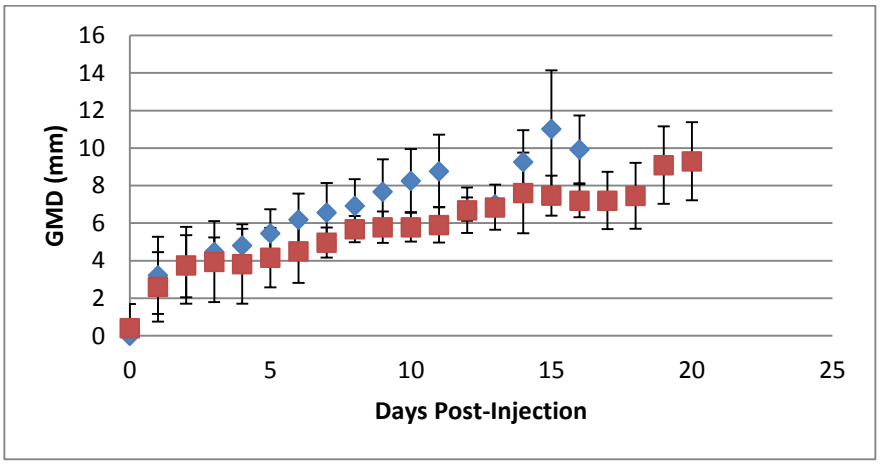

h3A4/3A7/hCAR/hPXR animals treated with corn oil and vehicle (blue), or corn oil and pazopanib (red).

d)

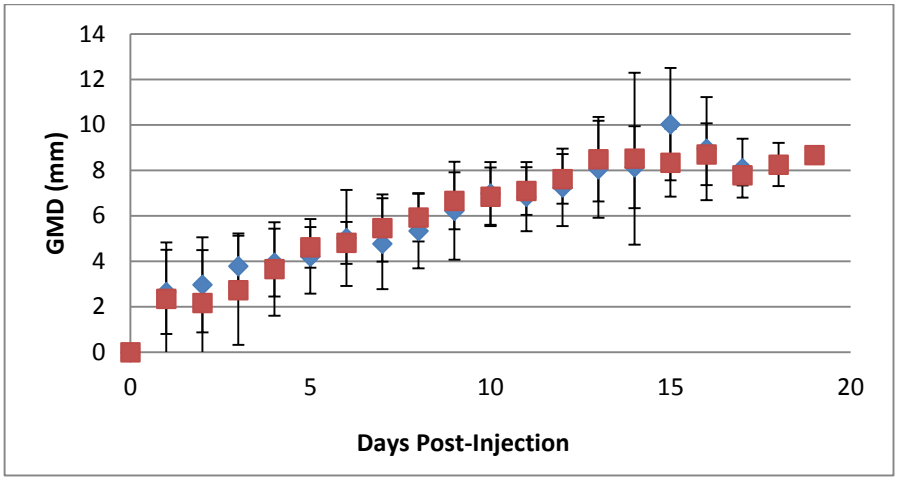

h3A4/3A7/hCAR/hPXR animals treated with Aroclor 1254 and vehicle (blue), or Aroclor 1254 and pazopanib (red).

e)

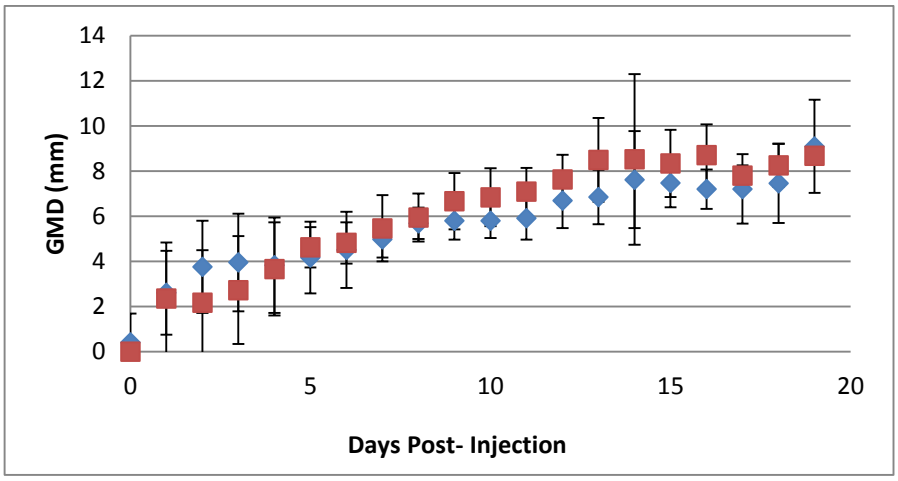

h3A4/3A7/hCAR/hPXR animals treated with corn oil and pazopanib (blue), or Aroclor 1254 and pazopanib.

f)

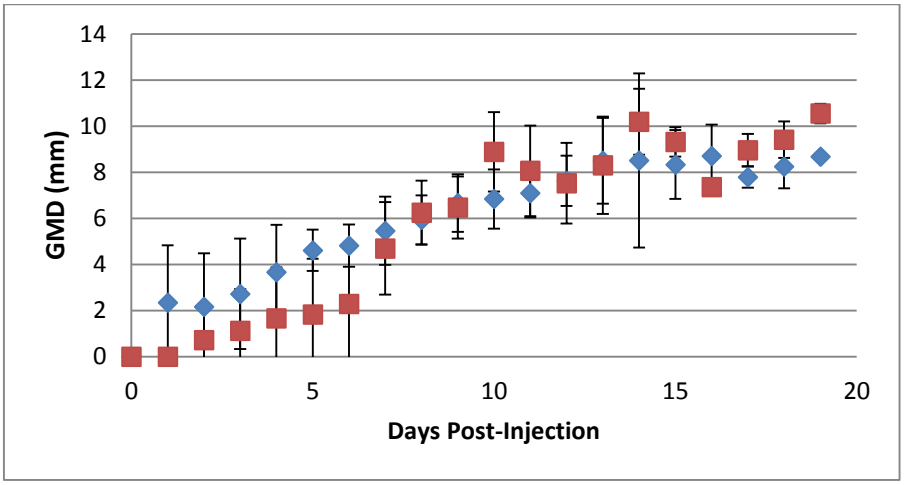

h3A4/3A7/hCAR/hPXR animals treated with Aroclor 1254 and pazopanib (blue), or, wild-type animals treated with Aroclor 1254 and pazopanib (red).

Figure 5.3. Tumour growth curves showing the growth of B16 melanoma tumours in wild-type and h3A4/3A7/hCAR/hPXR mice

Mice were pre-treated with either corn oil or Aroclor 1254, and dosed with vehicle or pazopanib. Data points show the mean tumour burden of both flanks across the entire cohort of mice. N=5 mice in all groups except h3A4/3A7/hCAR/hPXR pre-treated with corn oil and dosed with vehicle in which one mouse died prior to commencement of the experiment, giving a group n=4. Values expressed ± SD.

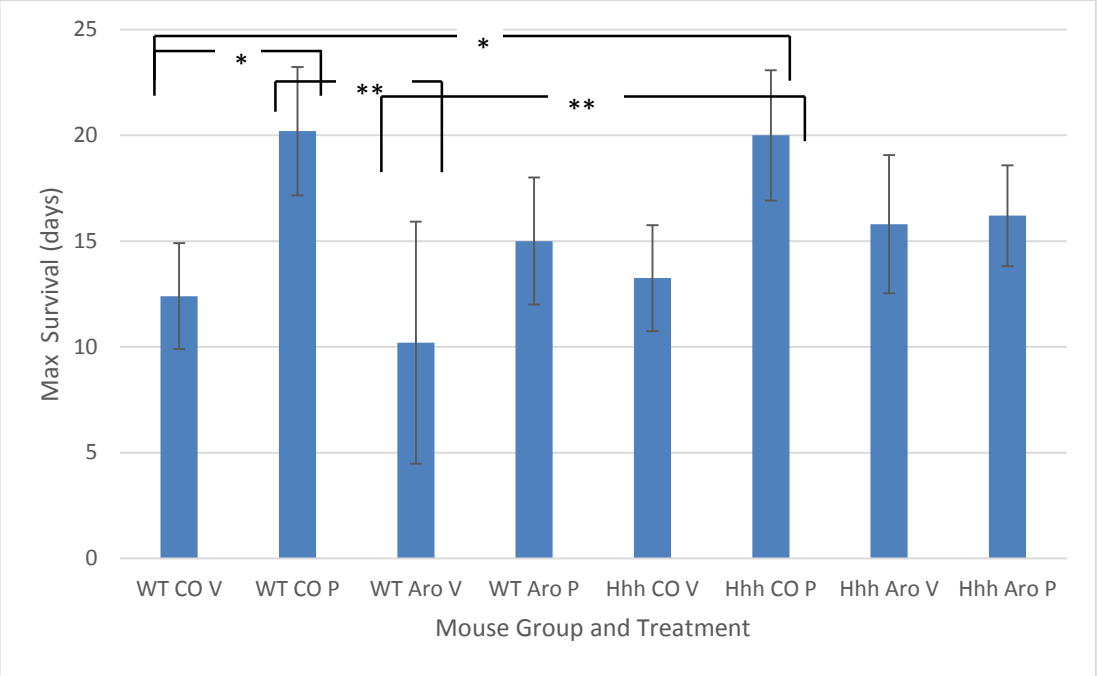

Mouse Genotype and Treatment	Maximum Survival Post-Injection (days)
Wild-type corn oil and vehicle	12.4 ± 2.5
Wild-type corn oil and pazopanib	20.2 ± 3
Wild-type Aroclor 1254 and vehicle	10.2 ± 5.7
Wild-type Aroclor 1254 and pazopanib	15 ± 3
h3A4/3A7/hCAR/hPXR corn oil and vehicle	13.3 ± 2.5
h3A4/3A7/hCAR/hPXR corn oil and pazopanib	20 ± 3
h3A4/3A7/hCAR/hPXR Aroclor 1254 and vehicle	15.8 ± 3.3
h3A4/3A7/hCAR/hPXR Aroclor 1254 and pazopanib	16.2 ± 2.4

Figure 5.4 Graph and table showing the average survival of mouse groups following the appearance of tumours in one or both flanks, and the commencement of treatment

WT corn oil and pazopanib vs WT corn oil and vehicle = * $P<0.05$, hhh corn oil and pazopanib vs WT corn oil and vehicle= * $P<0.05$, WT corn oil pazopanib vs WT Aroclor 1254 and vehicle= ** $P< 0.01$, hhh corn oil and pazopanib vs WT Aroclor 1254 and vehicle= ** $P < 0.01$. Values expressed ± SD.

5.2.4. Rate of B16 Tumour Growth from Normalised Data

Data obtained from the tumour growth curves were normalised by subtracting the initial GMD measurement from subsequent GMD measurements, i.e. the first measurable tumour GMD is considered the first measurement, and all subsequent measurements on following days have the first measurement subtracted from them. This provides a more linear plot in the early stages of growth until the growth rate increases or tumours become static. The linear sections of the normalised graphs are displayed in **Figure 5.5.** By normalising the data and obtaining the linear section of the growth curve, it is possible to calculate the initial rate of tumour growth per day by selecting a linear section of the plot and dividing the latest measurement by the earliest measurement, divided by the number of days elapsed. The mean initial growth rates of the tumours are detailed in **Table 5.1.** Statistical analysis was performed by means of a paired t-test.

a)

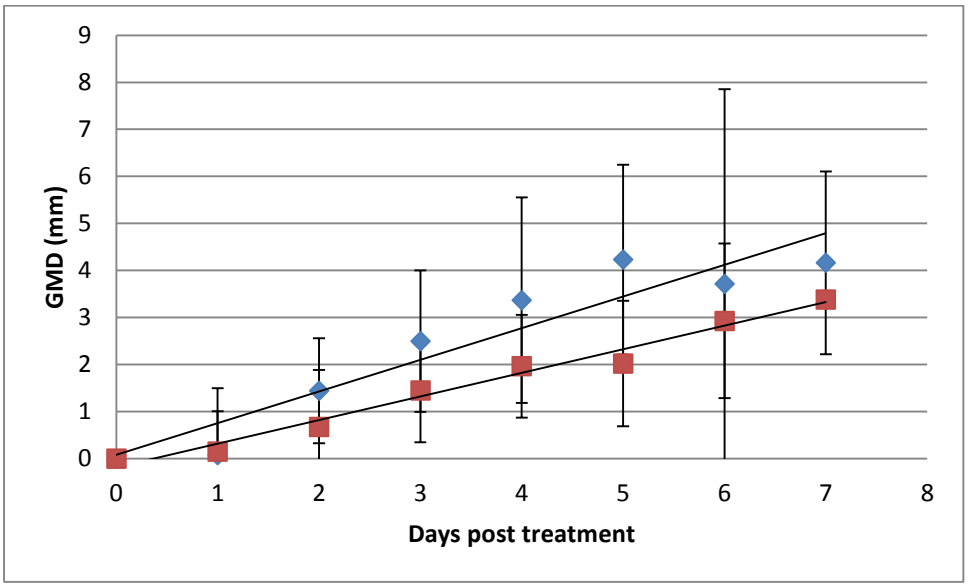

Wild-type animals treated with corn oil and vehicle (blue), or, corn oil and pazopanib (red). *, $P< 0.05$.

b)

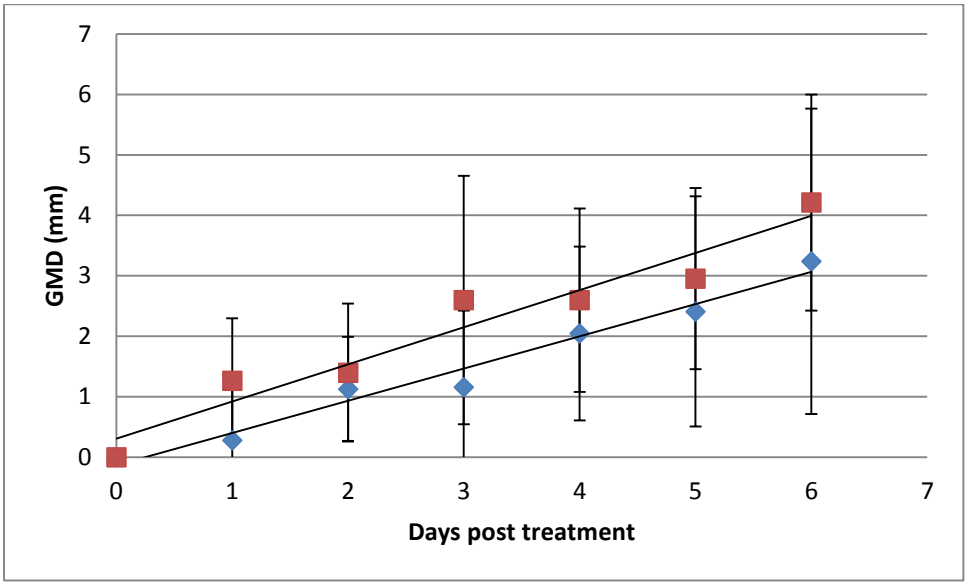

Wild-type animals treated with Aroclor 1254 and vehicle (blue), or, Aroclor 1254 and pazopanib (red). **, *P*<0.01

c)

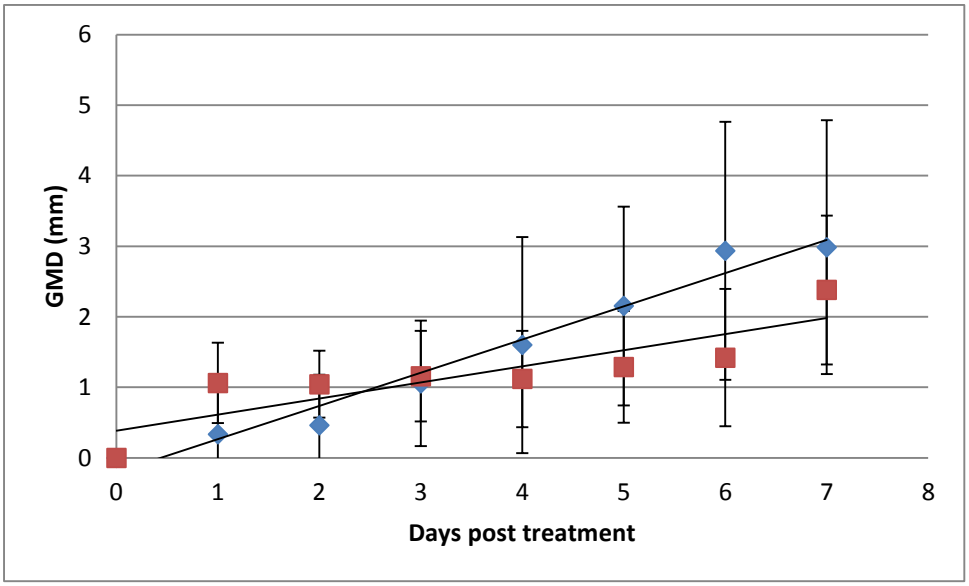

h3A4/3A7/hCAR/hPXR animals treated with corn oil and vehicle (blue), or, corn oil and pazopanib (red). No statistically significant difference was observed.

d)

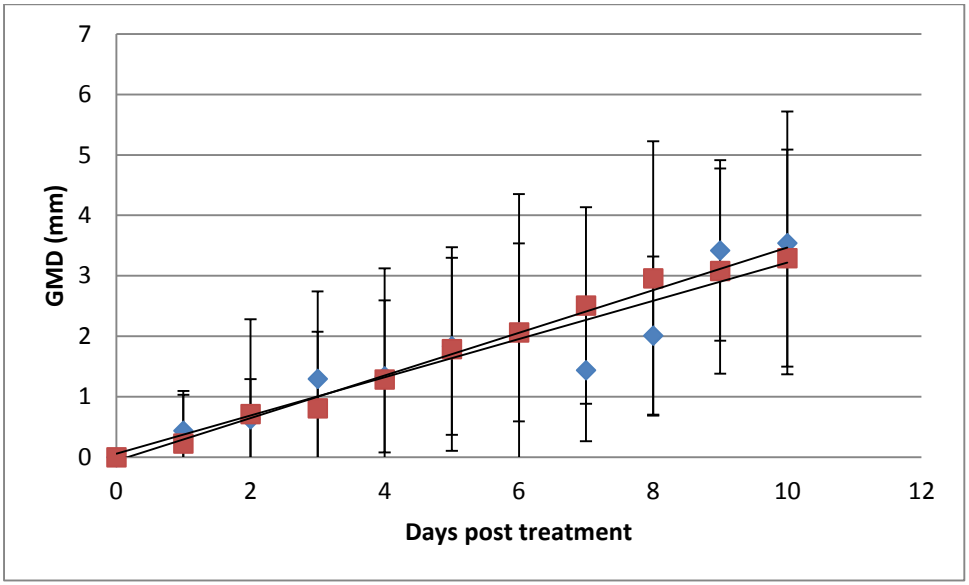

h3A4/3A7/hCAR/hPXR animals treated with Aroclor 1254 and vehicle (blue), or, Aroclor 1254 and pazopanib (red). No statistically significant difference was observed.

e)

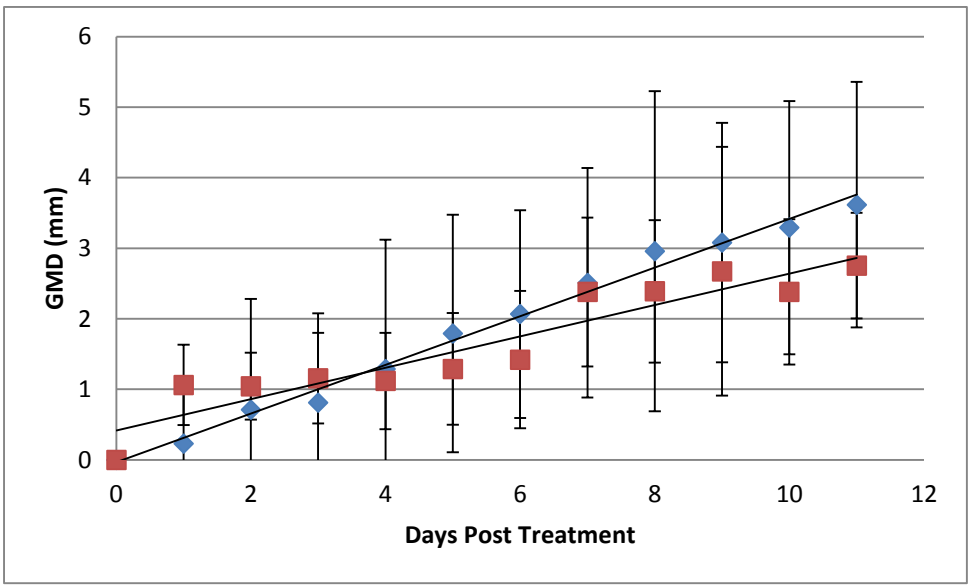

h3A4/3A7/hCAR/hPXR animals treated with Aroclor 1254 and pazopanib (blue), or, corn oil and pazopanib (red). No statistically significant difference was observed.

f)

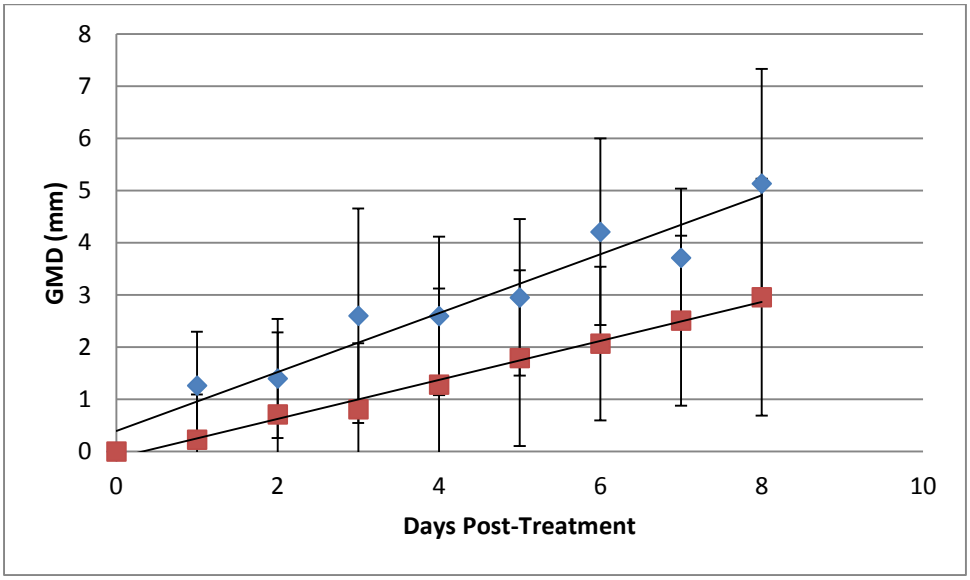

Wild-type animals treated with Aroclor 1254 and pazopanib (blue), or, h3A4/3A7/hCAR/hPXR animals treated with Aroclor 1254 and pazopanib (red). **, $P < 0.01$.

Figure 5.5. Graphs showing normalised linear growth rate curves of B16 melanoma tumour in wild-type and h3A4/3A7/hCAR/hPXR mice pre-treated with either corn oil or Aroclor 1254, and dosed with vehicle or pazopanib.

Data points show the mean tumour burden of both flanks across the entire cohort of mice. Data was normalised by subtracting the first GMD measurement from subsequent measurements. N=5 mice in all groups except h3A4/3A7/hCAR/hPXR pre-treated with corn oil and dosed with vehicle in which one mouse died prior to commencement of the experiment, giving a group n=4. Values expressed ± SD.

Mouse Genotype and Treatment	Rate of Initial Growth (mm^2) / day
Wild-type corn oil and vehicle	7.8
Wild-type corn oil and pazopanib	3.35
Wild-type Aroclor 1254 and vehicle	1.9
Wild-type Aroclor 1254 and pazopanib	0.6
h3A4/3A7/hCAR/hPXR corn oil and vehicle	1.2
h3A4/3A7/hCAR/hPXR corn oil and pazopanib	0.3
h3A4/3A7/hCAR/hPXR Aroclor 1254 and vehicle	0.8
h3A4/3A7/hCAR/hPXR Aroclor 1254 and pazopanib	1.49

Table 5.1. Mean initial tumour growth rates in mouse treatment groups

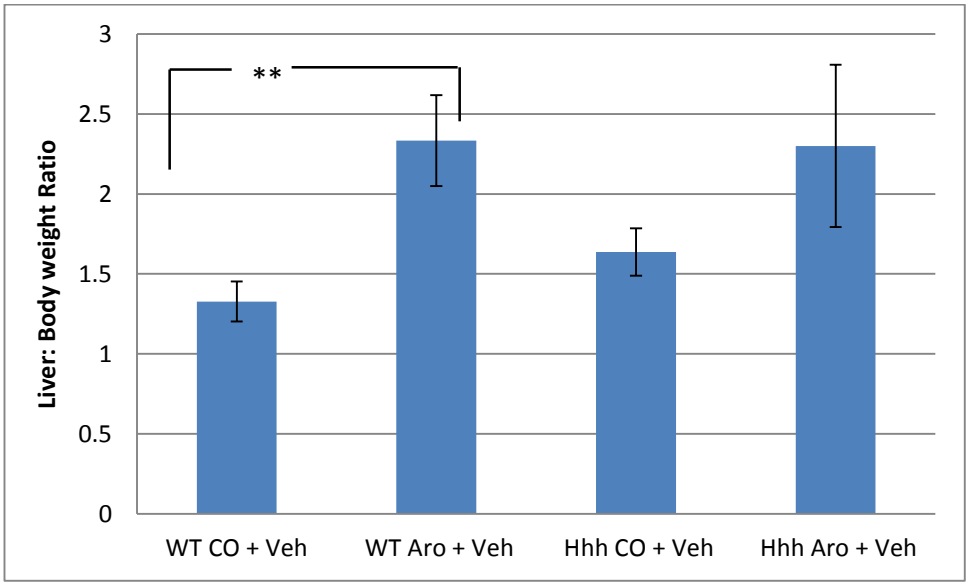

Figure 5.6. Liver to body weight ratios of wild-type and h3A4/3A7/hCAR/hPXR mice treated with corn oil or Aroclor 1254 and vehicle

Aroclor 1254-induced wild-type mice show enlarged livers compared to un-induced mice of the same genotype. **, $P<0.01$. Values expressed ± SD.

5.3 Discussion

5. 3.1 Summary

Data in this chapter describe the use of the polychlorinated biphenyl mixture, Aroclor 1254 as an effective long term enzyme inducing agent in mice compared to a single dose of rifampicin. A single dose of Aroclor 1254 in humanised 3A4/3A7/hCAR/hPXR mice lasts a minimum of 4 weeks, compared to rifampicin, which lasts approximately 48 hours. Furthermore, this chapter investigates the efficacy of pazopanib against syngeneic B16 melanoma tumours *in vivo,* in wild-type and humanised 3A4/3A7/hCAR/hPXR. Pazopanib significantly improved the survival of both genotypes following tumour implantation compared to vehicle treated animals. Interestingly, induction of cytochrome P450s by Aroclor 1254 did not have a radical effect on initial tumour growth rate, or survival.

5.3.2 Induction of Hepatic P450s by Aroclor 1254

Data described in this chapter show that a single dose of Aroclor 1254 (500 mg/kg, *i.p*) is sufficient to induce hepatic P450s in mice for a minimum of 4 weeks. This is consistent with several published studies in rodents, which have shown significant induction of cytochromes P450 in rodent liver following exposure to Aroclor 1254 (Easterbrook, Fackett et al. 2001). It is clear that Aroclor 1254 is a useful compound for studies requiring long term induction of the cytochromes P450; however, Aroclor 1254 is harmful and has been shown to have hepatotoxic effects. A study by Mayes *e al.* described a 24 month study, in which male and female Sprague-Dawley rats were exposed daily to various doses of Aroclor 1254 in the rat chow. Upon completion of the study, animals were killed and tissues harvested for analysis. Key findings outlined

in this study were elevated serum enzyme levels (AST and ALT), enlargement of the liver, hepatocellular hypertrophy, general discolouration of the liver, and an increased incidence of hepatocellular lesions and neoplasms. The frequency and severity of these abnormalities were dose-dependent and generally more common in females than in males (Mayes, McConnell et al. 1998).

While mice treated with Aroclor 1254 in the tumorigenesis study detailed in this chapter did not exhibit the mottled phenotype that was observed following rifampicin treatment described in Chapter 4, the livers were generally larger than corn oil treated animals at the time of harvest as can be seen in **Figure 5.5**. It would be of interest to stain liver sections of Aroclor 1254- and rifampicin-treated animals to identify any differences in liver morphology. Aroclor 1254 is a 'dirty' compound, and impacts on many different enzymes and pathways. Microarrays have been shown to be a highly sensitive technique for assessing chemical toxicity of drugs. They can be used to generate and characterise unique gene expression profiles for various drugs and models between which comparisons may be made between transcriptional expression of proteins associated with a particular toxic response. It would therefore be useful to perform microarray analysis on the livers and tumours of these induced and un-induced mice, to assess differences in gene expression. This is particularly important when considering an inducing agent such as Aroclor 1254 which has itself been shown to cause toxicity in both animals and humans, in combination with pazopanib, which also has the potential to elicit hepatotoxicity in man (Waring, Ciurlionis et al. 2001).

5.3.3 Pazopanib and B16 Melanoma Tumours

B16 melanoma cells were selected from a collection of syngeneic tumour cell lines for these tumour growth studies, based on their successful growth during a small pilot study with several syngeneic cell lines.

B16 melanoma tumours grow rapidly *in vivo* and must be monitored closely. These tumours are palpable typically between 5 and 10 days post implantation, and they have a propensity to develop ulcers which may bleed, and require the animal to be sacrificed (Overwijk and Restifo 2001). Angiogenesis is a hallmark of all solid cancers and is essential for primary tumour growth, metastasis and the growth of secondary tumours, and therefore it is reasonable to conclude that a drug capable of inhibiting angiogenesis may be useful in decreasing the rate of growth and metastasis of tumours (Ciardiello, Caputo et al. 2001).

A study by Manning *et al.* investigated the effect of sunitinib, a tyrosine kinase inhibitor developed by Pfizer which exerts its anti-cancer effect in a similar manner to pazopanib, on the growth and vascularisation of B16 melanoma tumours *in vivo.* The study began administering sunitinib to mice between 11 and 15 days following implantation of the cells. Their results showed vessel density of B16 melanoma was significantly decreased after treatment with 40 mg/kg sunitinib for 4–5 days, and melanoma growth was significantly slower (Manning 2013). This result reflects well the findings presented in this Chapter, which show that pazopanib significantly slows the rate of growth of B16 melanoma tumours in wild-type mice, as well as significantly improving their overall survival time. While data described in Chapter 5 does show tumour growth to slowing and beginning to plateau in mice receiving pazopanib, no tumour regression was observed. It is possible that tumour regression

may occur at higher daily doses of pazopanib, however, it is likely that toxicity issues would be encountered. Interestingly, the study by Manning *et al,* described the vascular heterogeneity of B16 melanoma tumours as being phenotypically zonal, with the peripheral tortuous zone vasculature proving sensitive to sunitinib chemotherapy, while the immediate sprouting vascular zone was refractory to sunitinib (Manning 2013). This may suggest that pazopanib, similarly to sunitinib is effective against one zone, and combination therapy of pazopanib and an adjuvant drug may elicit tumour regression in mice. Such a result may lead to better patient outcomes.

A study by Podar *et al,* in 2006 demonstrated that combined treatment regimens of pazopanib, bortezomib, and melphalan induce synergistic cytotoxicity in a multiple myeloma cell- endothelial cell co-culture. Such *in vitro* multiple myeloma co-culture experiments have typically proven to be highly predictive of patient responses, and the data presented in this study strongly suggest a role of low-dose pazopanib in a combination therapy with other chemotherapeutic agents as a method of improving tolerability and efficacy of chemotherapy, as well as overcoming dose-limiting toxicity as drugs may be given at lower doses when combined with another chemotherapeutic agent (Podar, Tonon et al. 2006). Combination therapy has also been used effectively *in vivo,* with promising results for the treatment of ovarian cancer. Ovarian cancer is typically very difficult to treat as patients often present with late stage disease. Furthermore, the development of chemoresistance to initially successful chemotherapy is common. A study by Faratian *et al.* described the use of trastuzumab in combination with pertuzumab as a combination therapy in an SKOV3 ovarian cancer xenograft model. While trastuzumab and pertuzumab slowed the growth of tumours when administered as a monotherapy, when given as a combined

therapy, complete regression of all tumours was observed. Not only was the combined therapy seen to be significantly more effective than either monotherapy, trastuzumab therapy was found to increase the sensitivity of these tumours to letrozole therapy. These findings have significant consequences for the design of personalised therapy for ovarian cancer patients, while also providing strong evidence for further investigations into combination therapies for a range of cancers (Faratian, Zweemer et al. 2011).

5.3.4 Effects of Induction on Pazopanib Efficacy

If human CYP3A4 was more heavily implicated in the metabolism of pazopanib compared with murine cyp3a, it would be expected that humanised 3A4/3A7/hCAR/hPXR mice, induced with Aroclor 1254 and treated with pazopanib, would show more rapid tumour growth and decreased survival compared to un-induced animals. It was hypothesised that the induction of the human CYP3A4 would cause pazopanib to be more rapidly metabolised than in un-induced animals, resulting in lower plasma concentrations of pazopanib. It can be seen in **Figure 5.4** that while overall survival of Aroclor 1254-induced humanised 3A4/3A7/hCAR/hPXR animals is shorter than un-induced animals, the difference is not quite significant. It may be the case that an additional dose of Aroclor 1254 may be required to maximise the induction of the CYP3A4 enzyme. Western Blots must be performed to assess the level of induction in these animals at the time of sacrifice. Furthermore, it can be seen in **Figure 5.5 e.** that Aroclor 1254 does not affect the initial rate of B16 melanoma tumour growth in humanised 3A4/3A7/hCAR/hPXR animals treated with pazopanib. The overall survival of wild-type mice was not expected to be altered by Aroclor 1254 induction, as it was shown in Chapter 4 **Figure 4.2**, that hepatic P450s were not

implicated in the metabolism of pazopanib in wild-type mice. Aroclor 1254 induction did reduce the overall survival of wild-type mice (**Figure 5.4**), however this was not significant. These data taken together raise the question of the contribution of intestinal metabolism of pazopanib. Thus far, this research has focussed on hepatic metabolism of pazopanib, as the liver is the major site of pazopanib metabolism and toxicity in humans. It is however likely that metabolism may also take place in the intestine of the mouse. It would be useful to perform further pharmacokinetic studies with pazopanib in a gut P450 knock out model such as the IE-Cpr-null model described by Zhang *et al.* (Zhang, Fang et al. 2009) in order to compare the pharmacokinetic profile to that seen in the HRN mouse.

Chapter 6

Final Conclusions

6.1 Final Conclusions and Further Work

This thesis attempted to investigate the activity of the novel tyrosine kinase inhibitor, pazopanib *in vitro* and *in vivo* in a panel of powerful humanised mice. Furthermore, the efficacy of pazopanib against syngeneic tumour cell lines *in vivo* was investigated. The research detailed in Chapter 3 is concerned with the *in vitro* metabolism of pazopanib in human liver microsomes, mouse liver microsomes and recombinant cytochrome P450 enzymes. Metabolism of pazopanib in a panel of human and mouse recombinant cytochrome P450 enzymes is in-keeping with the information presented by GSK, with CYP3A4 being the major contributor to pazopanib metabolism, with minor contributions from CYP2C8 and CYP1A2 (Agency 2013). One enzyme that showed pazopanib metabolising capacity which is not identified as being implicated *in* vivo by GSK, was CYP-1A1. This seemingly anomalous result may be attributed to the artificial nature of the experimental conditions. Furthermore, Chapter 3 demonstrated that humanised CYP3A4/3A7 mouse liver microsomes better reflect the metabolic capacity of human liver microsomes *in vitro,* suggesting that humanised mice may present a better model system for *in vitro* metabolic stability testing of emerging drugs compared to wild-type mice.

The data described in Chapter 4 is concerned with the pharmacokinetics of pazopanib in humanised 3A4/3A7, h3A4/3A7/hCAR/hPXR, Cyp3a knock-out and hepatic reductase null mouse models. Interestingly, results show that Cyp3a, and indeed any murine hepatic Cyps are not significantly implicated in the metabolism of pazopanib *in vivo.* The pharmacokinetics of pazopanib is altered in humanised mice in which the human CYP3A4 and CYP3A7 enzymes are present and induced. This suggests that a species difference exists between wild-type and humanised mice with regards to pazopanib metabolism. These data are in agreement with the *in vitro* data in Chapter

3 which illustrated faster metabolism of pazopanib by human liver microsomes compared to wild-type mouse liver microsomes. Additionally, differences in liver phenotypes following treatment with rifampicin and administration of high dose pazopanib were observed between wild-type and h3A4/3A7/hCAR/hPXR animals, with wild-type mice showing no changes in liver morphology and humanised mice showing a mottled, enlarged liver phenotype. This phenotype persists in h3A4/3A7/hCAR/hPXR mice pre-treated with ketoconazole, suggesting that CYP3A4 is not the causative factor. It would therefore be of interest to perform a microarray analysis on these livers to identify possible pathways involved in the development of this phenotype, and the mechanisms by which it arises.

Chapter 5 outlined preliminary studies into the growth of syngeneic B16 melanoma tumours in wild type and humanised 3A4/3A7/hCAR/hPXR mice, and their response to pazopanib with and without induction of the cytochrome P450s by Aroclor 1254. This is the first time pazopanib has been utilised in humanised mice bearing syngeneic B16 melanoma tumours. The data show that both wild-type and humanised 3A4/3A7/hCAR/hPXR show retarded tumour development when treated with pazopanib compared to control treated animals. It would be of interest to measure the plasma levels of pazopanib in tumour bearing animals to correlate any differences in steady state drug concentration with tumour response. Furthermore, high doses of pazopanib, administered over an extended period of time may have an effect on blood chemistry in these mice, which would be of interest to assess. Western blots on the liver microsomes and tumours harvested from these animals should be carried out to identify any differences in P450 expression between the treatment groups which again may be correlated with the efficacy of pazopanib between the wild-type and h3A4/3A7/hCAR/hPXR genotypes and treatments. This study involved repeated

high dosing of pazopanib or vehicle to induced and uninduced wild-type and h3A4/3A7/hCAR/hPXR animals. Sectioning of livers taken from these animals, coupled with micro-array analysis, may offer further insight into the origin of the abnormal liver phenotype described in Chapter 4. Given that pazopanib is an angiogenesis inhibitor, it would be of great interest to section excised melanoma tumours to carry out CD31 staining for vasculature in order to ascertain the effect of pazopanib in the development of these tumours.

This thesis is the first example of the utility of the humanised 3A4/3A7/hCAR/hPXR mouse as a pre-clinical model of human disease and drug metabolism. When compared to wild-type mice, the humanised 3A4/3A7/hCAR/hPXR mouse offers a better model of human metabolism of pazopanib *in vitro* and *in vivo.* The data described in this thesis provide compelling evidence which supports the use of humanised animal models in pre-clinical research, and may have significant implications in the fields of drug discovery, as well as personalised medicine and cancer modelling.

Appendix 1

Enzyme Measured	Assay
Total P450	Omura and Sato
OR	Cytochrome c Reductase
Cytochrome b_5	Spectrophotometric
CYP1A2	Phenacetin O-deethylase
CYP2A6	Coumarin 7-hydroxylase
CYP2B6	(S)-Mephynytoin N-Demethylase
CYP2C8	Paclitaxel 6α-hydroxylase
CYP2C9	Diclofenac 4'-hydroxylase
CYP2C19	(S)-Mephenytoin 4'-hydroxylase
CYP2D6	Bufuralol 1'-hydroxylase (the amount of activity inhibited by 1μM quinidine)
CYP2E1	Chlorzoxazone 6-hydroxylase
CYP3A4	Testosterone 6β-hydroxylase
CYP4A11	Lauric acid 12-hydroxylase

Table 6.1: P450 enzymes in human liver microsomes and the assays by which they are measured

Enzyme Measured	Donor 1	Donor 2	Donor 3	Donor 4	Donor 5	Donor 6
Total P450	400 pmol/mg	450 pmol/mg	210 pmol/mg	380 pmol/mg	96 pmol/mg	620 pmol/mg
OR	290	320	220	340	200	320
Cytochrome b_5	260 pmol/mg	1100 pmol/mg	270 pmol/mg	700 pmol/mg	450 pmol/mg	690 pmol/mg
CYP1A2	880	640	150	340	570	430
CYP2A6	1900	680	730	730	400	2100
CYP2B6	110	67	60	50	15	60
CYP2C8	310	240	97	110	100	230
CYP2C9	3900	3300	3600	560	3600	3000
CYP2C19	100	0	29	3	34	29
CYP2D6	91	63	160	70	86	30
CYP2E1	1700	3000	2700	3000	1700	940
CYP3A4	13700	970	2100	6900	4100	16000
CYP4A11	2100	980	2000	2100	2700	1300

Enzyme Measured	Donor 7	Donor 8	Donor 9	Donor 10	Donor 11	Donor 12
Total P450	360 pmol/mg	400 pmol/mg	440 pmol/mg	250 pmol/mg	170 pmol/mg	1200 pmol/mg
OR	280	130	290	270	96	260
Cytochrome b_5	350 pmol/mg	740 pmol/mg	690 pmol/mg	430 pmol/mg	500 pmol/mg	1000 pmol/mg
CYP1A2	240	110	700	570	84	260
CYP2A6	1500	1200	930	460	430	2100
CYP2B6	58	69	59	21	ND	98
CYP2C8	140	280	190	26	160	960
CYP2C9	5500	2100	5400	1200	2900	5400
CYP2C19	18	13	19	450	12	89
CYP2D6	73	81	250	7.3	46	180
CYP2E1	2900	1600	4100	960	860	1100
CYP3A4	7400	5700	6200	4800	2600	15000
CYP4A11	1800	450	2600	2500	1500	5300

Enzyme Measured	Donor 13	Donor 14
Total P450	250 pmol/mg	770 pmol/mg
OR	260	250
Cytochrome b_5	370 pmol/mg	550 pmol/mg
CYP1A2	780	2100
CYP2A6	250	810
CYP2B6	39	33
CYP2C8	160	100
CYP2C9	3300	4100
CYP2C19	41	59
CYP2D6	130	18
CYP2E1	1800	2000
CYP3A4	1950	5400
CYP4A11	2000	3100

Table 6.2 : Enzyme activity in human liver microsomes from 14 individual donors

Donor	Gender	Age (yrs)	Race	Cause of Death	Medical History	Medication Given During Hospitalisation
1	F	52	A	CVA	Hypertension, Acid Reflux, Constipation	Nipride, Naloxone, Mannitol, Cerebrex, Propofol, Morphine, Crystalloids, Neosynephrine, Heparin
2	M	55	A	Aneurysm	Hypertension, Arthritis	Heparin, Mannitol, Furosemide, Solumedrol, T4, Insulin, Dopamine
3	M	63	C	CVT	Warfarin	Morphine, Midazolam
4	M	70	C	Brain Stem Infarct	Type 2 Diabetes, nsulin, Parkinsons, Appendectomy	Dopamine, Glucernia, Cimetidine, Phenytoin, Nifedipine, Ceftriaxone, Humulin, Nitroglycerine, Atropin sulphate, Maalox, Acetaminophen, ACLS protocol, Furosemide
5	M	46	C	Anoxia	Hypertension, Brain Tumour	Dopamine, Cefazolin
6	F	47	C	CVA	Mitral Valve Prolapse, Hypertension, Intestinal Ulcers, Maxide, Metoprolol	Labetolol, Hydralazine, Mannitol, Magnesium, Cefazolin
7	M	68	C	Head Trauma	N/A	N/A
8	F	62	H	Brain Infarction	Verapamil, Diltiazem, Methyldopa	Heparin, Mannitol, Dopamine, Vasopressin, Methylprednisolone, Normodyne, Phenobarbitol, Vancomycin, Thrombin, Propofol, Crystalloids
9	M	54	C	Anoxia	Malaria, Darvocet	Epinephrine, Atropine

10	F	23	C	Head Trauma	N/A	Dexamethasone, Furosemide, Mannitol, Cefazolin, Naloxone, Pancuronium, Vasopressin, Phenytoin
11	F	42	H	Intracranial Haemorrhage	Gestational Diabetes, Fexofenadine	Dopamine, Thyroxin
12	F	60	C	Head Trauma	Hypertension, Gall Bladder Removed, Ex-smoker	Opranolol, Dicyclomine, Verapamil, Alendronate, Norepinephrine
13	M	41	C	Traffic Accident	N/A	N/A
14	M	58	C	Subarachnoid Haemorrhage	COPD, Emphysema, Hypertension, Peptic Ulcer, Myocardial Infarction	Esmalol, Nitroprusside, Blood Products

Table 6.3: Human Liver microsome donor information.

Abbreviations; ‘M’ Male, ‘F’ Female, ‘A’ Asian, ‘C’ Caucasian, ‘H’ Hispanic, ‘CVT’ Cerebrovascular Trauma, ‘CVA’ Cerebrovascular Accident, ‘COPD’ Chronic Obstructive nary Disease’.

Chapter 7

References

Agency, E. M. (2013, 21.07.13). "Votrient, pazopanib." Retrieved 15.01.14, 2014, from http://www.ema.europa.eu/docs/en_GB/document_library/EPAR_-_Product_Information/human/001141/WC500094272.pdf.

Andrews, E., M. Armstrong, et al. (2010). "A role for the pregnane X receptor in flucloxacillin-induced liver injury." Hepatology **51**(5): 1656-1664.

Backman, J. T., K. T. Kivisto, et al. (1998). "The area under the plasma concentration-time curve for oral midazolam is 400-fold larger during treatment with itraconazole than with rifampicin." European journal of clinical pharmacology **54**(1): 53-58.

Balciunaite, G., M. P. Keller, et al. (2002). "Wnt glycoproteins regulate the expression of FoxN1, the gene defective in nude mice." Nature immunology **3**(11): 1102-1108.

Balis, F. M. (2002). "Evolution of anticancer drug discovery and the role of cell-based screening." J Natl Cancer Inst **94**(2): 78-79.

Baranczewski, P., A. Stanczak, et al. (2006). "Introduction to in vitro estimation of metabolic stability and drug interactions of new chemical entities in drug discovery and development." Pharmacological reports : PR **58**(4): 453-472.

Bardou-Jacquet, E., L. Legros, et al. (2013). "Effect of alcohol consumption on liver stiffness measured by transient elastography." World journal of gastroenterology : WJG **19**(4): 516-522.

Bender, R. P., R. H. Lindsey, Jr., et al. (2004). "N-acetyl-p-benzoquinone imine, the toxic metabolite of acetaminophen, is a topoisomerase II poison." Biochemistry **43**(12): 3731-3739.

Berg, J., Stryer, L. (2002). "Biochemistry". Houndmills, W. H. Freeman Publishers.

Bible, K. C., V. J. Suman, et al. (2010). "Efficacy of pazopanib in progressive, radioiodine-refractory, metastatic differentiated thyroid cancers: results of a phase 2 consortium study." The lancet oncology **11**(10): 962-972.

Blumberg, B., W. Sabbagh, Jr., et al. (1998). "SXR, a novel steroid and xenobiotic-sensing nuclear receptor." Genes & development **12**(20): 3195-3205.

Boelsterli, U. A. (2003). "Diclofenac-induced liver injury: a paradigm of idiosyncratic drug toxicity." Toxicology and applied pharmacology **192**(3): 307-322.

Bozina, N., V. Bradamante, et al. (2009). "Genetic polymorphism of metabolic enzymes P450 (CYP) as a susceptibility factor for drug response, toxicity, and cancer risk." Arhiv za higijenu rada i toksikologiju **60**(2): 217-242.

Bradford, M. M. (1976). "A rapid and sensitive method for the quantitation of microgram quantities of protein utilizing the principle of protein-dye binding." Analytical biochemistry **72**: 248-254.

Brock, N. (1996). "The history of the oxazaphosphorine cytostatics." Cancer **78**(3): 542-547.

Bushardt, R. L., E. B. Massey, et al. (2008). "Polypharmacy: misleading, but manageable." Clin Interv Aging **3**(2): 383-389.

Calderwood, S. K. (2013). "Tumor heterogeneity, clonal evolution, and therapy resistance: an opportunity for multitargeting therapy." Discovery medicine **15**(82): 188-194.

Caldwell, J., I. Gardner, et al. (1995). "An introduction to drug disposition: the basic principles of absorption, distribution, metabolism, and excretion." Toxicologic pathology **23**(2): 102-114.

Carden, C. P., D. Sarker, et al. (2010). "Can molecular biomarker-based patient selection in Phase I trials accelerate anticancer drug development?" Drug Discov Today **15**(3-4): 88-97.

Carey, E. and W. D. Carey (2010). "Noninvasive tests for liver disease, fibrosis, and cirrhosis: Is liver biopsy obsolete?" Cleveland Clinic journal of medicine **77**(8): 519-527.

Carlson, G. A., D. R. Borchelt, et al. (1997). "Genetic modification of the phenotypes produced by amyloid precursor protein overexpression in transgenic mice." Human molecular genetics **6**(11): 1951-1959.

Chen, J. J., G. S. Chen, et al. (2003). "Inhibition of CYP 1A2-dependent MROD activity in rat liver microsomes: an explanation of the hepatic sequestration of a limited subset of halogenated aromatic hydrocarbons." Environmental toxicology **18**(2): 115-119.

Chen, Y., Y. Tang, et al. (2012). "Nuclear receptors in the multidrug resistance through the regulation of drug-metabolizing enzymes and drug transporters." Biochemical pharmacology **83**(8): 1112-1126.

Chowdhury, A., A. Santra, et al. (2006). "Mitochondrial oxidative stress and permeability transition in isoniazid and rifampicin induced liver injury in mice." Journal of hepatology **45**(1): 117-126.

Ciardiello, F., R. Caputo, et al. (2001). "Inhibition of growth factor production and angiogenesis in human cancer cells by ZD1839 (Iressa), a selective epidermal growth factor receptor tyrosine kinase inhibitor." Clinical cancer research : an official journal of the American Association for Cancer Research **7**(5): 1459-1465.

Craig, D. G., C. M. Bates, et al. (2011). "Overdose pattern and outcome in paracetamol-induced acute severe hepatotoxicity." British journal of clinical pharmacology **71**(2): 273-282.

Craig, R., Stitzel, R. E. (2004). "Modern Pharmacology with Clinical Applications". Baltimore, Lippincott Williams and Wilkins.

Culo, F., M. Renic, et al. (1995). "Ketoconazole inhibits acetaminophen-induced hepatotoxicity in mice." European journal of gastroenterology & hepatology **7**(8): 757-762.

Debajyoti, D. (1978). "Biochemistry". Kolkata, Academic Publishers.

DeGorter, M. K., C. Q. Xia, et al. (2012). "Drug transporters in drug efficacy and toxicity." Annual review of pharmacology and toxicology **52**: 249-273.

Denton, P. W., J. D. Estes, et al. (2008). "Antiretroviral pre-exposure prophylaxis prevents vaginal transmission of HIV-1 in humanized BLT mice." PLoS medicine **5**(1): e16.

Desta, Z., B. A. Ward, et al. (2004). "Comprehensive evaluation of tamoxifen sequential biotransformation by the human cytochrome P450 system in vitro: prominent roles for CYP3A and CYP2D6." The Journal of pharmacology and experimental therapeutics **310**(3): 1062-1075.

DiMasi, J. A., R. W. Hansen, et al. (2003). "The price of innovation: new estimates of drug development costs." Journal of health economics **22**(2): 151-185.

Dvorak, H. F. (2002). "Vascular permeability factor/vascular endothelial growth factor: a critical cytokine in tumor angiogenesis and a potential target for diagnosis and therapy." Journal of clinical oncology : official journal of the American Society of Clinical Oncology **20**(21): 4368-4380.

Easterbrook, J., D. Fackett, et al. (2001). "A comparison of aroclor 1254-induced and uninduced rat liver microsomes to human liver microsomes in phenytoin O-deethylation, coumarin 7-hydroxylation, tolbutamide 4-hydroxylation, S-mephenytoin 4'-hydroxylation, chloroxazone 6-hydroxylation and testosterone 6beta-hydroxylation." Chemico-biological interactions **134**(3): 243-249.

Eden, S. (1979). "Age- and sex-related differences in episodic growth hormone secretion in the rat." Endocrinology **105**(2): 555-560.

Ekroos, M. and T. Sjogren (2006). "Structural basis for ligand promiscuity in cytochrome P450 3A4." Proceedings of the National Academy of Sciences of the United States of America **103**(37): 13682-13687.

Ellis, G. A. and D. R. Blake (1993). "Why are non-steroidal anti-inflammatory drugs so variable in their efficacy? A description of ion trapping." Annals of the rheumatic diseases **52**(3): 241-243.

Ensoli, B., P. Markham, et al. (1994). "Block of AIDS-Kaposi's sarcoma (KS) cell growth, angiogenesis, and lesion formation in nude mice by antisense oligonucleotide targeting basic fibroblast growth factor. A novel strategy for the therapy of KS." The Journal of clinical investigation **94**(5): 1736-1746.

Faratian, D., A. J. Zweemer, et al. (2011). "Trastuzumab and pertuzumab produce changes in morphology and estrogen receptor signaling in ovarian cancer xenografts revealing new treatment strategies." Clinical cancer research : an official journal of the American Association for Cancer Research **17**(13): 4451-4461.

FDA (2012) "Voitrient."

Figlin, R., C. Sternberg, et al. (2012). "Novel agents and approaches for advanced renal cell carcinoma." The Journal of urology **188**(3): 707-715.

Forrester, L. M., C. J. Henderson, et al. (1992). "Relative expression of cytochrome P450 isoenzymes in human liver and association with the metabolism of drugs and xenobiotics." The Biochemical journal **281 (Pt 2)**: 359-368.

Gelmon, K. (2008). "Part II: Milestones in personalised medicine--trastuzumab." Lancet Oncol **9**(7): 698.

Ghibellini, G., E. M. Leslie, et al. (2006). "Methods to evaluate biliary excretion of drugs in humans: an updated review." Molecular pharmaceutics **3**(3): 198-211.

Gibson, G., Skett, P. (2001). "Introduction to Drug Metabolism". Andover, Cengage Learning EMEA.

Gillette, J. R. (1971). "Factors affecting drug metabolism." Annals of the New York Academy of Sciences **179**: 43-66.

Giovanella, B. C., J. S. Stehlin, et al. (1989). "DNA topoisomerase I--targeted chemotherapy of human colon cancer in xenografts." Science **246**(4933): 1046-1048.

GlaxoSmithKline (2013) "VOTRIENT."

Gonzalez, F. J. (2005). "Role of cytochromes P450 in chemical toxicity and oxidative stress: studies with CYP2E1." Mutation research **569**(1-2): 101-110.

Gossler, A., T. Doetschman, et al. (1986). "Transgenesis by means of blastocyst-derived embryonic stem cell lines." Proceedings of the National Academy of Sciences of the United States of America **83**(23): 9065-9069.

Gottesman, M. M. (2002). "Mechanisms of cancer drug resistance." Annu Rev Med **53**: 615-627.

Gough, A. C., J. S. Miles, et al. (1990). "Identification of the primary gene defect at the cytochrome P450 CYP2D locus." Nature **347**(6295): 773-776.

Graham, M. J. and B. G. Lake (2008). "Induction of drug metabolism: species differences and toxicological relevance." Toxicology **254**(3): 184-191.

Grover, A. and L. Z. Benet (2009). "Effects of drug transporters on volume of distribution." The AAPS journal **11**(2): 250-261.

Guo, G. L., G. Lambert, et al. (2003). "Complementary roles of farnesoid X receptor, pregnane X receptor, and constitutive androstane receptor in protection against bile acid toxicity." The Journal of biological chemistry **278**(46): 45062-45071.

Hagenbuch, B. (2010). "Drug uptake systems in liver and kidney: a historic perspective." Clin Pharmacol Ther **87**(1): 39-47.

Hapgood, R. (2003). "The potential and limitations of personalised medicine in primary care." Br J Gen Pract **53**(497): 915-916.

Harmsen, S., I. Meijerman, et al. (2009). "Nuclear receptor mediated induction of cytochrome P450 3A4 by anticancer drugs: a key role for the pregnane X receptor." Cancer Chemother Pharmacol **64**(1): 35-43.

Hasegawa, M., Y. Kapelyukh, et al. (2011). "Quantitative prediction of human pregnane X receptor and cytochrome P450 3A4 mediated drug-drug interaction in a novel multiple humanized mouse line." Molecular pharmacology **80**(3): 518-528.

Hasemann, C. A., R. G. Kurumbail, et al. (1995). "Structure and function of cytochromes P450: a comparative analysis of three crystal structures." Structure **3**(1): 41-62.

Hassan, M., U. S. Svensson, et al. (1999). "A mechanism-based pharmacokinetic-enzyme model for cyclophosphamide autoinduction in breast cancer patients." Br J Clin Pharmacol **48**(5): 669-677.

Henderson, C. J., D. M. Otto, et al. (2003). "Inactivation of the hepatic cytochrome P450 system by conditional deletion of hepatic cytochrome P450 reductase." J Biol Chem **278**(15): 13480-13486.

Henderson, C. J., D. M. Otto, et al. (2003). "Knockout mice in xenobiotic metabolism." Drug Metab Rev **35**(4): 385-392.

Hickman, S. E., E. K. Allison, et al. (2008). "Microglial dysfunction and defective beta-amyloid clearance pathways in aging Alzheimer's disease mice." The Journal of neuroscience : the official journal of the Society for Neuroscience **28**(33): 8354-8360.

Higgins, M. J. and V. Stearns (2010). "CYP2D6 polymorphisms and tamoxifen metabolism: clinical relevance." Curr Oncol Rep **12**(1): 7-15.

Hill, A. V. (1913). "The Combinations of Haemoglobin with Oxygen and with Carbon Monoxide. I." The Biochemical journal **7**(5): 471-480.

Hinson, J. A. and P. G. Forkert (1995). "Phase II enzymes and bioactivation." Canadian journal of physiology and pharmacology **73**(10): 1407-1413.

Huang, G., C. Tong, et al. (2011). "Beyond knockout rats: new insights into finer genome manipulation in rats." Cell cycle **10**(7): 1059-1066.

Huang, H., H. Wang, et al. (2007). "Inhibition of drug metabolism by blocking the activation of nuclear receptors by ketoconazole." Oncogene **26**(2): 258-268.

Hucker, H. B. (1970). "Species differences in drug metabolism." Annual review of pharmacology **10**: 99-118.

Hudziak, R. M., G. D. Lewis, et al. (1989). "p185HER2 monoclonal antibody has antiproliferative effects in vitro and sensitizes human breast tumor cells to tumor necrosis factor." Mol Cell Biol **9**(3): 1165-1172.

Hurwitz, H. I., A. Dowlati, et al. (2009). "Phase I trial of pazopanib in patients with advanced cancer." Clinical cancer research : an official journal of the American Association for Cancer Research **15**(12): 4220-4227.

Iannaccone, P. M. and H. J. Jacob (2009). "Rats!" Dis Model Mech **2**(5-6): 206-210.

Ihunnah, C. A., M. Jiang, et al. (2011). "Nuclear receptor PXR, transcriptional circuits and metabolic relevance." Biochimica et biophysica acta **1812**(8): 956-963.

Ittner, L. M. and J. Gotz (2007). "Pronuclear injection for the production of transgenic mice." Nature protocols **2**(5): 1206-1215.

Iwamoto, F. M., K. R. Lamborn, et al. (2010). "Phase II trial of pazopanib (GW786034), an oral multi-targeted angiogenesis inhibitor, for adults with recurrent glioblastoma (North American Brain Tumor Consortium Study 06-02)." Neuro-oncology **12**(8): 855-861.

Jones, H. M. and J. B. Houston (2004). "Substrate depletion approach for determining in vitro metabolic clearance: time dependencies in hepatocyte and microsomal incubations." Drug metabolism and disposition: the biological fate of chemicals **32**(9): 973-982.

Juliano, R. L. and V. Ling (1976). "A surface glycoprotein modulating drug permeability in Chinese hamster ovary cell mutants." Biochim Biophys Acta **455**(1): 152-162.

Kato, R. and K. Onoda (1970). "Studies on the regulation of the activity of drug oxidation in rat liver microsomes by androgen and estrogen." Biochemical pharmacology **19**(5): 1649-1660.

Keisner, S. V. and S. R. Shah (2011). "Pazopanib: the newest tyrosine kinase inhibitor for the treatment of advanced or metastatic renal cell carcinoma." Drugs **71**(4): 443-454.

Kerbel, R. S. (2003). "Human tumor xenografts as predictive preclinical models for anticancer drug activity in humans: better than commonly perceived-but they can be improved." Cancer biology & therapy **2**(4 Suppl 1): S134-139.

Kirstein, M. N., P. J. Houghton, et al. (2001). "Relation between 9-aminocamptothecin systemic exposure and tumor response in human solid tumor xenografts." Clinical cancer research : an official journal of the American Association for Cancer Research **7**(2): 358-366.

Klempner, S. J., T. K. Choueiri, et al. (2012). "Severe pazopanib-induced hepatotoxicity: clinical and histologic course in two patients." Journal of clinical oncology : official journal of the American Society of Clinical Oncology **30**(27): e264-268.

Kliewer, S. A., J. T. Moore, et al. (1998). "An orphan nuclear receptor activated by pregnanes defines a novel steroid signaling pathway." Cell **92**(1): 73-82.

Knowles, S. R., J. Uetrecht, et al. (2000). "Idiosyncratic drug reactions: the reactive metabolite syndromes." Lancet **356**(9241): 1587-1591.

Koch, S., S. Tugues, et al. (2011). "Signal transduction by vascular endothelial growth factor receptors." The Biochemical journal **437**(2): 169-183.

Krausova, L., L. Stejskalova, et al. (2011). "Metformin suppresses pregnane X receptor (PXR)-regulated transactivation of CYP3A4 gene." Biochemical pharmacology.

Kronbach, T., D. Mathys, et al. (1989). "Oxidation of midazolam and triazolam by human liver cytochrome P450IIIA4." Molecular pharmacology **36**(1): 89-96.

Kumar, R., V. B. Knick, et al. (2007). "Pharmacokinetic-pharmacodynamic correlation from mouse to human with pazopanib, a multikinase angiogenesis inhibitor with potent antitumor and antiangiogenic activity." Mol Cancer Ther **6**(7): 2012-2021.

Kumar, R., V. B. Knick, et al. (2007). "Pharmacokinetic-pharmacodynamic correlation from mouse to human with pazopanib, a multikinase angiogenesis inhibitor with potent antitumor and antiangiogenic activity." Molecular cancer therapeutics **6**(7): 2012-2021.

Kumar, S., K. Samuel, et al. (2002). "Extrapolation of diclofenac clearance from in vitro microsomal metabolism data: role of acyl glucuronidation and sequential oxidative metabolism of the acyl glucuronide." The Journal of pharmacology and experimental therapeutics **303**(3): 969-978.

Lancaster, R. D., A. C. McDougall, et al. (1984). "Leprosy in the nude mouse." Experimental cell biology **52**(1-2): 154-157.

Li, P., C. Tong, et al. (2008). "Germline competent embryonic stem cells derived from rat blastocysts." Cell **135**(7): 1299-1310.

Limdi, J. K. and G. M. Hyde (2003). "Evaluation of abnormal liver function tests." Postgraduate medical journal **79**(932): 307-312.

Macchiarini, F., M. G. Manz, et al. (2005). "Humanized mice: are we there yet?" The Journal of experimental medicine **202**(10): 1307-1311.

Mahmood, I. (1999). "Allometric issues in drug development." Journal of pharmaceutical sciences **88**(11): 1101-1106.

Manning, C. S., Jenkins, R., Hooper, S., Gerhardt, H., Marais, R., Adams, S., Adams, R. H., Rheenen, J., Sahi, E. (2013). ""Intravital Imaging Reveals Conversion Between Distinct Tumour Vascular Morphologies and Localized Vascular Response to Sunitinib"." IntraVital **2.1**.

Marangoni, A., G. (2002). Enzyme Kinetics: A Modern Approach. Hoboken, John Wiley and Sons.

Marcucci, F., R. Fanelli, et al. (1970). "Further studies on species difference in diazepam metabolism." European journal of pharmacology **9**(2): 253-256.

Marechal, J. D., J. Yu, et al. (2006). "In silico and in vitro screening for inhibition of cytochrome P450 CYP3A4 by comedications commonly used by patients with cancer." Drug Metab Dispos **34**(4): 534-538.

Maruyama, C., H. Suemizu, et al. (2002). "Genotyping the mouse severe combined immunodeficiency mutation using the polymerase chain reaction with confronting two-pair primers (PCR-CTPP)." Experimental animals / Japanese Association for Laboratory Animal Science **51**(4): 391-393.

Matthews, H., G. Fries, et al. (1978). "Metabolism and biochemical toxicity of PCBs and PBBs." Environmental health perspectives **24**: 147-155.

Mayes, B. A., E. E. McConnell, et al. (1998). "Comparative carcinogenicity in Sprague-Dawley rats of the polychlorinated biphenyl mixtures Aroclors 1016, 1242, 1254, and 1260." Toxicological sciences : an official journal of the Society of Toxicology **41**(1): 62-76.

McLean, A. J. and D. G. Le Couteur (2004). "Aging biology and geriatric clinical pharmacology." Pharmacological reviews **56**(2): 163-184.

Meehan, R. R., L. M. Forrester, et al. (1988). "Regulation of phenobarbital-inducible cytochrome P-450s in rat and mouse liver following dexamethasone administration and hypophysectomy." The Biochemical journal **254**(3): 789-797.

Mode, A., J. A. Gustafsson, et al. (1982). "Association between plasma level of growth hormone and sex differentiation of hepatic steroid metabolism in the rat." Endocrinology **111**(5): 1692-1697.

Moore, L. B., D. J. Parks, et al. (2000). "Orphan nuclear receptors constitutive androstane receptor and pregnane X receptor share xenobiotic and steroid ligands." The Journal of biological chemistry **275**(20): 15122-15127.

Motzer, R. J., J. Bacik, et al. (2004). "Prognostic factors for survival in previously treated patients with metastatic renal cell carcinoma." Journal of clinical oncology : official journal of the American Society of Clinical Oncology **22**(3): 454-463.

Muruganandan, S. and C. J. Sinal (2008). "Mice as clinically relevant models for the study of cytochrome P450-dependent metabolism." Clin Pharmacol Ther **83**(6): 818-828.

Nagy, A. (2000). "Cre recombinase: the universal reagent for genome tailoring." Genesis **26**(2): 99-109.

Neve, E. P. and M. Ingelman-Sundberg (2008). "Intracellular transport and localization of microsomal cytochrome P450." Analytical and bioanalytical chemistry **392**(6): 1075-1084.

Nolan, C. M., S. V. Goldberg, et al. (1999). "Hepatotoxicity associated with isoniazid preventive therapy: a 7-year survey from a public health tuberculosis clinic." JAMA : the journal of the American Medical Association **281**(11): 1014-1018.

Obach, R. S., J. G. Baxter, et al. (1997). "The prediction of human pharmacokinetic parameters from preclinical and in vitro metabolism data." The Journal of pharmacology and experimental therapeutics **283**(1): 46-58.

Omiecinski, C. J., J. P. Vanden Heuvel, et al. (2011). "Xenobiotic metabolism, disposition, and regulation by receptors: from biochemical phenomenon to predictors of major toxicities." Toxicol Sci **120 Suppl 1**: S49-75.

Omura, T. and R. Sato (1962). "A new cytochrome in liver microsomes." The Journal of biological chemistry **237**: 1375-1376.

Omura, T. and R. Sato (1964). "The Carbon Monoxide-Binding Pigment of Liver Microsomes. I. Evidence for Its Hemoprotein Nature." The Journal of biological chemistry **239**: 2370-2378.

Orimo, A., P. B. Gupta, et al. (2005). "Stromal fibroblasts present in invasive human breast carcinomas promote tumor growth and angiogenesis through elevated SDF-1/CXCL12 secretion." Cell **121**(3): 335-348.

Osborne, C. K. (1998). "Steroid hormone receptors in breast cancer management." Breast Cancer Res Treat **51**(3): 227-238.

Overwijk, W. W. and N. P. Restifo (2001). "B16 as a mouse model for human melanoma." Current protocols in immunology / edited by John E. Coligan ... [et al.] **Chapter 20**: Unit 20 21.

Padda, M. S., M. Sanchez, et al. (2011). "Drug-induced cholestasis." Hepatology **53**(4): 1377-1387.

Pantazis, P., H. R. Hinz, et al. (1992). "Complete inhibition of growth followed by death of human malignant melanoma cells in vitro and regression of human melanoma xenografts in immunodeficient mice induced by camptothecins." Cancer research **52**(14): 3980-3987.

Pantazis, P., A. J. Kozielski, et al. (1993). "Camptothecin derivatives induce regression of human ovarian carcinomas grown in nude mice and distinguish between non-tumorigenic and tumorigenic cells in vitro." International journal of cancer. Journal international du cancer **53**(5): 863-871.

Pascussi, J. M., L. Drocourt, et al. (2001). "Dual effect of dexamethasone on CYP3A4 gene expression in human hepatocytes. Sequential role of glucocorticoid receptor and pregnane X receptor." European journal of biochemistry / FEBS **268**(24): 6346-6358.

Pass, G. J., D. Carrie, et al. (2005). "Role of hepatic cytochrome p450s in the pharmacokinetics and toxicity of cyclophosphamide: studies with the hepatic cytochrome p450 reductase null mouse." Cancer Res **65**(10): 4211-4217.

Podar, K., G. Tonon, et al. (2006). "The small-molecule VEGF receptor inhibitor pazopanib (GW786034B) targets both tumor and endothelial cells in multiple myeloma." Proceedings of the National Academy of Sciences of the United States of America **103**(51): 19478-19483.

Pond, S. M. and T. N. Tozer (1984). "First-pass elimination. Basic concepts and clinical consequences." Clinical pharmacokinetics **9**(1): 1-25.

Potter, G. K., R. N. Shen, et al. (1984). "Nude mice as models for human leukemia studies." The American journal of pathology **114**(3): 360-366.

Preckel, B. and J. Bolten (2005). "Pharmacology of modern volatile anaesthetics." Best practice & research. Clinical anaesthesiology **19**(3): 331-348.

Raynal, C., J. M. Pascussi, et al. (2010). "Pregnane X Receptor (PXR) expression in colorectal cancer cells restricts irinotecan chemosensitivity through enhanced SN-38 glucuronidation." Mol Cancer **9**: 46.

Rezen, T., V. Tamasi, et al. (2009). "Effect of CAR activation on selected metabolic pathways in normal and hyperlipidemic mouse livers." BMC genomics **10**: 384.

Richmond, A. and Y. Su (2008). "Mouse xenograft models vs GEM models for human cancer therapeutics." Disease models & mechanisms **1**(2-3): 78-82.

Rini, B. I. and E. J. Small (2005). "Biology and clinical development of vascular endothelial growth factor-targeted therapy in renal cell carcinoma." Journal of clinical oncology : official journal of the American Society of Clinical Oncology **23**(5): 1028-1043.

Roberts, M. S., B. M. Magnusson, et al. (2002). "Enterohepatic circulation: physiological, pharmacokinetic and clinical implications." Clinical pharmacokinetics **41**(10): 751-790.

Rodriguez-Antona, C. and M. Ingelman-Sundberg (2006). "Cytochrome P450 pharmacogenetics and cancer." Oncogene **25**(11): 1679-1691.

Saxena, A., K. P. Tripathi, et al. (2008). "Pharmacovigilance: effects of herbal components on human drugs interactions involving cytochrome P450." Bioinformation **3**(5): 198-204.

Scheer, N., J. Ross, et al. (2008). "A novel panel of mouse models to evaluate the role of human pregnane X receptor and constitutive androstane receptor in drug response." J Clin Invest **118**(9): 3228-3239.

Scott, R. R. and W. L. Miller (2008). "Genetic and clinical features of p450 oxidoreductase deficiency." Hormone research **69**(5): 266-275.

Scripture, C. D., A. Sparreboom, et al. (2005). "Modulation of cytochrome P450 activity: implications for cancer therapy." The lancet oncology **6**(10): 780-789.

Shitara, Y., H. Sato, et al. (2005). "Evaluation of drug-drug interaction in the hepatobiliary and renal transport of drugs." Annual review of pharmacology and toxicology **45**: 689-723.

Shukla, S. J., S. Sakamuru, et al. (2011). "Identification of clinically used drugs that activate pregnane X receptors." Drug metabolism and disposition: the biological fate of chemicals **39**(1): 151-159.

Sjogren, E., H. Lennernas, et al. (2009). "The multiple depletion curves method provides accurate estimates of intrinsic clearance (CLint), maximum velocity of the metabolic reaction (Vmax), and Michaelis constant (Km): accuracy and robustness evaluated through experimental data and Monte Carlo simulations." Drug metabolism and disposition: the biological fate of chemicals **37**(1): 47-58.

Slamon, D. J., W. Godolphin, et al. (1989). "Studies of the HER-2/neu proto-oncogene in human breast and ovarian cancer." Science **244**(4905): 707-712.

Sleijfer, S., I. Ray-Coquard, et al. (2009). "Pazopanib, a multikinase angiogenesis inhibitor, in patients with relapsed or refractory advanced soft tissue sarcoma: a phase II study from the European organisation for research and treatment of cancer-soft tissue and bone sarcoma group (EORTC study 62043)." Journal of clinical oncology : official journal of the American Society of Clinical Oncology **27**(19): 3126-3132.

Smith, G. C., D. G. Tew, et al. (1994). "Dissection of NADPH-cytochrome P450 oxidoreductase into distinct functional domains." Proceedings of the National Academy of Sciences of the United States of America **91**(18): 8710-8714.

Smith, R. A., V. Cokkinides, et al. (2009). "Cancer screening in the United States, 2009: a review of current American Cancer Society guidelines and issues in cancer screening." CA: a cancer journal for clinicians **59**(1): 27-41.

Sternberg, C. N., I. D. Davis, et al. (2010). "Pazopanib in locally advanced or metastatic renal cell carcinoma: results of a randomized phase III trial." Journal of clinical oncology : official journal of the American Society of Clinical Oncology **28**(6): 1061-1068.

Swami, S., A. V. Krishnan, et al. (2011). "Inhibitory effects of calcitriol on the growth of MCF-7 breast cancer xenografts in nude mice: selective modulation of aromatase expression in vivo." Hormones & cancer **2**(3): 190-202.

Szakacs, G., J. K. Paterson, et al. (2006). "Targeting multidrug resistance in cancer." Nature reviews. Drug discovery **5**(3): 219-234.

Takahashi, A., I. Asakawa, et al. (2002). "Radiation-induced apoptosis in the scid mouse spleen after low dose-rate irradiation." International journal of radiation biology **78**(8): 689-693.

Takimoto, C. H. (2001). "Why drugs fail: of mice and men revisited." Clinical cancer research : an official journal of the American Association for Cancer Research **7**(2): 229-230.

Taylor, S. K., S. Chia, et al. (2010). "A phase II study of pazopanib in patients with recurrent or metastatic invasive breast carcinoma: a trial of the Princess Margaret Hospital phase II consortium." The oncologist **15**(8): 810-818.

Trauner, M. and J. L. Boyer (2003). "Bile salt transporters: molecular characterization, function, and regulation." Physiological reviews **83**(2): 633-671.

Tutt, A., M. Robson, et al. (2010). "Oral poly(ADP-ribose) polymerase inhibitor olaparib in patients with BRCA1 or BRCA2 mutations and advanced breast cancer: a proof-of-concept trial." Lancet **376**(9737): 235-244.

Uetrecht, J. (2007). "Idiosyncratic drug reactions: current understanding." Annual review of pharmacology and toxicology **47**: 513-539.

van Herwaarden, A. E., J. W. Smit, et al. (2005). "Midazolam and cyclosporin a metabolism in transgenic mice with liver-specific expression of human CYP3A4." Drug metabolism and disposition: the biological fate of chemicals **33**(7): 892-895.

van Schaik, R. H. (2008). "CYP450 pharmacogenetics for personalizing cancer therapy." Drug Resist Updat **11**(3): 77-98.

Vasudev, N. S. and J. M. Larkin (2011). "Tyrosine kinase inhibitors in the treatment of advanced renal cell carcinoma: focus on pazopanib." Clinical Medicine Insights. Oncology **5**: 333-342.

Verbeeck, R. K. and F. T. Musuamba (2009). "Pharmacokinetics and dosage adjustment in patients with renal dysfunction." European journal of clinical pharmacology **65**(8): 757-773.

Wade, C. M. and M. J. Daly (2005). "Genetic variation in laboratory mice." Nature genetics **37**(11): 1175-1180.

Walko, C. M. and H. L. McLeod (2008). "Will we ever be ready for blood level-guided therapy?" J Clin Oncol **26**(13): 2078-2079.

Wandel, C., R. Bocker, et al. (1994). "Midazolam is metabolized by at least three different cytochrome P450 enzymes." Br J Anaesth **73**(5): 658-661.

Wang, M., D. L. Roberts, et al. (1997). "Three-dimensional structure of NADPH-cytochrome P450 reductase: prototype for FMN- and FAD-containing enzymes." Proceedings of the National Academy of Sciences of the United States of America **94**(16): 8411-8416.

Waring, J. F., R. Ciurlionis, et al. (2001). "Microarray analysis of hepatotoxins in vitro reveals a correlation between gene expression profiles and mechanisms of toxicity." Toxicology letters **120**(1-3): 359-368.

Watkins, R. E., G. B. Wisely, et al. (2001). "The human nuclear xenobiotic receptor PXR: structural determinants of directed promiscuity." Science **292**(5525): 2329-2333.

Weiss, J. N. (1997). "The Hill equation revisited: uses and misuses." FASEB journal : official publication of the Federation of American Societies for Experimental Biology **11**(11): 835-841.

West, R. B. and M. van de Rijn (2007). "Experimental approaches to the study of cancer-stroma interactions: recent findings suggest a pivotal role for stroma in carcinogenesis." Lab Invest **87**(10): 967-970.

Wolbold, R., K. Klein, et al. (2003). "Sex is a major determinant of CYP3A4 expression in human liver." Hepatology **38**(4): 978-988.

Wood, J. M., G. Bold, et al. (2000). "PTK787/ZK 222584, a novel and potent inhibitor of vascular endothelial growth factor receptor tyrosine kinases, impairs vascular endothelial growth factor-induced responses and tumor growth after oral administration." Cancer research **60**(8): 2178-2189.

Xie, W., J. L. Barwick, et al. (2000). "Reciprocal activation of xenobiotic response genes by nuclear receptors SXR/PXR and CAR." Genes & development **14**(23): 3014-3023.

Xie, X., N. Brunner, et al. (1992). "Comparative studies between nude and scid mice on the growth and metastatic behavior of xenografted human tumors." Clinical & experimental metastasis **10**(3): 201-210.

Xu, C. F., N. X. Bing, et al. (2011). "Pazopanib efficacy in renal cell carcinoma: evidence for predictive genetic markers in angiogenesis-related and exposure-related genes." Journal of clinical oncology : official journal of the American Society of Clinical Oncology **29**(18): 2557-2564.

Yamakado, H., Y. Moriwaki, et al. (2012). "alpha-Synuclein BAC transgenic mice as a model for Parkinson's disease manifested decreased anxiety-like behavior and hyperlocomotion." Neuroscience research **73**(2): 173-177.

Yap, T. A., S. K. Sandhu, et al. (2010). "Envisioning the future of early anticancer drug development." Nat Rev Cancer **10**(7): 514-523.

Yennurajalingam, S., S. Frisbee-Hume, et al. (2013). "Reduction of cancer-related fatigue with dexamethasone: a double-blind, randomized, placebo-controlled trial in patients with advanced cancer." Journal of clinical oncology : official journal of the American Society of Clinical Oncology **31**(25): 3076-3082.

Yoshiki, A. and K. Moriwaki (2006). "Mouse phenome research: implications of genetic background." ILAR journal / National Research Council, Institute of Laboratory Animal Resources **47**(2): 94-102.

Zhang, L., J. M. Strong, et al. (2006). "Scientific perspectives on drug transporters and their role in drug interactions." Molecular pharmaceutics **3**(1): 62-69.

Zhang, Q. Y., C. Fang, et al. (2009). "An intestinal epithelium-specific cytochrome P450 (P450) reductase-knockout mouse model: direct evidence for a role of intestinal p450s in first-pass clearance of oral nifedipine." Drug metabolism and disposition: the biological fate of chemicals **37**(3): 651-657.